ornl

ORNL/TM-6970

OAK
RIDGE
NATIONAL
LABORATORY

UNION
CARBIDE

Materials Analyses of Ceramics for Glass Furnace Recuperators

G. W. Weber
V. J. Tennery

OPERATED BY
UNION CARBIDE CORPORATION
FOR THE UNITED STATES
DEPARTMENT OF ENERGY

DISCLAIMER

Printed in the United States of America. Available from
National Technical Information Service
U.S. Department of Commerce
5285 Port Royal Road, Springfield, Virginia 22161
NTIS price codes—Printed Copy: A06 Microfiche A01

ORNL/TM-6970

Contract No. W-7405-eng-26

METALS AND CERAMICS DIVISION

MATERIALS ANALYSES OF CERAMICS FOR GLASS FURNACE RECUPERATORS

G. W. Weber and V. J. Tennery

Prepared for
Office of Industrial Programs
Conservation and Solar Applications

Date Published: November 1979

OAK RIDGE NATIONAL LABORATORY
Oak Ridge, Tennessee 37830
operated by
UNION CARBIDE CORPORATION
for the
DEPARTMENT OF ENERGY

THIS PAGE

WAS INTENTIONALLY

LEFT BLANK

CONTENTS

MATERIALS ANALYSES OF CERAMICS FOR GLASS FURNACE RECUPERATORS

G. W. Weber* and V. J. Tennery

ABSTRACT

The use of waste heat recuperation systems offers significant promise for meaningful energy conservation in the process heat industries. The potential for fuel savings realizable from the four major industrial users — steel, glass, aluminum, and cement — amounts to approximately 1.4 EJ (1.3×10^{15} Btu) per year. Glass furnaces alone account for a potential savings of $800,000/d in equivalent oil at $12 per barrel. The higher efficiencies available through the use of glass furnace recuperation in place of current regeneration systems has not been realized primarily because of technology and material limitations. A program sponsored by the Office of Industrial Programs/Conservation of the Department of Energy at Terra Tek, Inc., Salt Lake City, Utah, has as its objective the development of acceptable recuperator technology for the glass industry. This report details the analysis of candidate ceramic recuperator materials exposed by Terra Tek to simulated industrial glass furnace hot flue gas environments.

Several candidate structural ceramic materials including various types of silicon carbide, several grades of alumina, mullite, cordierite, and silicon nitride were exposed to high-temperature flue gas atmospheres from specially constructed day tank furnaces. Furnace charging, operation, and batch composition were selected to closely simulate industrial practice. Material samples were exposed in flues both with and without glass batch in the furnace for times up to 116 d at temperatures from 1150 to 1550°C (2100–2800°F). Exposed materials were examined by optical microscopy, scanning electron microscopy, energy dispersive x-ray analysis, x-ray diffraction, and x-ray fluorescence to identify material degradation mechanisms. The materials observations were summarized as:

1. Silicon carbide exhibited enhanced corrosion at lower temperatures (1150°C) when alkalies were deposited on the carbide from the flue gas and less corrosion at higher temperatures (1550°C) when alkalies were not deposited on the carbide.
2. Alumina corrosion depended strongly upon purity and density . Alumina contents less than 99.8% were unsatisfactory above 1400°C.
3. Mullite and corderite are generally unacceptable for application in soda-lime glass melting environments at temperatures above 1100°C.

---

*Now with Carborundum Company, Niagara Falls, N. Y.

4. Reaction-bonded silicon nitride exhibited behavior generally inferior to that of silicon carbide and displayed a corrosion rate dependence on temperature similar to the carbide. This similarity to the carbide is due to the same sensitivity to accelerated corrosion due to the degradative action of alkalies on the protective silica film normally formed on the nitride.

The conclusion is that structural ceramics relying upon either a protective SiO_2 film (such as SiC or Si_3N_4) or an extensive silicate bonding phase (such as cordierite, mullite, and aluminas with $\leq 94\%$ Al_2O_3) were severely corroded by the fluxing action of alkalies and iron in the test environment used. The alkalies and iron increase the fluidity of the siliceous film and impair its oxidation protection ability.

INTRODUCTION

Recent developments concerning the limitations and economy associated with energy availability in the United States, particularly from fossil fuels for industrial process heat, have indicated that a primary means for offsetting increasing demand and cost along with dwindling supplies is through economically feasible energy conservation. This conservation can take the forms of (1) minimizing heat loss from the equipment to the surroundings with appropriate insulation, (2) improved higher efficiency processes, and (3) utilization of traditionally rejected heat for other purposes such as for power generation or increasing process efficiency through preheating process gases or raw materials. The concept of preheating process or combustion air to increase the thermodynamic efficiency of the process has received increasing support in current Department of Energy (DOE) programs. The four largest industries in terms of waste heat rejected in the U.S. are steel, glass, aluminum, and cement. Together they account for estimated potential energy savings of 1.4 EJ (1.3 quads or 1.3×10^{15} Btu) if certain process improvements are assumed. Development of a high-performance glass furnace recuperator offers potential for 70% recovery of the available flue gas heat, and this would represent $800,000/d savings in equivalent oil at $12 per barrel.[1,2] Approximately 11 GJ (10^7 Btu) is required in a continuous glass furnace to melt 1 Mg (one ton) of glass. Of this heat, 80% is emitted as waste heat from the furnace, with 50% being lost in the

hot gas exhaust.[3] This large energy source contains, in fact, more than enough energy to preheat incoming combustion air and represents a possible source of energy to produce cogenerated electricity.[4]

Some studies[5] have concluded that regenerators are more efficient than recuperators (fixed-boundary heat exchangers) for using hot waste gases at 1500°C (2700°F) to preheat combustion air to 650°C (1200°F). However, as the thermodynamic quality requirements of the preheated air are increased to increase process efficiency, recuperators are expected to become increasingly attractive.[5]

A program was initiated by DOE Office of Industrial Programs/ Conservation within the past two years to evaluate potential refractory structural ceramic materials as candidates for use in glass furnace recuperators with anticipated exhaust gas temperatures up to 1350°C (2500°F). The concomitant material temperatures in this application would exceed 1250°C (2300°F). These temperatures coupled with the generally hostile glass furnace exhaust environment and mechancial integrity requirements represent a demanding materials application.

The samples that were evaluated in this report were carefully selected structural ceramic candidates for use in a glass-furnace recuperator. These materials were exposed by Terra Tek, Inc., Salt Lake City, Utah, at different temperatures for varying lengths of time to the flue gas stream from a specially constructed glass day tank containing a composition closely approximating one employed for container and flat glass manufacture. Materials exposed included several types of silion carbide, several grades of alumina, mullite, cordierite, and silicon nitride. This report will deal with the analyses of the test specimen behavior, microstructure, macrostructure, and microcomposition of these materials as they relate to their potential use in a glass furnace recuperator.

SPECIMEN HISTORY

Special day tank furnaces were constructed at Millcreek Glass Company of Salt Lake City, Utah, to conduct the materials testing as subcontractors of Terra Tek, Inc. We then analyzed these exposed samples to form the basis for this report.

A schematic diagram of the special day tank furnaces is shown in Fig. 1. The blocks lining the tank were alumina-zirconia-silica (AZS) fused cast refractory called Monofrax S3.* Fused cast AZS is widely recognized as the industry standard for soda-lime glass furnace blocks for containing the molten glass. The furnace side walls above glass level are superduty firebricks containing over 40% alumina and about 50% silica. The roof is a high-alumina castable refractory. Silica refractory would normally be used in continuous melting glass furnaces in place of the high alumina, but silica was not suitable for this small furnace because of frequent reheating and furnace maintenance.[4]

These furnaces could closely simulate the conditions in a continuous soda-lime glass melting furnace. These small furnaces could simulate flue conditions found in larger furnaces at least within the variability between different large furnaces and between different exhaust ports on the same industrial-size furnace. Large furnace environmental characteristics were replicated by simulating industrial furnace operating conditions, such as batch carryover into the flue containing the test specimens caused by charging new batch materials into the furnace.

Two furnaces were used at Terra Tek for the specimen exposure tests to permit simultaneous testing in combustion product exhaust and glass furnace exhaust. Glass batch was charged into the furnace used for glass melting four times a day to simulate the actual dust carryover experienced in an industrial furnace. Temperatures in the furnace varied from 1290 to 1625°C (2360–2955°F) with an average of about 1540°C (2800°F).

The glass batch used in the recuperator material test furnaces is given in Table 1. As previously described, this batch was representative of soda-lime glass used in the plate and container glass industries. Although it is unlikely that any one plant would incorporate barium carbonate, borax, and cryolite together, it was felt that all should be included to better simulate all possible components in the exhaust of any operating plant.

---

*Carborundum Company, Niagara Falls, N. Y.

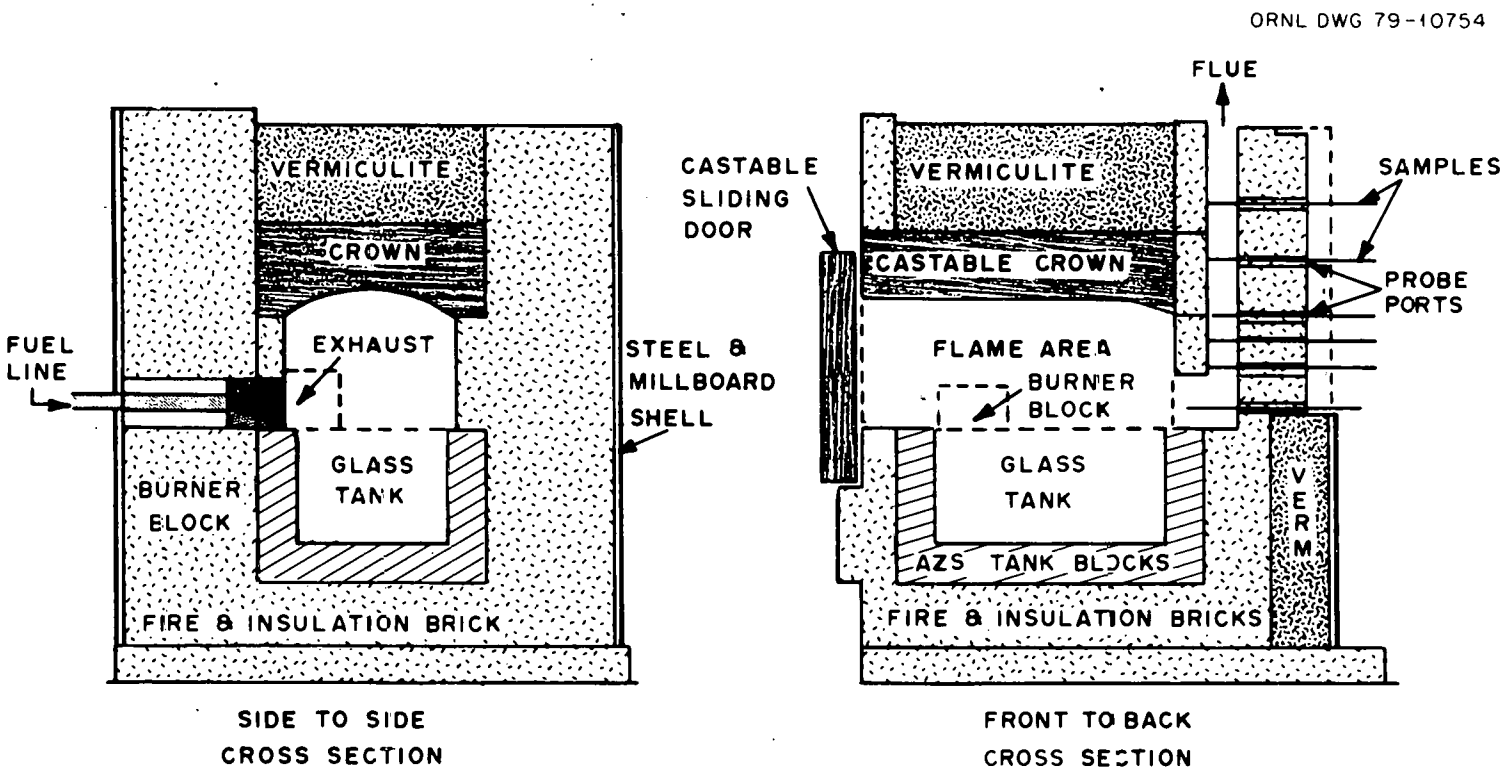

Fig. 1. Cross Sections of the Special Day Tank Furnaces Used at Millcreek Glass for Material Tests.

Table 1. Batch Composition Used in Glass Furnace Recuperator Materials Testing

Material	Charge (wt %)	Equivalent Oxide Delivered to Glass	Equivalent Oxide Glass Composition (wt %)[a]
SiO_2	50.64	SiO_2	50.64
$CaCO_3$	14.47	CaO	8.10
Na_2CO_3	17.69	Na_2O	10.35
Dolomite	7.24	CaO	2.20
		MgO	1.56
Feldspar	8.04	Al_2O_3	1.45
$BaCO_3$	0.56	BaO	0.44
Cryolite	0.80	F	0.43
		Al_2O_3	0.19
		Na_2O	0.35
Borax	0.56	B_2O_3	0.38
		Na_2O	0.17

[a]Based on charge.

The samples were inserted into the probe ports of the furnace flues as shown in Fig. 1. The rectangular flue was 230 by 60 mm (9 by 2.5 in.), and the probes extended across the flue. The actual exhaust test configuration is shown in Fig. 2. Temperatures measured by Pt vs Pt—10% Rh thermocouples varied from 1150°C (2100°F) at ports 25 through 27 to 1550°C (2800°F) at port 1, depending upon the height and location in the furnace flue as indicated in the graphic test port representation in Fig. 3. It is apparent that significant alterations in flow in the lower test section of the exhaust gas path could affect the types and concentrations of impurities deposited in upper test sections in the flue. The condensation, slagging, and enhanced reaction often observed on the downstream side of sections in flow streams as a result of flow interruptions could modify the results. The modification would depend

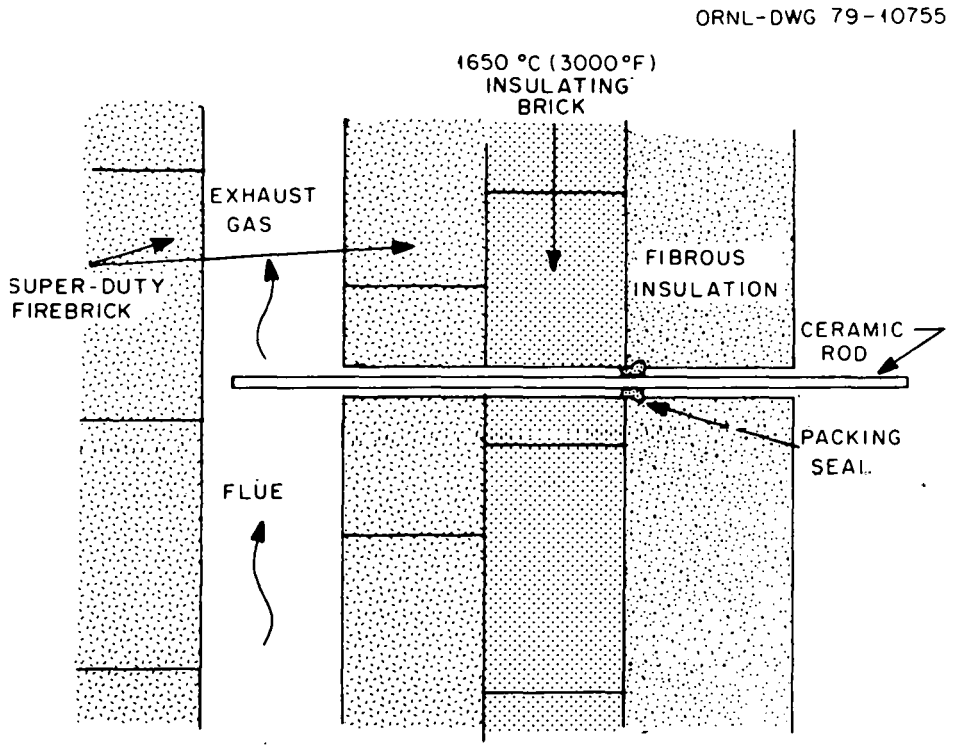

Fig. 2. Detail of Recuperation Material Coupon Furnace Exhaust Test Configuration.

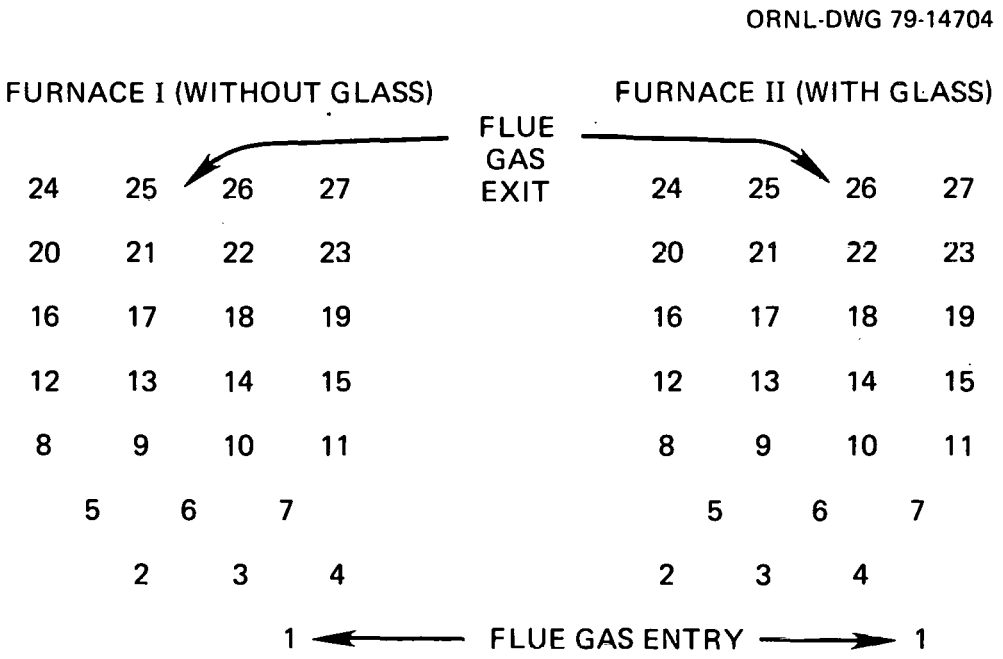

Fig. 3. Flue Gas Port Arrangement.

upon the concentration and composition of deposited species from the glass batch. This situation would be particularly unclear for samples in the back of columns such as 24, 25, 26, and 27, and particular attention was given in the test specimen analyses to detect such anomalies. The Furnace I test specimen results for conditions without glass in the furnace were anticipated to be simpler to interpret than those from Furnace II, which had glass batch carryover contributing to the test specimen corrosion process. The comparisons between material A in position 25 and material B in position 1, for example, need to be interpreted carefully because of the very different environments experienced by the two specimens.

Descriptions of the materials by supplier, density, and fabrication technique are detailed in Table 2. The material sample observations made by Terra Tek and Millcreek Glass personnel on the samples upon removal from the test furnaces are given in Tables 3 and 4.

Table 2. Ceramic Materials Tested

Material	Designation	Supplier	Density Mg/m^3	Comments
SiC	Sintered alpha	Carborundum	3.16	0.3%, 0.5% B added Sintered to <1-μm particle size.
SiC	NC-400	Norton	2.61	Recrystallized
SiC	NC-430	Norton	3.08	Reaction-sintered (self-bonded), bonded with Si and C.
SiC	KT	Carborundum	3.01	Reaction-sintered (self-bonded), bonded with Si and C.
SiC	CVD	MTC	3.24	Chemically vapor deposited.
Si_2ON_2	Sioxyn[a]	Norton		
Al_2O_3	Vistal[b]	Coors	4.00	High-purity polycrystalline
Al_2O_3	AD998	Coors	3.80	High-purity polycrystalline
Al_2O_3	AD-94	Coors	3.64	94% Al_2O_3
Al_2O_3	AD-85	Coors	3.40	85% Al_2O_3
Mullite		Coors	2.85	75% Al_2O_3 — 25% SiO_2
Cordierite	CD-1	Coors	2.40	Low thermal expansion
ZrO_2	Zirconia	Coors	5.64	
Si_3N_4	RBN	AiResearch	2.74	Reaction bonded

[a] Trademark of the Norton Company.

[b] Trademark of Coors Porcelain Company.

Table 3. Sample Observations for Furnace I (Without Glass)

Material	Sample	Port	Approximate Average Temperature (°C)	Approximate Average Temperature (°F)	Exposure (d)	Observations
SiC-CVD	1	1	1550	2800	116	Glazed with some foam. Apparent decrease in diameter over part of exposed length.
SiC-CVD	3	22	1225	2250	92	Glazed. No dimensional deterioration.
SiC-Sintered α	1	4	1450	2650	36	Slight glazing. No dimensional deterioration. No change. Moved to port 7.
	1	7	1425	2600	44	Milky coating. No dimensional deterioration.
SiC-NC-430	1	2	1450	2650	104	Glazed. No dimensional deterioration. Milky coating.
SiC-NC-400	1	8	1400	2550	116	Some glazing and foam. No dimensional deterioration.
SiC-KT	1B	13	1350	2450	116	Glazed. No dimensional deterioration. Possible slight rounding of sharp edge.
Al_2O_3-AD-94	1	2	1450	2650	8	Slumping slightly. Moved to port 11.
	1	11	1400	2550	109	Iron staining from another sample. No dimensional deterioration.
Al_2O_3-VISTAL	1	9	1400	2550	7	No change observed. Moved to port 3.
	1	3	1450	2650	105	Iron staining from sample above. No dimensional deterioration. Loss of "waxy" surface.
Al_2O_3-AD-998	1	4	1450	2650	39	No apparent deterioration.
Al_2O_3-AD-85	1	10	1400	2550	7	Severe slumping. Withdrawn.
Mullite	1	3	1450	2650	8	Easily bent at temperature. Greatly reduced resistance to thermal shock. Withdrawn.
Mullite	3	17	1250	2300	14	Darkening of surface, crystalline development on one side. Greatly reduced resistance to thermal shock. Withdrawn.
Cordierite	1	5	1425	2600	4	Hot end slumped, then fell off. Withdrawn. Recovered end curled and badly deteriorated.
Cordierite	3	18	1250	2300	14	Exposed side of sample darkened, blistered, and expanded, causing sample to curl upwards. Withdrawn.
Cordierite	4	25	1150	2100	92	Slight edge deterioration. Surface darkened. Edge slightly rounded.
Si_3N_4	1B	12	1350	2450	46	Sample broken upon extraction for observation. Possible flaw apparent. Possible slight deterioration of exposed surface.
Si_3N_4	3B	21	1225	2250	62	Glazed. Little if any dimensional deterioration. Sample broken easily upon extraction. Break very similar to sample 1B.
ZrO_2	1	4	1450	2650	21	Hot end slumped slightly. Severe multiple fracturing in intermediate region inside flue wall. Withdrawn.
Stainless Steel-426	1	26	1150	2100	28	Severe scaling. Withdrawn.

Table 4. Sample Observations for Furnace II (With Glass)

Material	Sample	Port	Approximate Average Temperature (°C)	Approximate Average Temperature (°F)	Exposure (d)	Observations
SiC-CVD	2	1	1550	2800	70	Glazed with some foam. Apparent decrease in diameter over part of exposed length — 48 d. Sample eroded into two parts. Most erosion at or near supporting wall where glass condensate is apparent — 70 d.
SiC-Sintered α	2	2, 3, or 4	1450	2650	4	Sample moved to port 1.
	2	1	1550	2800	17	Sample eroded almost into two parts. Erosion limited to zone at supporting wall where material temperature is well below 1550°C (2800°F).
SiC-Sintered α	3	21	1225	2250	18	Major disappearance of material over exposed length.
SiC-NC 430	2	2	1450	2650	104	Glazed. Sample circumference decreased at sample wall zone of lowered temperature.
SiC-NC 400	2	8	1400	2550	116	Some glazing and foam. No dimensional deterioration. Some decrease in circumference at support wall zone.
SiC-KT	4	1	1550	2800	69	Slight decrease in diameter inside supporting wall at much lower temperature.
SiC-KT	2	13	1350	2450	47	Glazed. Slight decrease in diameter of exposed length. Moved to port 6.
	2	6	1425	2600	48	Slight edge deterioration. Slight decrease in circumference 13 mm (0.5 in.) inside support wall.
SiC-KT	3	21	1225	2250	69	Major decrease in circumference of exposed material.
Al_2O_3-AD-94	2	2	1450	2650	8	Slumping slightly. Moved to port 11.
	2	11	1400	2550	109	Decrease in circumference at support wall zone.
Al_2O_3-Vistal	2	9	1400	2550	11	No change observed. Moved to port 3.
	2	3	1450	2650	146	Surface no longer feels waxy. No dimensional deterioration. Slight slumping. Diameter decreased 0.5 mm (0.02 in.) at supporting wall zone only.
Al_2O_3-Vistal	4		1150	2100	90	Material coated with a glaze on lower side. Glaze easily breaks off.
Al_2O_3-AD-85	2	10	1400	2550	5	Severe slumping. Withdrawn.
Al_2O_3-AD-85	3		1150	2100	90	Glass apparently combining into the surface on lower side.
Mullite	2	3	1450	2650	8	Easily bent at temperature. Crystalline development in ceramic body. Greatly reduced resistance to thermal shock.
Mullite	4		1150	2100	90	Slight disappearance of material from lower side.
Cordierite	2	5	1425	2600	4	Hot end slumped, then fell off. Withdrawn.
Cordierite	5		1150	2100	90	Sample warped upward with some deterioration of lower side.
Si_3N_4	2	12	1350	2450	70	Glazed with some foaming initially. Slight surface deterioration. Sample broken easily upon extraction. Break and discoloration similar to 1B.
Si_3N_4	4	21	1225	2250	23	Major decrease in diameter over entire exposed length. Withdrawn.
Si_2ON_2	1	7	1425	2600	18	Surface covered with foam. Decrease in volume of exposed material. Sample subsequently broken in port. Exposed portion not extractable.
ZrO_2	2	4	1450	2650	21	Severe multiple fracturing in intermediate temperature region inside flue wall. Withdrawn. Sample broken upon withdrawal and exposed portion lost.

ANALYTICAL PROCEDURES

X-Ray Analysis

Standard x-ray diffraction techniques were utilized to identify crystalline phases present in the ceramic recuperator test samples. Powdered samples were mounted on a silicon single crystal to reduce the x-ray background. The silicon was oriented in such a way as to provide no contribution to the x-ray spectrum. A vertical Norelco diffractometer using copper radiation with a graphite crystal differential beam monochromator was used to provide the x-ray data. Data collection was at a 2θ scan rate of 0.0021°/s with 6 s integrating time, providing a final plot of diffracted intensity against 2θ.

X-ray fluorescence techniques were used to determine the qualitative elemental composition of deposits present on the samples. The samples were the same as those used in the x-ray diffraction analysis. Silver radiation was used for excitation and a lithium-drifted silicon detector and multichannel analyzer were used for data collection.

Ceramographic Preparation and Examination

Samples were removed by fracturing and/or diamond sawing from the original specimens and were placed in hollow cylindrical mounting molds. The sample was covered with a catalyzed epoxy resin (Shell Epon 815)* and then impregnated with the epoxy by use of vacuum.

Grinding and polishing was done by use of successively coarser media with water as a coolant. Typical abrasives used were 180-, 320-, 400-, and 600-grit silicon carbide papers, 0.3-μm alumina and 1-μm diamond paste. The finished sample was washed with ethyl alcohol and air dried.

---

*Product of Shell Oil Company, New York.

A reflected-light metallurgical microscope was used to observe the microstructures. Bright field, dark field, and polarized light were used in the analysis as appropriate.

Scanning Electron Microscopy

Fractured and as-received ceramic specimen surfaces and deposits were examined by scanning electron microscopy (SEM). A JEOL U-3 microscope was employed. The nonconducting samples were vapor coated with a very thin layer of gold to eliminate charging effects in the instrument.

Qualitative chemical analysis on SEM samples used characteristic x-ray emissions. A lithium-drifted silicon detector with a multichannel analyzer was used for data collection.

Electron Microprobe

Polished ceramographic sections were analyzed for elemental compositional distribution with an electron microprobe. Backscattered electons were used for determination of the distribution of high-atomic-number elements, while characteristic x-ray emissions were used for individual elemental distributions.

RESULTS

Silicon Carbide

Several different types of silicon carbide representing a range of densities, fabrication techniques, impurity levels, and costs were evaluated in the previously described furnace tests. The high thermal conductivity, good mechanical properties, relatively low thermal expansion with resultant thermal shock resistance, and generally good corrosion resistance make SiC an attractive candidate structural ceramic material for use in high-temperature recuperators. The SiC ceramics will be discussed individually as their performance was quite varied in this environment.

Reaction Sintered or "Siliconized" SiC

The material in this category is generally fabricated by reaction sintering of primary silicon carbide grains with additions of silicon and carbon, which form a secondary silicon carbide phase upon firing at high temperature. This ceramic body can also be prepared by infiltration of silicon into a prefired SiC and carbon precursor mixture. A second firing converts much of the free silicon and carbon to silicon carbide. These bodies are typified by a primary silicon carbide phase and a dispersion of smaller secondary silicon carbide grains, free silicon, and porosity. Materials in this category include KT* and NC-430†. Silicon carbide of this type that was exposed in the furnace tests is shown in Figs. 4 and 5 for KT and Figs. 6 and 7 for NC-430 with exposure times, temperatures, and furnace conditions. This material will apparently withstand exposure to these combustion gases without glass in the furnace, as evidenced by the performance of Specimen KT-1B at 1350°C (2450°F) for 116 d and NC-430-1 at 1450°C (2650°F) for 104 d. Both samples had a glazed appearing surface with a milky white coating and no significant dimensional deterioration except for some slight rounding of sharp edges in the KT material. Both samples did show some deposition of brownish "iron-type" scale, which may attack or react with the silicon carbide. The samples were broken for ceramographic examination.

Microstructures of cross sections of these two samples taken about 20 or 25 mm from the exposed end are shown in Fig. 8. This region was located approximately in the middle of the flue gas duct and would thus be minimally influenced by the refractory walls and edge effects. For this reason, this portion of each specimen was given major emphasis throughout this study unless specifically mentioned otherwise. The more extensive porosity and microstructural disruption of the KT material at the glass-SiC interface region relative to the NC-430 silicon carbide would appear to make it less desirable for application in this environment. This behavioral difference was surprising because the NC-430 material was exposed to somewhat higher temperatures and was

*Carborundum Company, Niagara Falls, N.Y.

†Norton Company, Worcester, Mass.

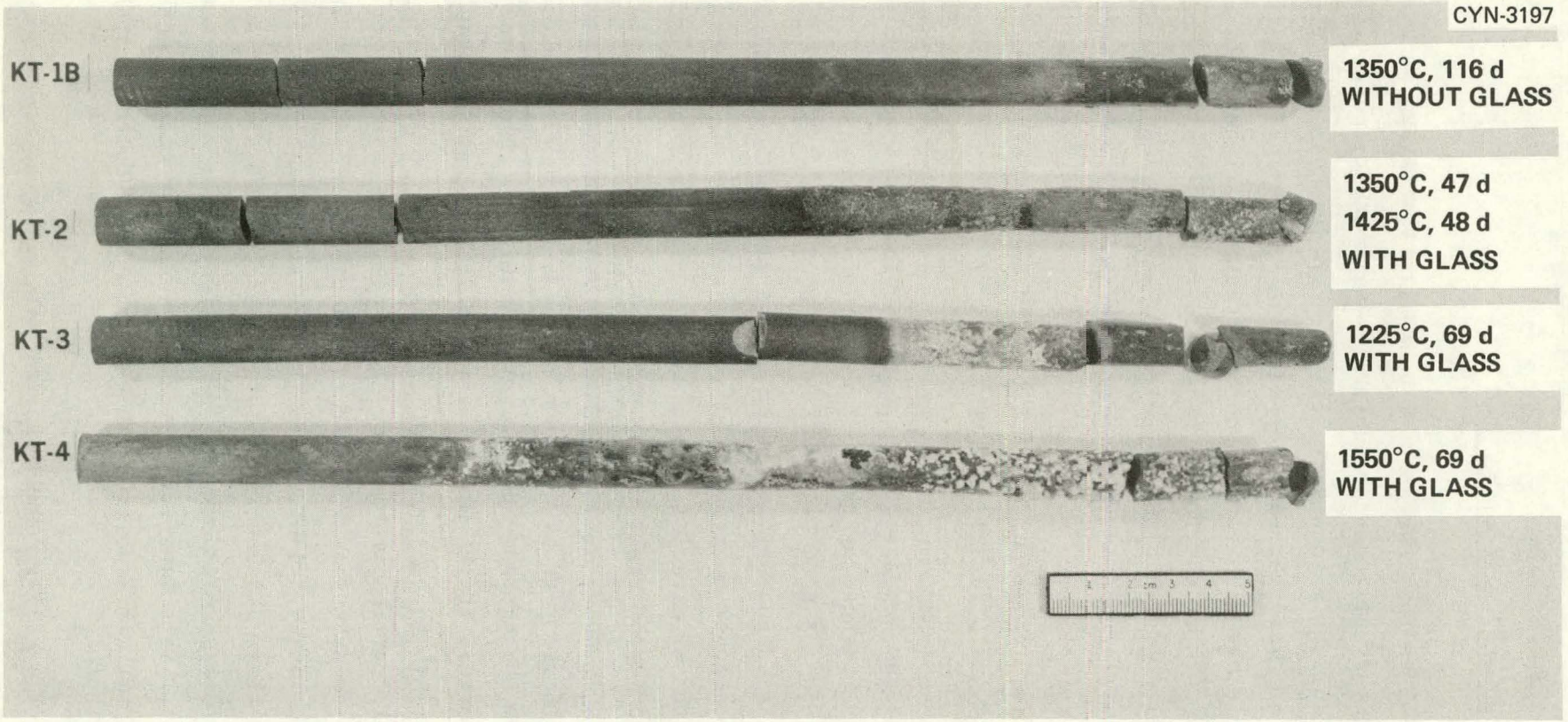

Fig. 4. Reaction Bonded (Siliccnized) Silicon Carbide Exposed to Glass Furnace Environment.

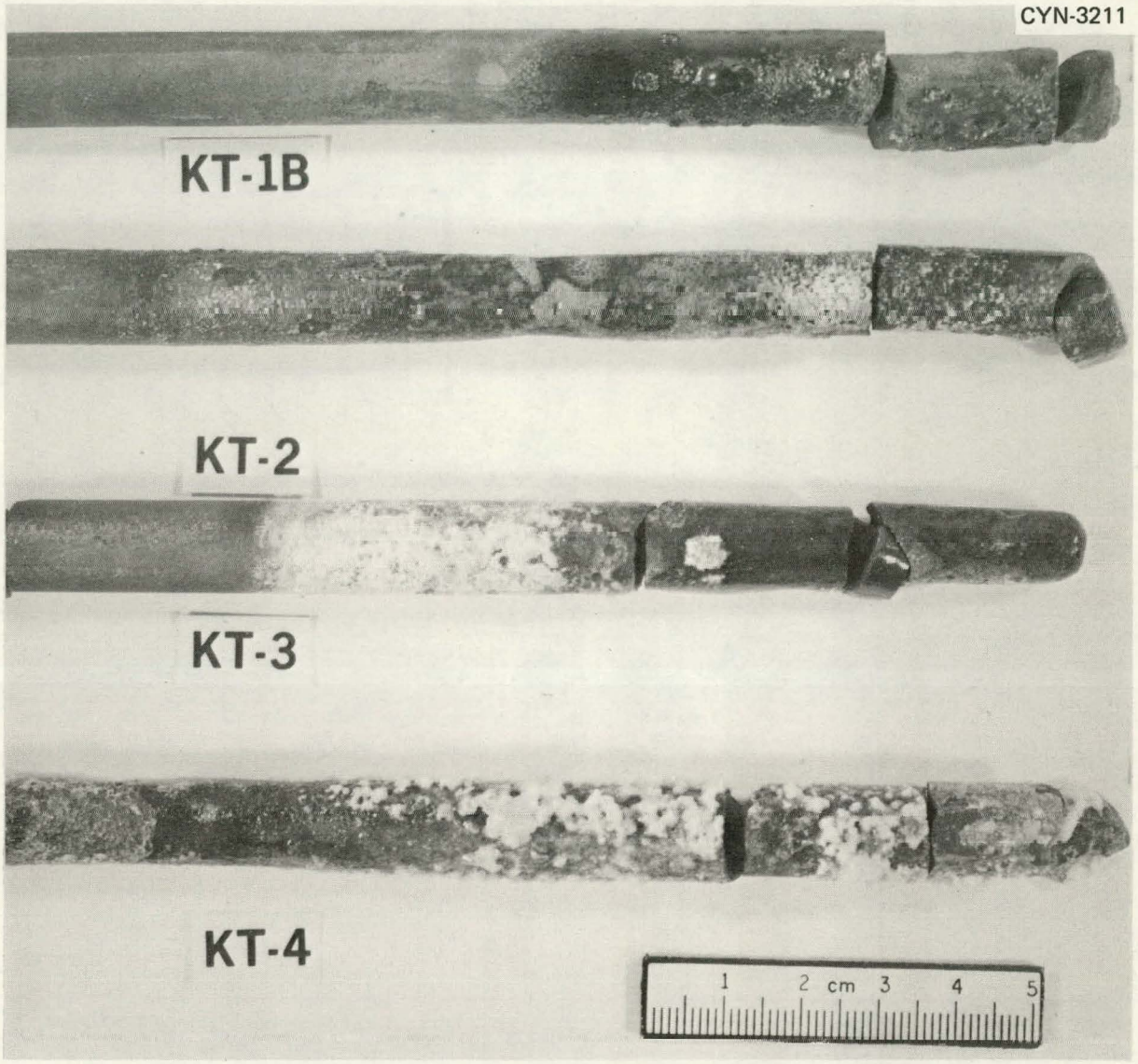

Fig. 5. Close-Up of Reaction Bonded (Siliconized) Silicon Carbide Exposed to Glass Furnace Environment.

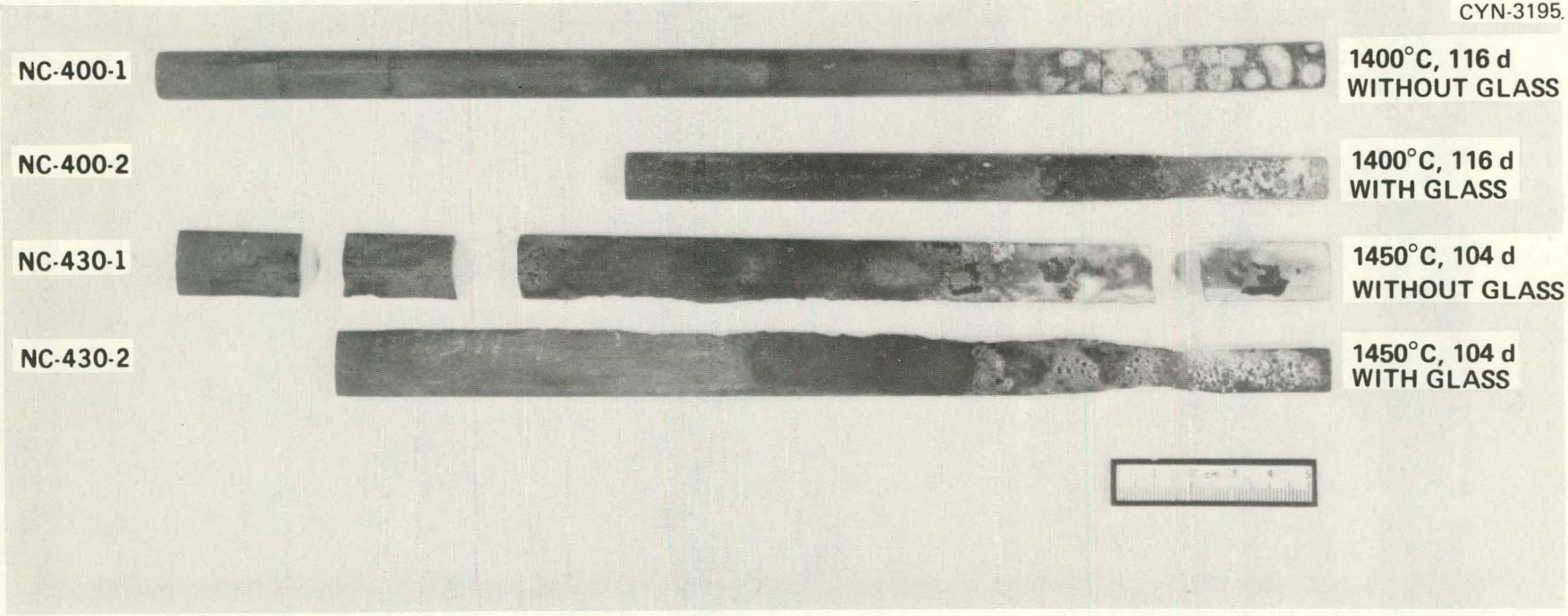

Fig. 6. Recrystallized and Reaction Sintered (Siliconized) Silicon Carbide Exposed to Glass Furnace Environment.

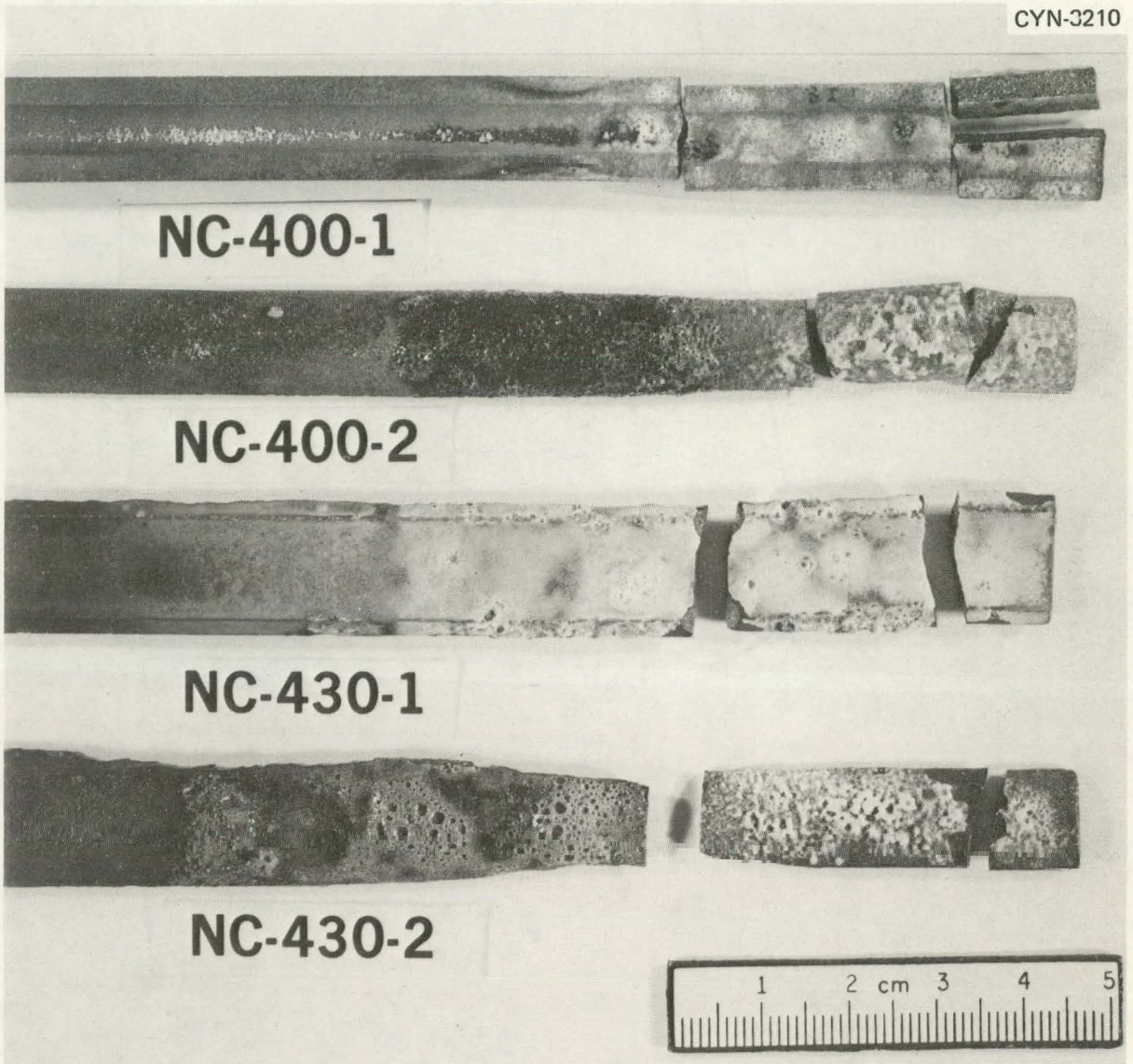

Fig. 7. Close-Up of Recrystallized and Reaction Sintered (Siliconized) Silicon Carbide Exposed to Glass Furnace Environment.

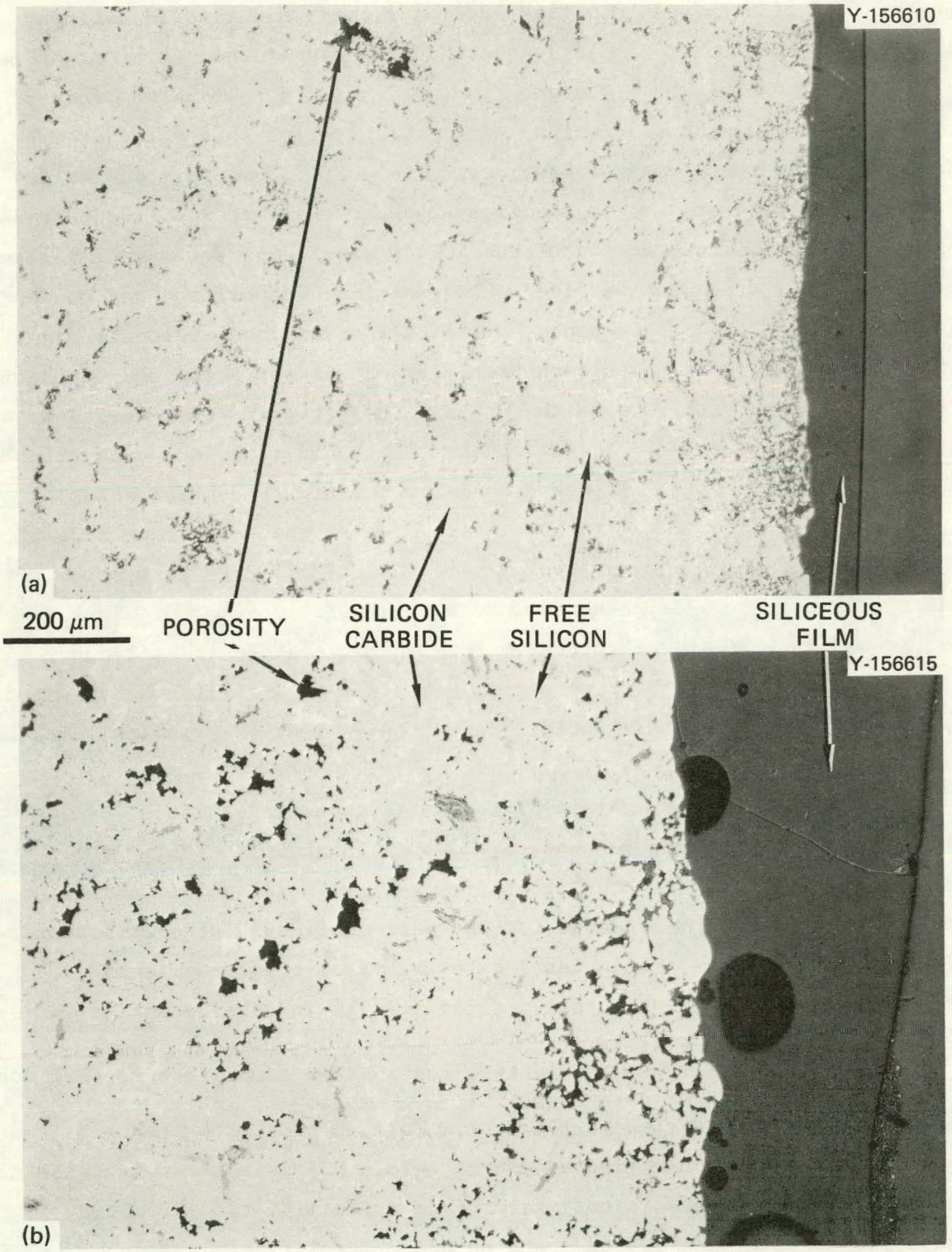

Fig. 8. Microstructure of Siliconized Silicon Carbide Exposed to Furnace Flue Atmosphere with No Glass in the Furnace. (a) NC-430-1, 104 d at 1450°C (2650°F) in test port 2. (b) KT-1B, 116 d at 1340°C (2450°F) in port 13.

in the form of a curved thin flat section rather than a solid cylinder like the KT specimen. Sample location in the test furnace flue might be a possible cause of the difference in behavior. The NC-430 was in port 2 (at a higher temperature), which is essentially open to the furnace exhaust, while the KT sample was located in port 13, where the flow is interrupted by several other specimens between the port and flue entry. Assuming that the convex side of the NC-430 was facing downward into the exhaust system, the concave side would experience deposition and condensation from the flow disturbance on the downstream lower velocity side. Only the concave side of this specimen showed discoloration and deposition of extraneous material, while the convex side was primarily covered with glass and cristobalite. The downstream side would therefore appear to be more subject to chemical attack because of the higher concentration of deposits on this surface. Material deposited on the downstream side of the sample in port 2 (NC-430) completely covered the exposed portion of another sample located further downstream in port 13 (KT-1B). This increased availability of corrosive foreign material on the silicon carbide at a point in the flue considerably downstream from the location of maximum gas temperature would be expected to increase chemical attack on the silicon carbide.

X-ray diffraction analysis of the milky-appearing surface coating about 15 mm from the exposed end on NC-430-1 is shown in Table A1 of the Appendix. The data correlate fairly well with the Joint Committee on Powder Diffraction Standards (JCPDS) pattern 11-695 for α-cristobalite (SiO_2). Exposure of silicon carbide to oxidizing environments at elevated temperatures characteristically results in development of an amorphous glass and cristobalite on the surface, so this observation was as anticipated.

The x-ray diffraction analysis of a portion of a brown scale appearing 10 mm from the exposed end of sample KT-1B is shown in Table A2 of the Appendix. There is only fair correlation with two different polytypes of SiC — 21R and 6H — and no other identifiable phases.

Exposure of siliconized silicon carbide to the exhaust flue of a furnace containing glass resulted in significantly different behavior than when the furnace contained no glass. Three samples of the KT

material were exposed: KT-4 at 1550°C (2800°F) for 69 d in port 1, KT-2 at 1350°C (2450°F) for 47 d in port 13 and 1425°C (2600°F) for 48 d in port 6, and KT-3 at 1225°C (2250°F) for 69 d in port 3, representing high, medium, and low flue gas temperature. The qualitative behavior of this silicon carbide was again worst at the lowest temperature; KT-3 (at the lowest temperature) had a major decrease in the diameter of the exposed specimen end, while KT-4 (at the highest temperature) showed minimal dimensional changes, except at a location close to the flue wall where the specimen temperature was lowest. The intermediate-temperature material showed a qualitatively intermediate corrosion rate.

The NC-430 sample 2, which was exposed at 1450°C (2650°F) for 104 d at port 2, again showed little silicon carbide loss at the exposed end but had severe surface recession close to the flue wall, where the silicon carbide temperature was lowest.

The microstructure of the siliconized silicon carbide exposed to glass is shown in Figs. 9 and 10. Comparison of these figures indicates that the attack on the free silicon present as a second phase in this material increases with increasing temperature in the range 1350 to 1550°C (2450–2800°F). The disappearance of the free silicon (mp 1410°C) secondary phase and its replacement by glass or porosity is significantly more extensive at higher temperatures (>1410°C) and is much worse for the KT material than for the NC material. Comparsion with Fig. 8(a) also indicates that the microstructure of the KT silicon carbide may be disrupted more extensively than that of NC-430 silicon carbide during long-term flue tests in the furnace containing no glass.

The most striking observation, however, is that the sample exposed to the lowest temperature (1225°C) did not show the characteristic removal of the free silicon phase, but showed a roughly uniform removal of silicon and silicon carbide from the sample at an appreciable rate. The conclusion is that two very different degradation mechanisms are operative in this type of silicon carbide, depending upon the temperature. Fairly rapid reaction and corrosion occur at low temperatures and much slower corrosion occurs at higher temperature, with the microstructural degradation of the free silicon secondary phase having little apparent effect on the bulk corrosion or surface recession rate.

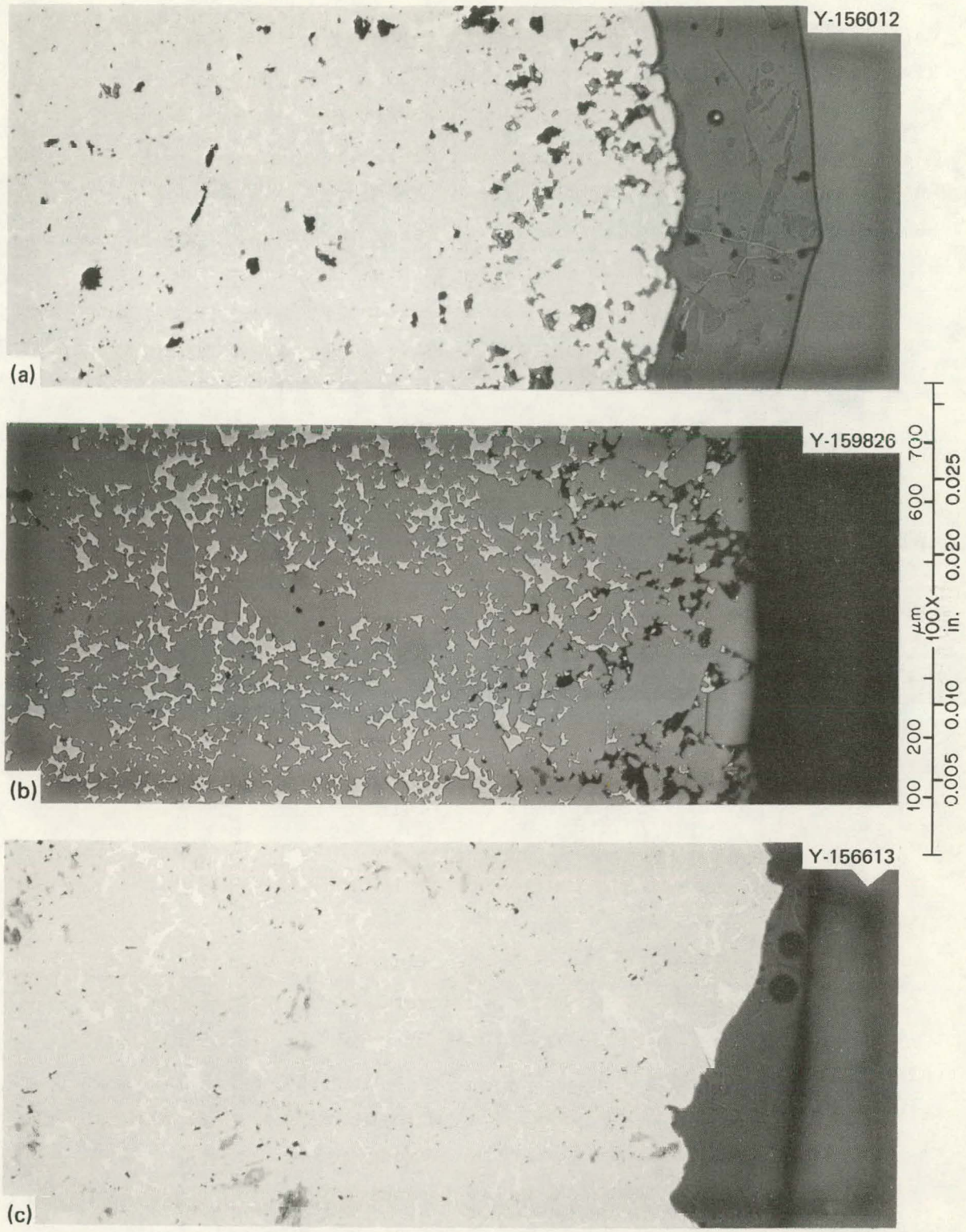

Fig. 9. Microstructure of Siliconized Silicon Carbide Exposed to Furnace Flue Atmosphere with Glass in the Furnace. (a) KT-4 at 1550°C (2800°F) for 69 d. (b) KT-2 at 1350°C (2450°F) for 48 d. (c) KT-3 at 1225°C (2250°F) for 69 d.

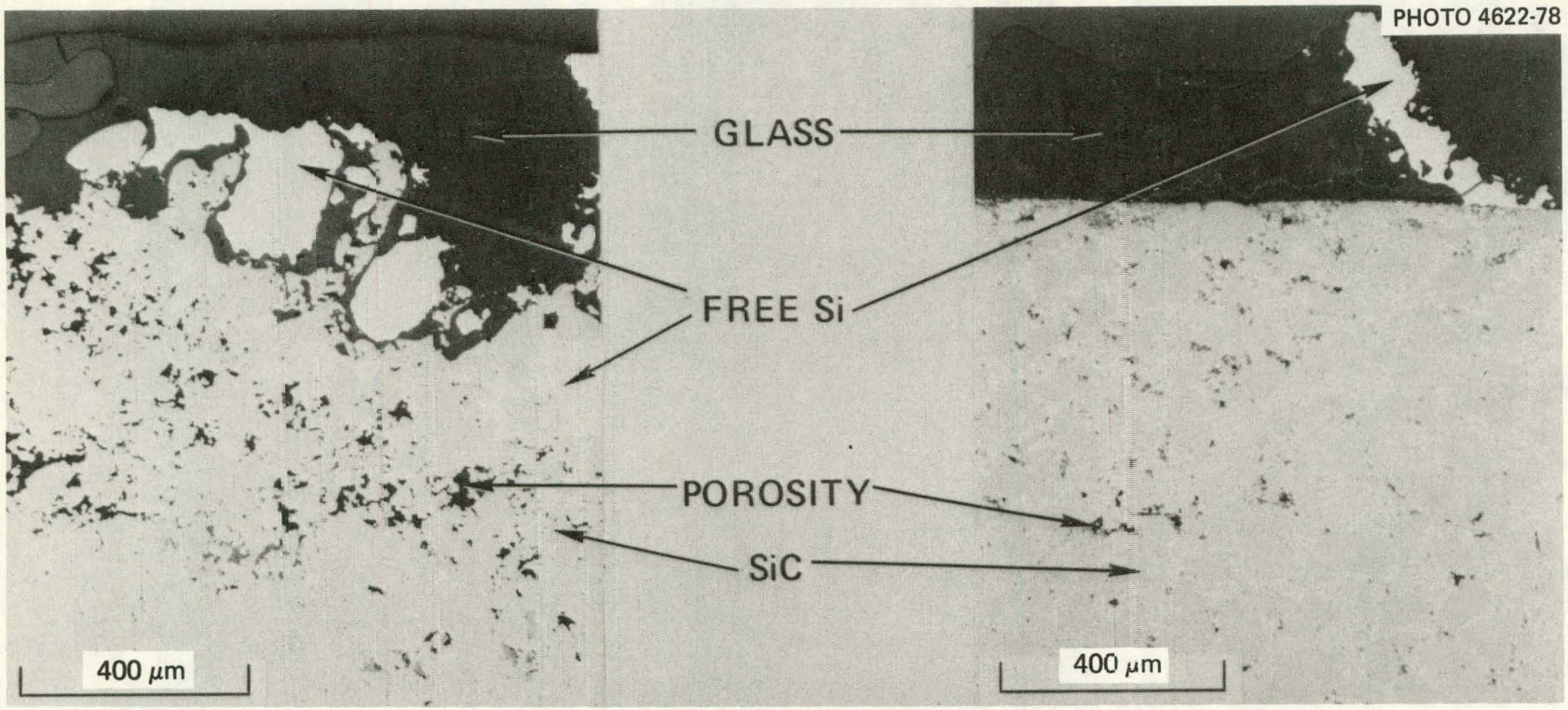

Fig. 10. Comparison of Microstructure of Two Types of Siliconized Silicon Carbide Exposed to Furnace Flue Atmosphere with Glass in the Furnace. Left: specimen KT-2 exposed 47 d at 1350°C (2450°F) and 48 d at 1425°C (2600°F). Right: specimen NC-430-2 exposed 104 d at 1450°C (2650°F).

X-ray diffraction analysis of the siliconized silicon carbide tested with glass in the furnace is given in the Appendix Tables A3 through A6. The white "foam" scale approximately 25 mm from the exposed end on NC-430-2, which was exposed at 1450°C (2650°F) for 104 d, corresponds reasonably well to α-cristobalite. Bluish-white deposits 15 mm from the exposed end of specimen KT-4 exposed at 1550°C (2800°F) for 69 d apparently contained both α-cristobalite and tridymite. The grayish surface material 30 mm from the end of KT-3 exposed at 1225°C (2250°F) for 69 d shows α-cristobalite and $Na_4Ca(SiO_3)_3$ (Table A5). The x-ray diffraction pattern also indicated the presence of some tridymite. Two diffraction patterns of KT-2 (1350°C, 47 d; 1425°C, 48 d) were obtained. Material 40 mm from the end contained α-cristobalite, 21R SiC, and $Na_4Ca(SiO_3)_3$. A whitish deposit 30 mm from the exposed end exhibited similar diffraction peaks and may have contained all three of these phases, but the correspondence of the *d*-spacings with ASTM reference values was not particularly strong except for $Na_4Ca(SiO_3)_3$. The difficulty of interpreting complex silicate x-ray diffraction patterns was well demonstrated in the case of these specimens. The solubility of foreign atoms in the structure, the complex polymorphism of silica, and the great number of possible silicate phases make an unambiguous interpretation of the phase composition of these samples very difficult.

Scanning electron microscopy was also used to investigate the region 5 mm from the exposed end of sample NC-430-2. This region resembled a solid white foam, as shown in Fig. 11. Figure 11(a) shows the blistering of the surface and the open holes through the coating to the underlying material, presumably SiC. Figure 11(b) at higher magnification (1000×) shows the glassy appearance of the coating and (c) the energy-dispersive x-ray analysis of this region. The high concentrations of Si, Na, Ca, and K are expected from the glass composition used in the furnace. The white cellular deposit was apparently the result of a significant amount of glass batch carryover during the test. This sample was very close to the flue entry in a region with possible flow stagnation (port 2), as shown in Fig. 3 (p. 7).

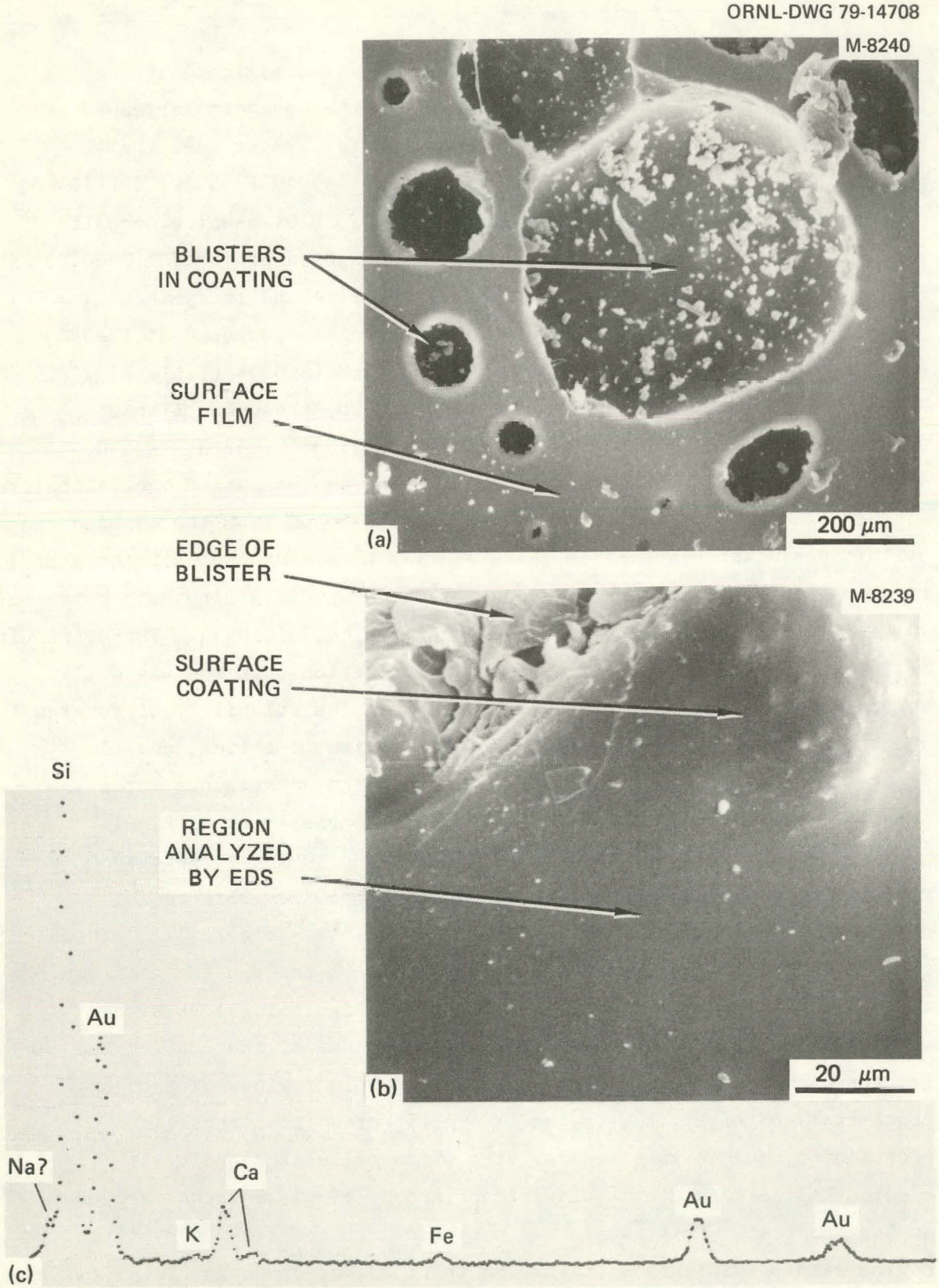

Fig. 11. Scanning Electron Micrographs and Microcomposition of the Glassy Surface on Siliconized Silicon Carbide (NC-430-2) Exposed to Glass Furnace Exhaust at 1450°C for 104 d. (a) Holes in glassy layer. (b) High magnification. (c) Microcomposition by energy-dispersive x-ray spectroscopy (EDS). Gold peaks are from conductive coating, not part of specimen.

Recrystallized or "Self-Bonded" SiC

Material in this category is fabricated from fine-grained silicon carbide by sintering without additions of sintering aids or secondary phases. The material is characteristically porous, having significantly poorer mechanical properties and lower thermal conductivity than the "siliconized" silicon carbide previously discussed. Two samples of this recrystallized silicon carbide (NC-400) are shown in Figs. 6 and 7 (pp. 16 and 17). The samples were exposed at 1400°C (2550°F) for 116 d with (NC-400-2) and without (NC-400-1) glass at port 8 in the test furnace. Sample NC-400-1 exhibited some glazing on its surface and a foamlike deposit of yellowish material distributed on the exposed surface. This silicon carbide sample exhibited little dimensional change during the high-temperature test with no glass in the test furnace. Sample NC-400-2 showed glazing, foam, and some dimensional reduction in the low-temperature region adjacent to the flue wall. The dimensional behavior was analogous to that observed for the siliconized NC-430 material at a 50°C (100°F) higher temperature.

Representative microstructures are shown in Fig. 12 (NC-400-1 and NC-400-2). The microstructures are somewhat similar. An amorphous surface coating penetrated easily into the extensive large open porosity present in this silicon carbide. The material exposed to glass in the furnace [Fig. 12(b)] shows more evidence of significant dissolution and possible reprecipitation at the interface between the silicon carbide and the surface coating. Relicts of a second phase in the amorphous surface coating are visible in both samples.

X-ray diffraction analysis of the yellowish "foamed" deposits 30 to 40 mm from the end of sample NC-400-1 is shown in Table A7 of the Appendix along with two different JCPDS patterns for α-cristobalite. The correspondence to α-cristobalite is fairly good, particularly with respect to JCPDS standard pattern 4-0379.

A similar powder diffraction analysis of the foamed deposit 5 mm from the end of sample NC-400-2 in Table A8 correlates well with JCPDS α-cristobalite pattern 11-695.

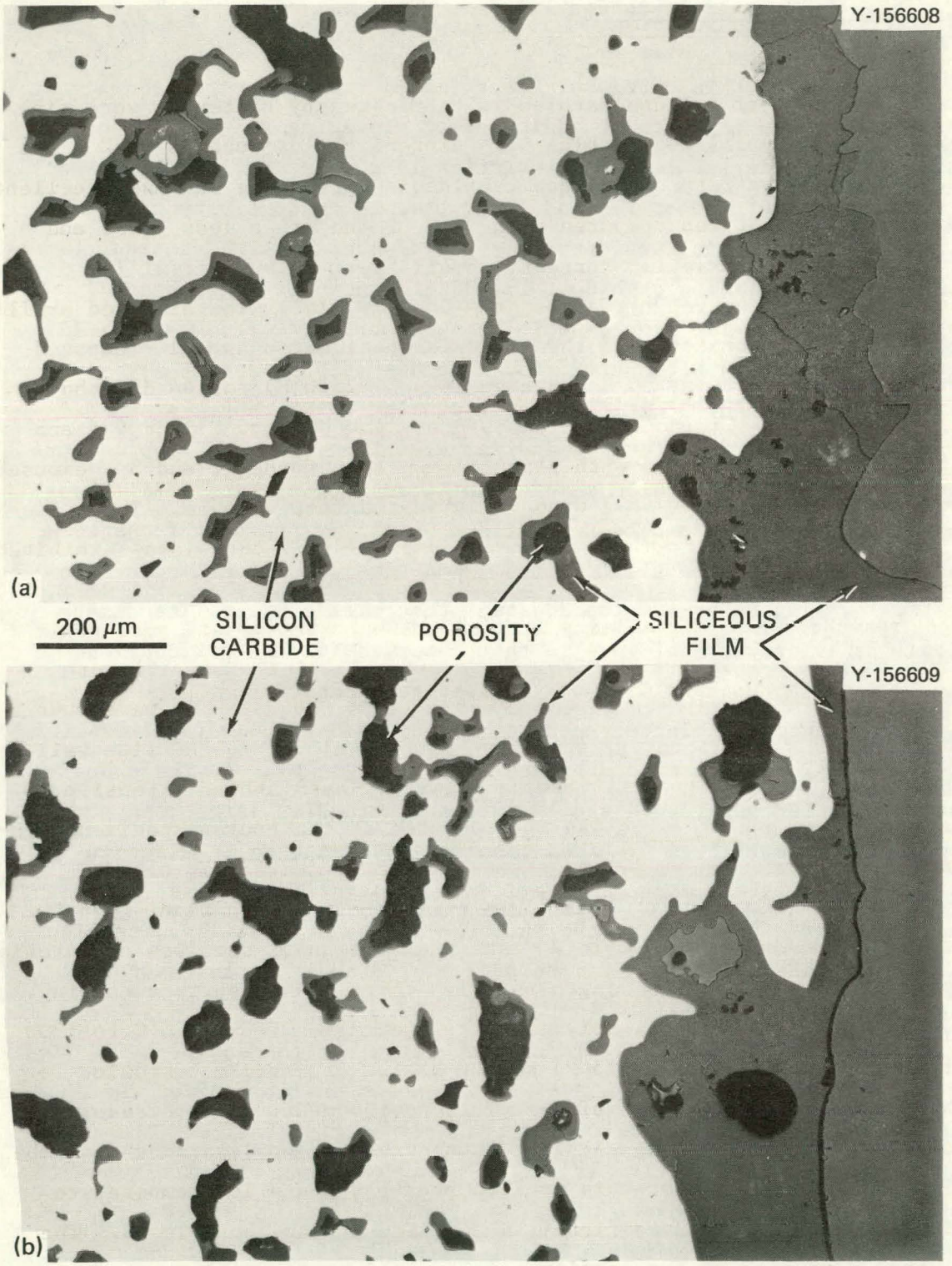

Fig. 12. Microstructure of Recrystallized Silicon Carbide Exposed at 1400°C (2550°F) for 116 d. (a) NC-400-1 exposed without glass in the furnace. (b) NC-400-2 exposed with glass in the furnace.

Sintered α-Silicon Carbide

This form of silicon carbide is fabricated by sintering very fine grained (<1 μm) silicon carbide with sintering aids such as 0.5% B and 0.3% C. This variety of silicon carbide is very dense and has excellent mechanical properties compared with some of the other less dense and coarser grained varieties currently available. This material is currently manufactured by Carborundum Company, Inc. The sintered α-silicon carbide tested consisted of three samples designated as: 1 — exposed at 1450°C (2650°F) for 36 d and then 1425°C (2600°F) for 44 d without glass in the test furnace, 2 — exposed at 1450°C (2650°F) for 4 d and 1550°C (2800°F) for 17 d with glass in the test furnace, and 3 — exposed at 1225°C (2250°F) for 18 d with glass in the test furnace. These specimens are shown in Figs. 13 and 14. Sample 1 (without glass) exhibited a milky coating with "circular" deposits very similar to those seen on specimen NC-400-1, which had a similar thermal history and port position. The edges of the flat concave section exhibited significant rounding and material loss. The material loss and deposits were most marked at a location on the specimen that was closer to the flue wall and thus presumably cooler. Sample 2 (with glass) showed extensive material loss, which again was concentrated at the cooler specimen location adjacent to the wall. An extensive glassy coating is also apparent. Sample 3 (with glass), which was tested at a significantly lower temperature than sample 2, exhibited a significant loss of material over most of the exposed length and also had a glassy surface coating.

These two samples clearly identify the region from 1225°C to 1300 or 1400°C (2250–2400 or 2575°F) as the region of maximum corrosion for this variety of silicon carbide in this environment. The decreasing corrosion rate seen along sample 3 toward the cooler locations near the flue wall indicates that this process probably has a low temperature limit, which was not specifically identified during these tests. The minimal corrosion of the portions of sample 2 at the higher test temperatures and an almost linear increase in corrosion rate as the temperature decreased into the wall give indication of the kinetic profile

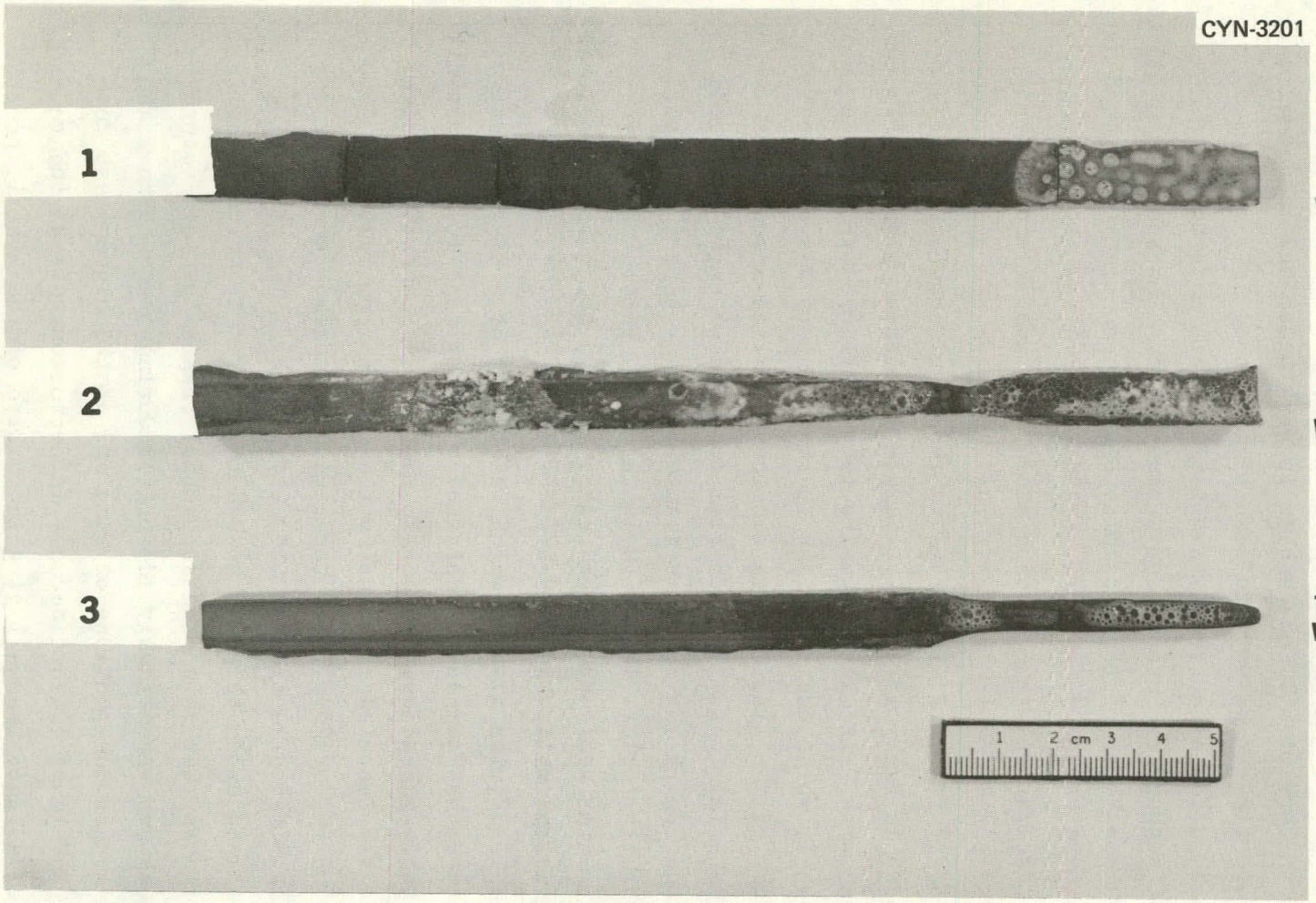

Fig. 13. Sintered α-Silicon Carbide Subjected to Glass Furnace Exposure Testing.

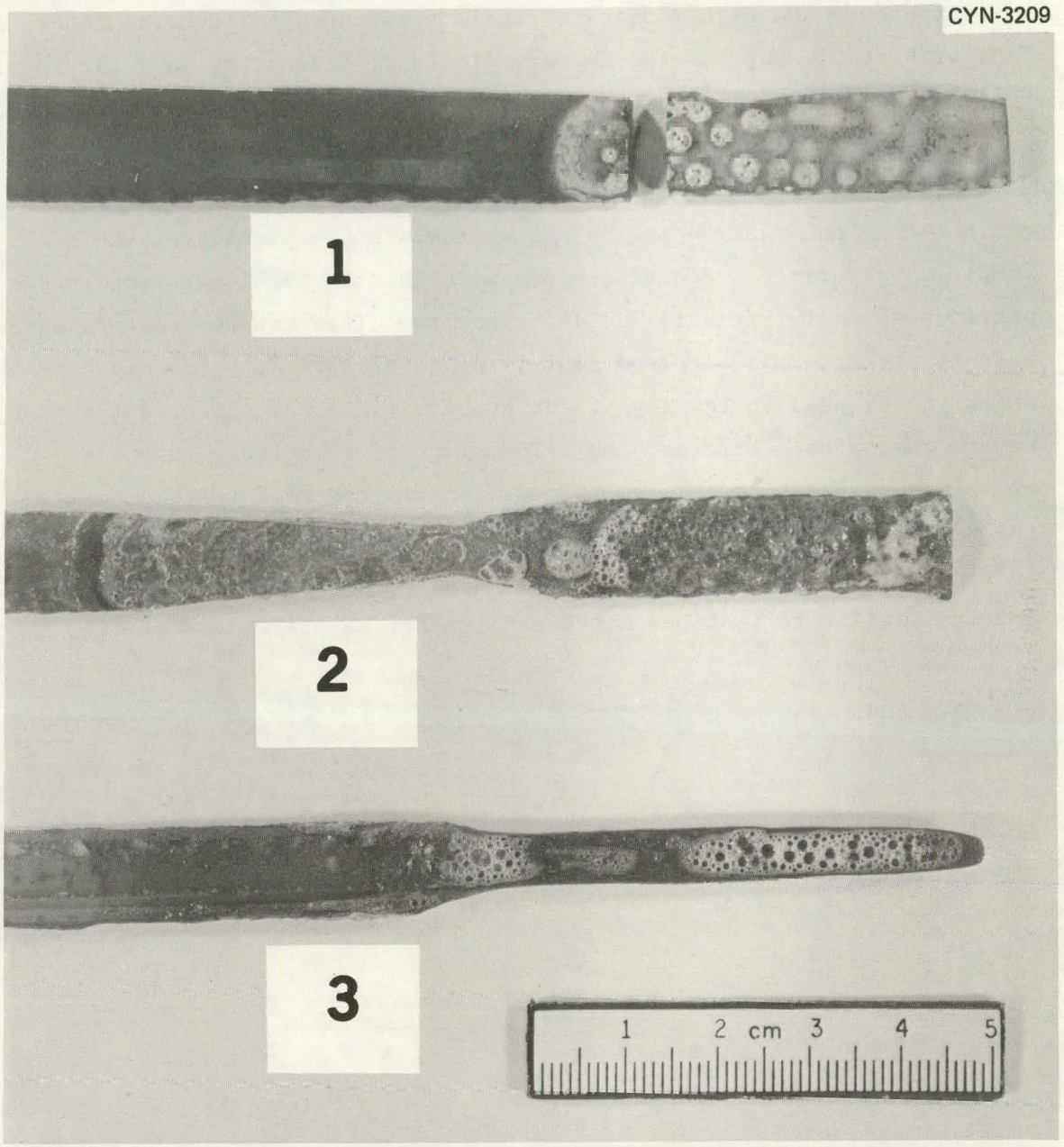

Fig. 14. Close-Up of Sintered α-Silicon Carbide Subjected to Glass Furnace Exposure Testing.

of the operative corrosive reaction. Isothermal corrosion tests would be required to obtain data for predicting the temperature ranges in which the corrosion rates for this silicon carbide are sufficiently low to satisfy the required design life criteria for the material.

The micrograph, Fig. 15, of sample 1 shows the very fine grained microstructure and high density typical of sintered α-SiC. The interface with the glassy coating is very distinct, indicating that little penetration or attack occurs at these temperatures (1425—1450°C) without glass in the furnace.

Figure 16 of sample 2 indicates that the sintered alpha material was attacked and removed in the higher temperature portion of the sample. This removal occurred along with that in the lower temperature portions shown in Figs. 13 and 14. That two different removal processes were at work is apparent from Fig. 17 of sample 3. This test specimen, which was exposed to the lowest temperature (1225°C), suffered the most severe corrosion. However, the SiC surface is relatively smooth and contained only a very thin amorphous film, in contrast to the much thicker amorphous coating and roughened SiC surface seen on sample 2 in Fig. 16. This mass removal behavior as a function of temperature is very similar to that described earlier for KT silicon carbide.

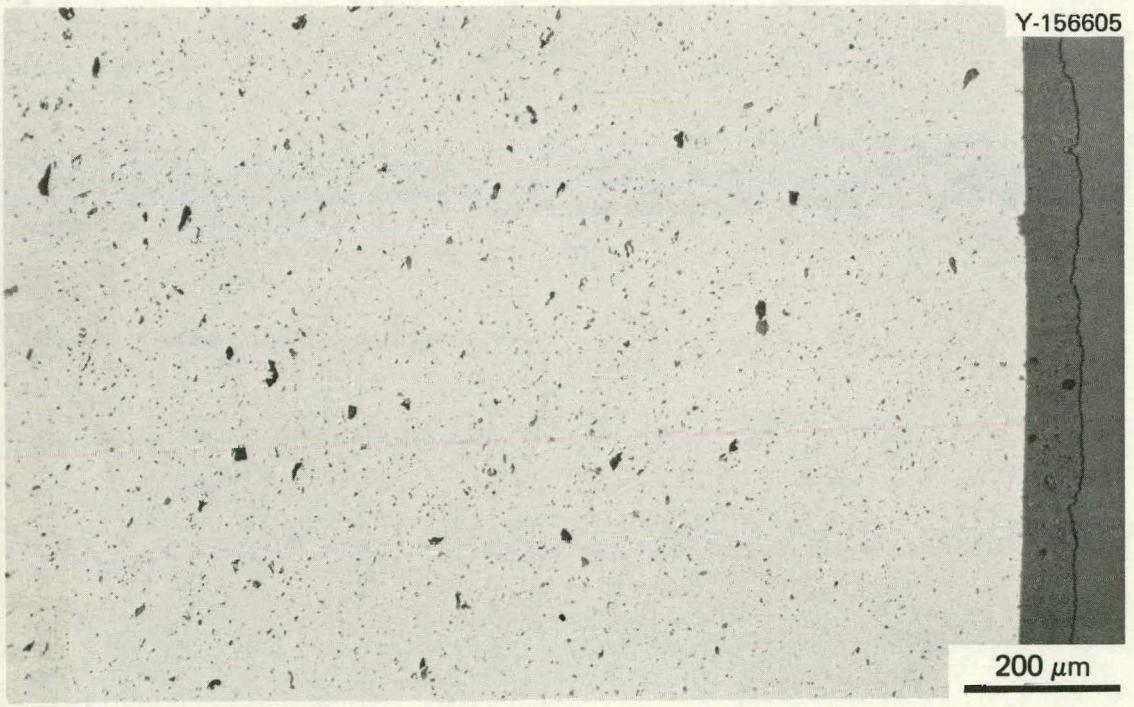

Fig. 15. Microstructure of Sintered α-Silicon Carbide (Sample 1) Exposed at 1425°C (2600°F) for 36 d and 1450°C (2650°F) for 44 d with No Glass in the Furnace.

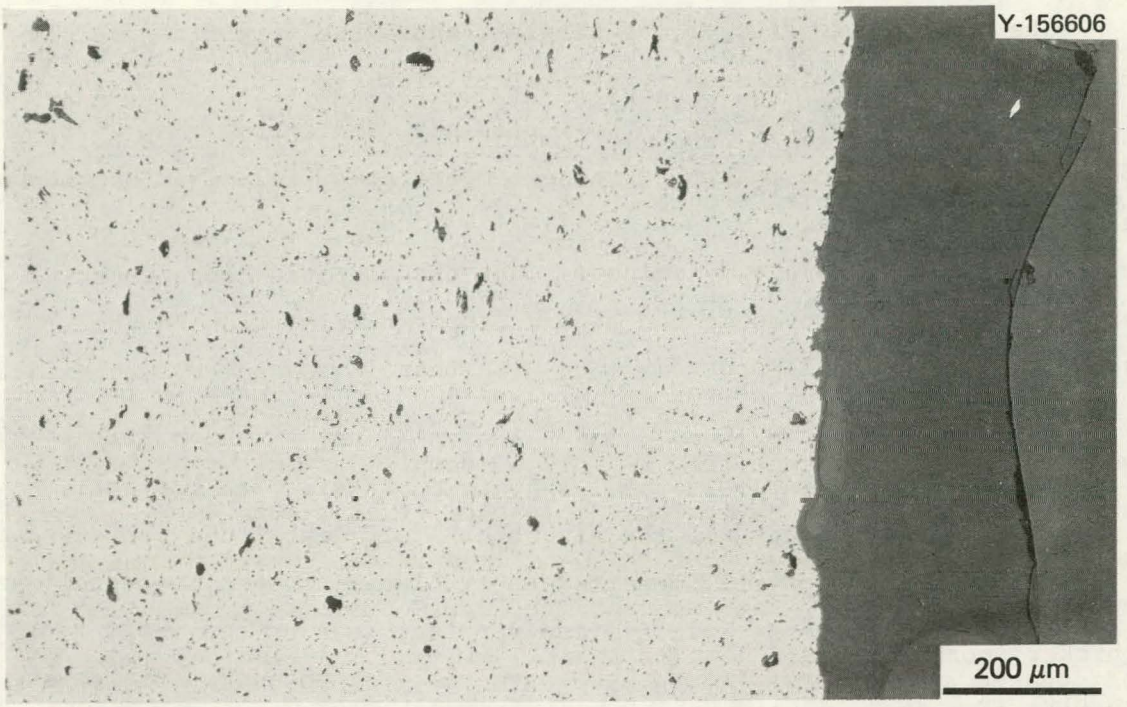

Fig. 16. Microstructure of Sintered α-Silicon Carbide (Sample 2) Exposed at 1450°C (2650°F) for 4 d and 1550°C (2800°F) for 17 d with Glass in the Furnace.

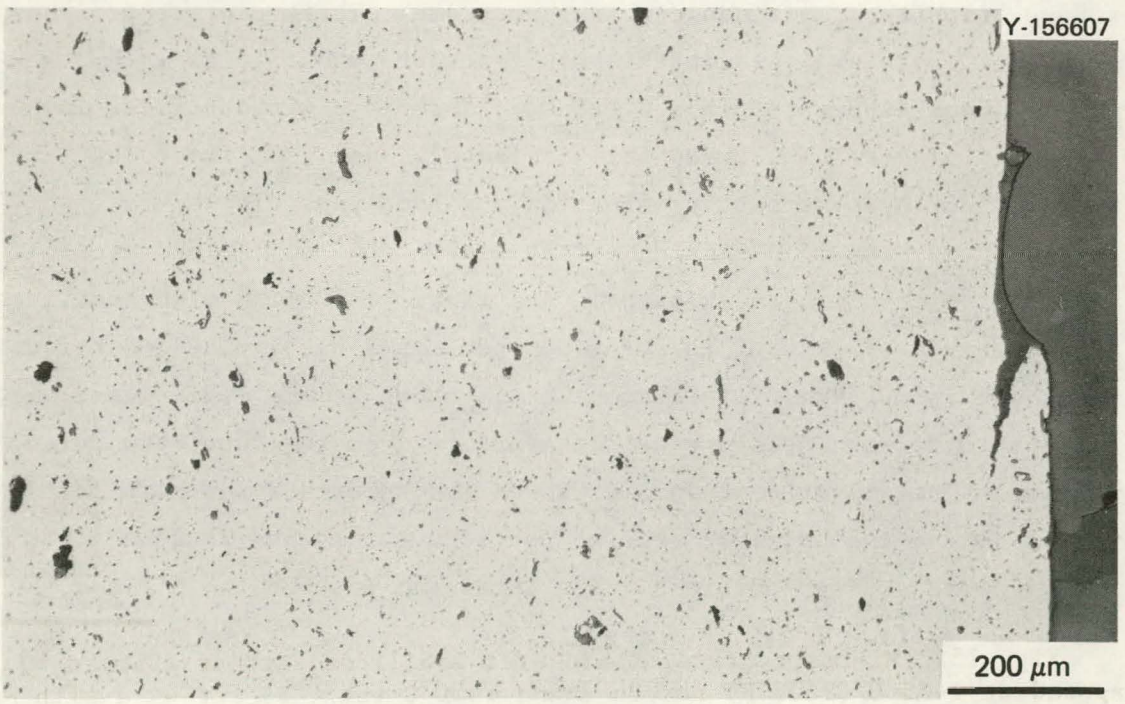

Fig. 17. Microstructure of Sintered α-Silicon Carbide (Sample 3) Exposed at 1225°C (2250°F) for 18 d with Glass in the Furnace.

The x-ray diffraction results for samples 1 and 2 are shown in Tables A9 and A10 of the Appendix. Alpha cristobalite was the only identifiable extraneous crystalline phase observed in the surface coatings of both samples.

Chemically Vapor Deposited Silicon Carbide

Chemically vapor deposited (CVD) silicon carbide can be produced so as to be theoretically dense, impervious to gases, and with high mechanical strength in relatively small shapes. However, with currently demonstrated technology, if the size of the SiC deposit is increased to dimensions of tens of millimeters, the available properties degrade and approach those of dense bulk silicon carbide, such as the α-SiC discussed previously. Presently, a generally accepted materials development goal regarding CVD SiC includes production of an equiaxed microstructure in large pieces by carefully controlling the process parameters such as temperature, gases used, or gas phase nucleating agents. Most current approaches deposit the CVD SiC onto a moderately porous graphite or silicon carbide substrate. Three different pieces of CVD SiC were examined in this study and are shown in Fig. 18. Sample 1 was exposed at 1550°C (2800°F) for 116 d without glass in the test furnace. This material was fragile, and many fractures occurred during post-test examination and handling. The surface of this specimen showed a glazing effect with some "foam" type deposit over most of the length exposed in the flue. There was also some loss in diameter over part of the exposed specimen length. The impervious dense microstructure of this specimen is shown in Fig. 19. There also appears to be some evidence of delamination from the substrate during testing. This is evident in Fig. 18 as the substrate was tightly bonded in the cooler, less exposed portions but became detached from the hotter, more exposed portions. The interface between the SiC and the amorphous surface layer is quite distinct in Fig. 19, but the heavy concentration of a second phase immediately adjacent to the interface indicates that under the test conditions a mechanism involving dissolution

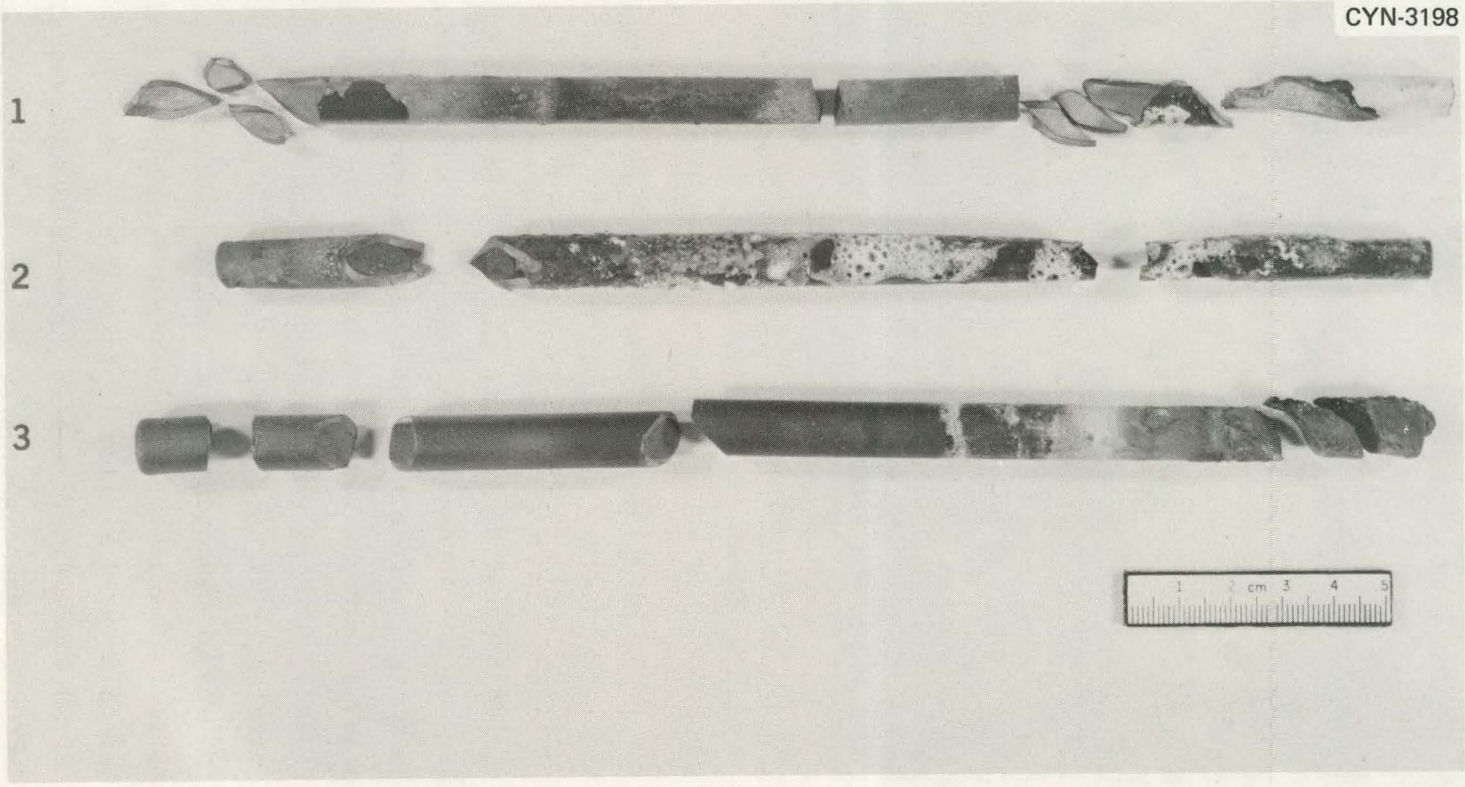

Fig. 18. Chemically Vapor Deposited Silicon Carbide Exposed to Glass Furnace Testing.

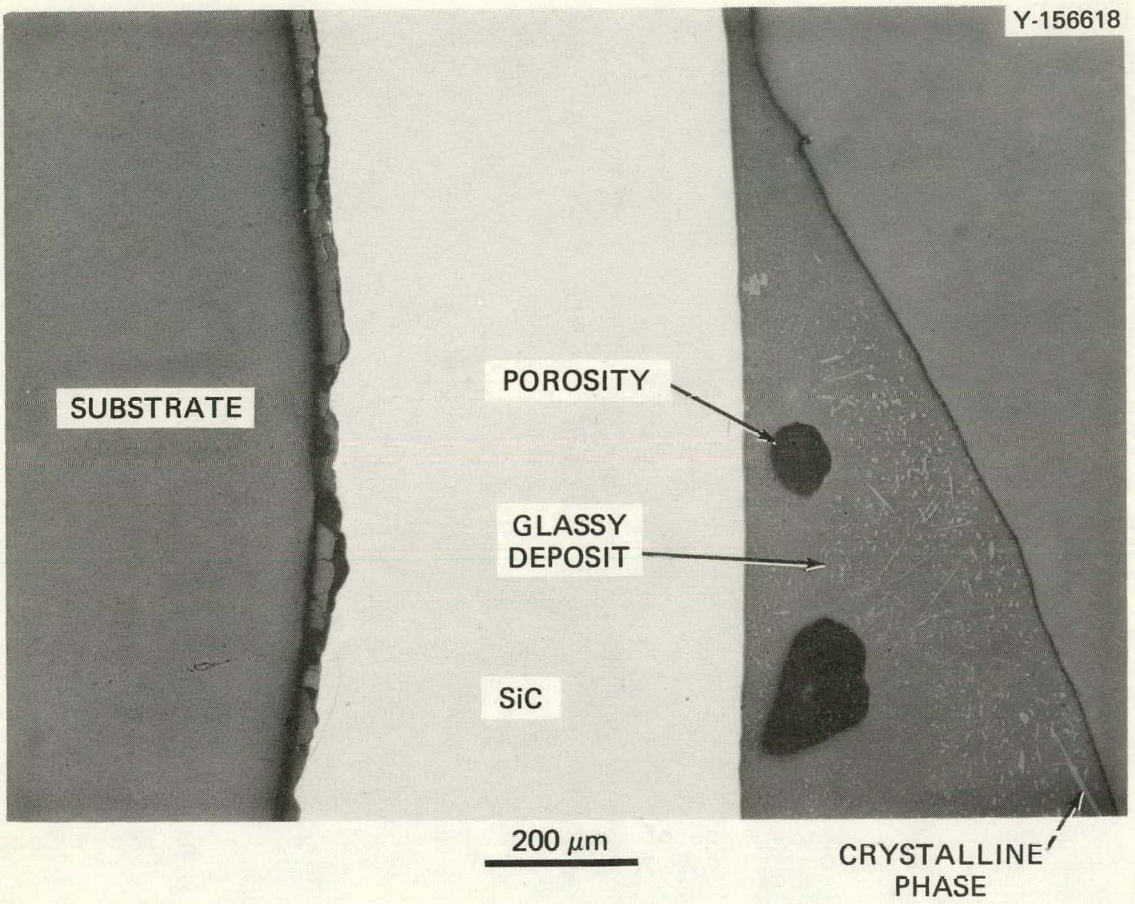

Fig. 19. Microstructure of CVD Silicon Carbide Exposed at 1550°C (2800°F) for 116 d with No Glass in the Furnace.

of the SiC may have been operating. The well-developed crystals visible in the surface layer are probably cristobalite, which crystallized from the melt during cooling.

Sample 2 was also exposed to flue gas at 1550°C (2800°F) for 70 d, but with glass in the furnace. After 48 d the specimen showed some decrease in diameter. After 70 d the sample was corroded into two parts at a location near the supporting wall, where the specimen temperature was lowest. Glazing was apparent over the entire surface. Even with this severe material loss during the test, the microstructure in Fig. 20 shows a very distinct interface with the surface coating. The large material loss of this CVD SiC during the test when glass was present in the furnace is very similar to that already described for samples of siliconized and α-SiC tested at lower temperatures. There is no obvious explanation for the higher mass losses observed with the CVD

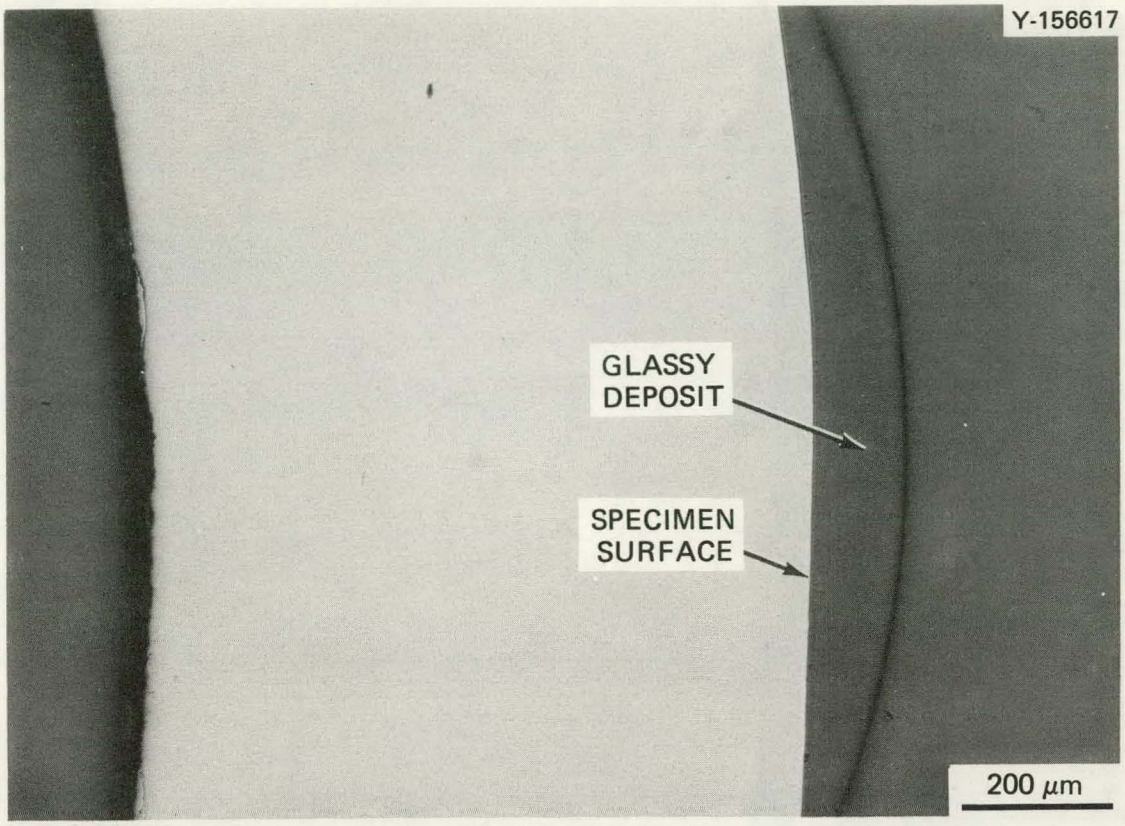

Fig. 20. Microstructure of Chemically Vapor Deposited Silicon Carbide Exposed at 1550°C (2800°F) for 70 d with Glass in the Furnace.

SiC at temperatures higher than those seen for the other types of SiC in these tests. This behavior is seen in sample 3, which at low temperatures [1225°C (2250°F)] for 92 d without glass underwent little mass loss or dimensional change. This is a contrast to the behavior of sintered α-SiC with glass in the furnace at a similar test temperature. The microstructure seen in Fig. 21 shows several phases present in the surface coating and well-developed crystals located in the coating, particularly near the SiC-coating interface. The interface is fairly distinct with some possible sites of exaggerated attack visible in the ceramographic sections.

The x-ray diffraction data for samples taken from these specimens are given in Tables A11, A12, and A13 of the Appendix. The major crystalline phase in the coating on all three samples was α-cristobalite. There was also evidence of some $Ca_3Al_2Si_3O_{12}$ on sample 3 and a phase containing iron, silicon, and carbon on sample 1, although the x-ray diffraction line correlations for either of these two latter phases were not unambiguous.

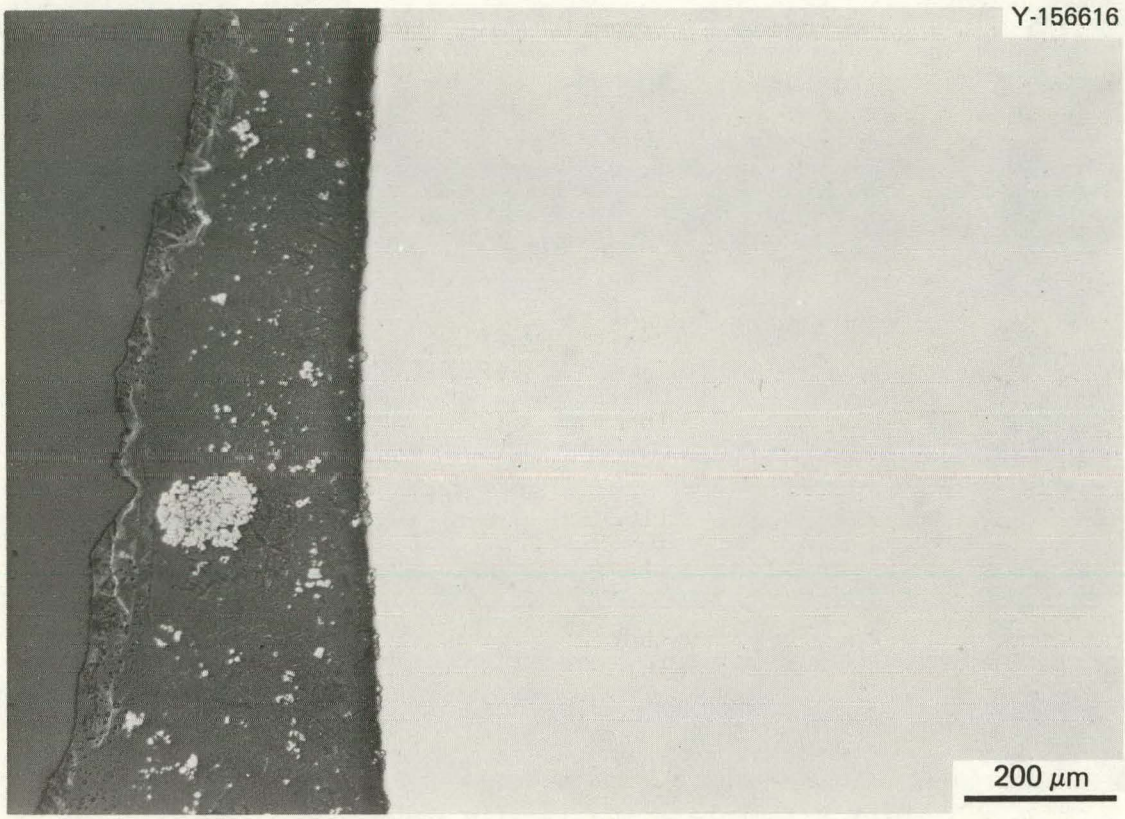

Fig. 21. Microstructure of Chemically Vapor Deposited Silicon Carbide Exposed at 1225°C (2250°F) for 92 d with Glass in the Furnace.

Approximate silicon carbide loss rates are shown in Table 5. These loss rates were calculated from measurements taken on the exposed material of the maximum "clean" diameter and the minimum diameter observed near the midplane of the exposed section, except in the case of the second sintered α-2 measurement, which was made at a location adjacent to the wall for comparison. These measurements are subject to considerable error because of the thickness of deposits on the surfaces developed during exposure and should be regarded only as a first approximation of material degradation. Even with the uncertainties involved, the radial loss rate measurements are surprisingly consistent. The exposed end of sintered alpha sample 3 and the section of sintered alpha sample 2 adjacent to the furnace wall were, as described earlier, believed to be at similar temperatures. The similarity in corrosion rates for 400 to 500 h exposure is encouraging in showing internal consistency in the results. Ceramographic examination of specimens exposed at higher temperatures showed evidence of a different material loss mechanism compared with

Table 5. Diametral Changes of SiC Specimens

Sample	Midplane Temperature (°C)	Exposure (h)	Post-Test Diameter, mm		Half of Loss in Diameter (mm)	Radial Loss (μm/h)
			max	min		
Sintered α-3	1225	430	11.4	6.0	2.69	6.3
Sintered α-2	1450	96				
	1550	408	12.7	11.6	0.5	1.1
	a	504	12.7	6.4	3.2	6.3
CVD-2	1550	1680	10.7	8.3	1.2	0.7
NC-430-2	1450	2500	17.2	10.5	3.2	1.3
KT-2	1350	1100				
	1450	1150	12.7	11.2	0.8	0.3

[a]Measured not at midplane but at minimum diameter, adjacent to wall, where the temperature was probably about 1250°C.

silicon carbide tested at lower temperatures. This difference in mechanism is reflected in one-sixth the loss rates at 1450 to 1550°C compared with those observed at 1250°C for similar silicon carbide materials. This observation was consistent for the sintered alpha, NC-430, and CVD silicon carbide for times varying by a factor of 5. The CVD silicon carbide had a slightly lower than average loss rate, which may have been due to a slower parabolic law time dependence, possibly because it was a purer denser material. The KT silicon carbide exhibited an anomalously low loss rate. This excellent performance at similar times and temperatures (a surface recession rate about one-fourth the rate observed for NC-430) may be because the KT specimens were solid cylinders rather than the relatively "flat" specimens of the NC and sintered alpha silicon carbide. A better understanding of the loss mechanism of all these silicon carbides under the test conditions used, determined with identical sample geometries, should be the objective of future work to establish if the KT material actually has superior corrosion resistance.

Alumina

We tested four different types of commercial alumina ceramic specimens, which had different densities and silica contents and had been made with selected fabrication techniques. Although alumina has a lower thermal conductivity and poorer thermal shock resistance than silicon carbide, its chemical stability in this environment makes it an attractive candidate for use in glass furnace recuperators. The ceramics tested represent a set of increasing purity including 85 wt % Al_2O_3 (AD-85), 94 wt % Al_2O_3 (AD-94), 99.8 wt % Al_2O_3 (AD-998), and high-purity Vistal* alumina (>99.8 wt % Al_2O_3).

The AD-94 and -998 alumina samples are shown in Figs. 22 and 23. Tables 3 and 4, (pp. 9–10) identify the three samples of AD-85 that were tested. Specimen AD-85-1 was exposed at 1400°C (2550°F) without glass in the furnace and experienced such severe slumping that it was withdrawn after 7 d. Sample AD-85-2 was exposed also at 1400°C (2550°F), with glass in the furnace; it slumped so severely that it was withdrawn after 5 d. A third sample, AD-85-3, was tested at lower temperatures 1150°C (2250°F) and after 90 d showed evidence of considerable interaction with materials in the flue gas on its lower exposed side. Alumina ceramics of this purity are apparently not satisfactory above 1150°C (2250°F) in the environment used in this test and are of questionable value even below that temperature in this environment.

Ceramic AD-94 has higher purity than AD-85. Sample AD-94-1 was tested at 1450°C (2650°F) for 8 d without glass. Slumping was observed, and the sample was then moved to a location at 1400°C (2550°F) and maintained there for 109 d. A brown staining is apparent on this sample, but there was little dimensional deterioration. Sample AD-94-2 had an identical thermal history to sample 1 but was exposed with glass in the furnace. A significant buildup of a dark coating was observed on this sample along with some slight dimensional loss adjacent to the flue wall, and slumping was noticeable.

---

*Coors, Inc., Golden, Colorado.

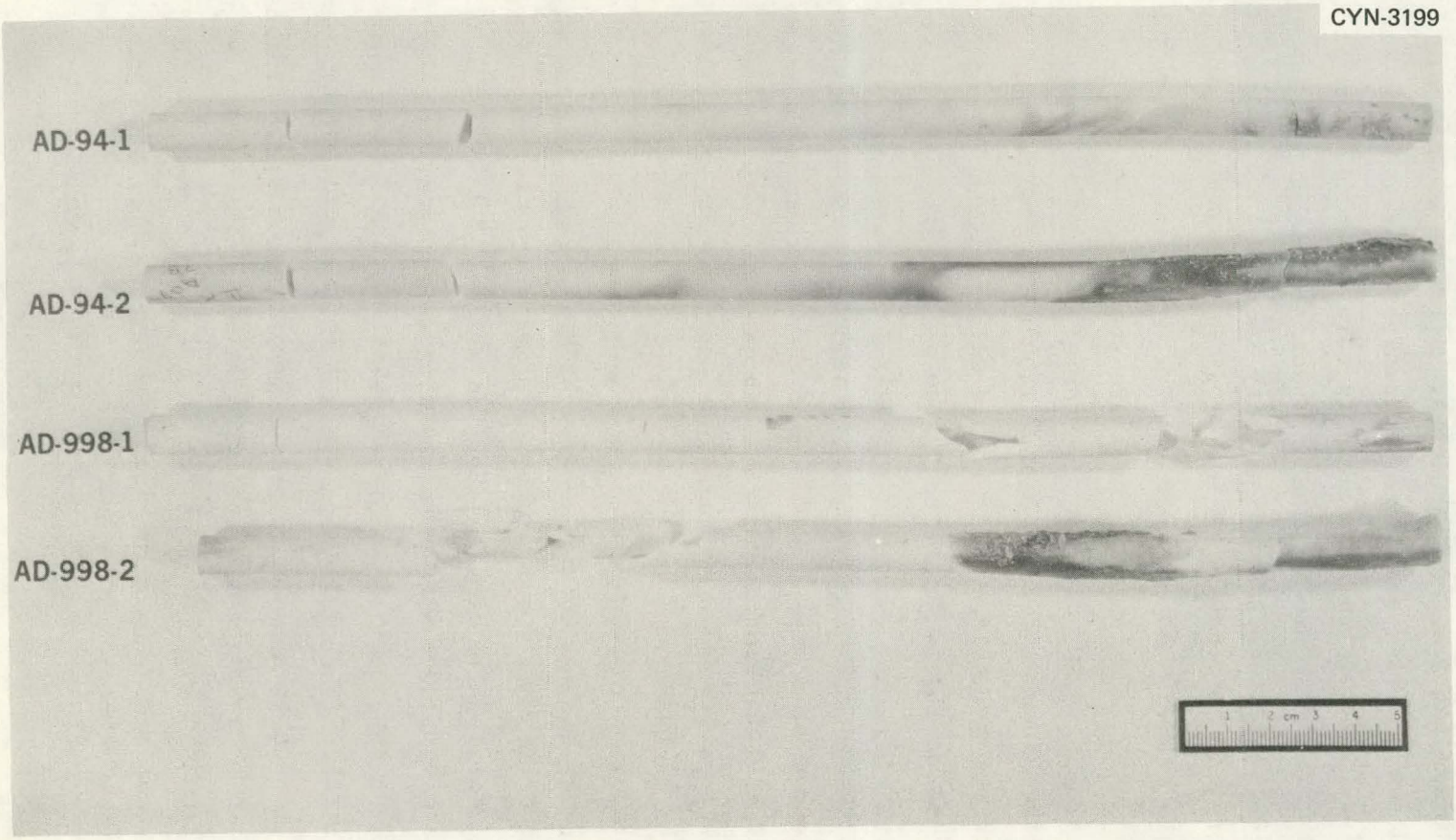

Fig. 22. High-Purity Alumina Ceramic Specimens Exposed to Glass-Furnace Off-Gas Atmosphere.

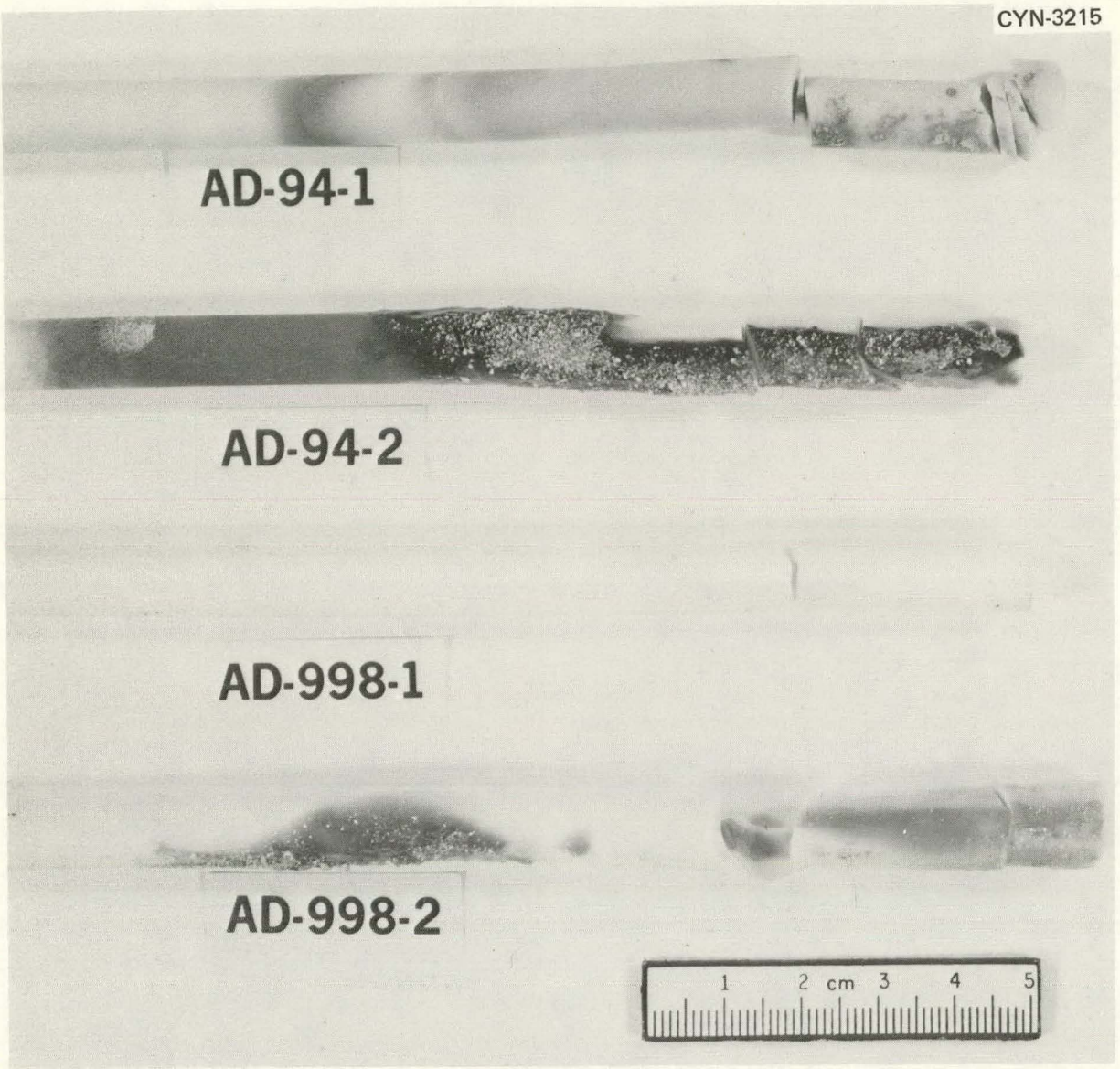

Fig. 23. Close-Up of High-Purity Alumina Ceramic Specimens Exposed to Glass Furnace Off-Gas Atmosphere.

The microstructures of these two samples are shown in Fig. 24. The sample tested without glass (AD-94-1) retained the characteristic microstructure of a high-alumina ceramic, consisting of small alumina grains surrounded by a siliceous bonding phase and small scattered porosity. A significant change was apparent in the sample tested with glass in the furnace. An amorphous phase from the surface, probably an alkali

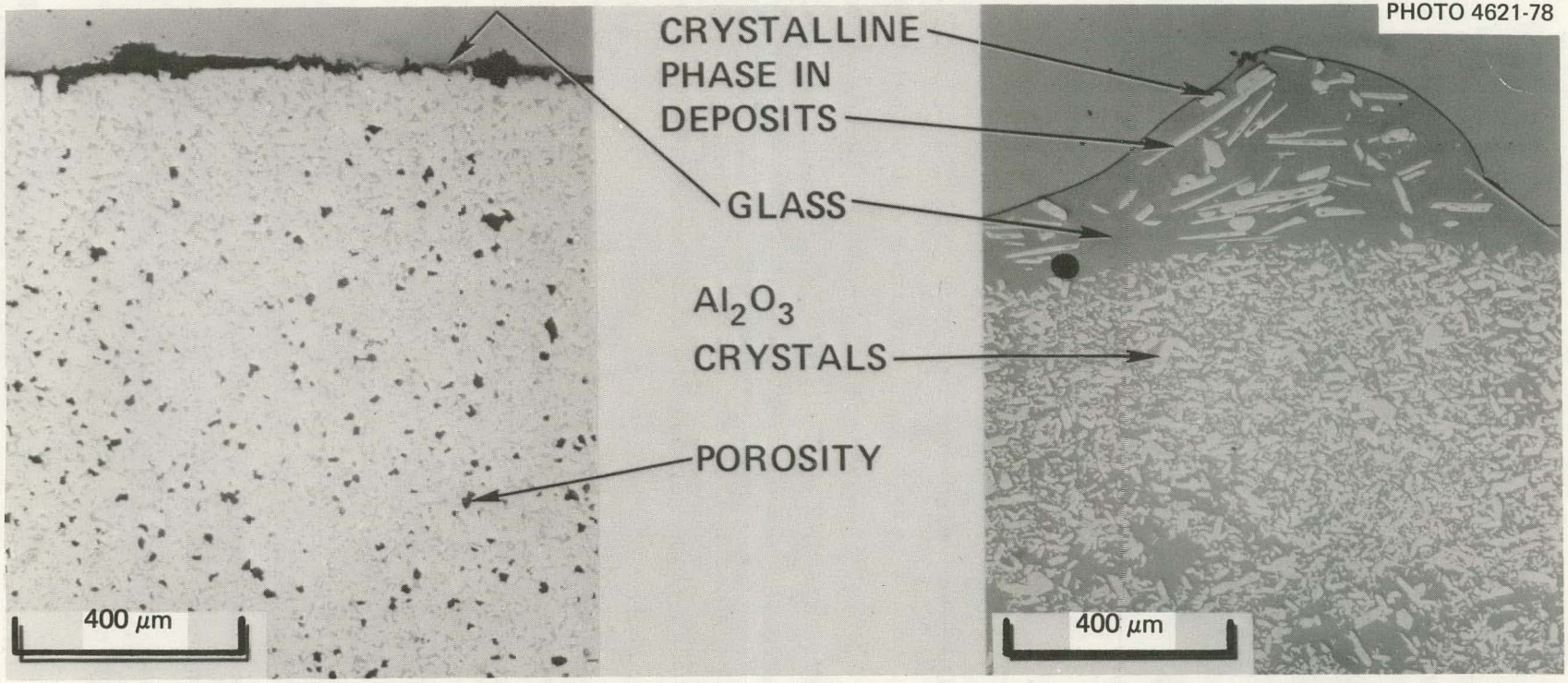

Fig. 24. Microstructure of Alumina Porcelain AD-94 Exposed at 1450°C (2650°F) for 8 d and 1400°C (2550°F) for 109 d. Left: without glass in the furnace. Right: with glass.

silicate melt, completely penetrated the ceramic, separated the individual grains, and filled the available porosity. The lack of a discrete interface between the original specimen and the surface deposit illustrates the extensive penetration of the melt into the alumina ceramic microstructure. As the crystals observed in the surface deposit have a morphology unlike that found in the bulk ceramic, they apparently developed upon cooling and are not discrete corundum crystals removed from the matrix. The AD-94-2 specimen would be expected to have very poor high-temperature mechanical properties as a result of the presence of this extensive and continous amorphous material. This ceramic would, therefore, be an unlikely candidate for structural use in recuperators for this application.

X-ray diffraction analyses of a pink region and a white deposit 10 mm from the end of AD-94-1 specimen indicated that the principal phase present in the surface sample was α-alumina, with a possibility of a phase resembling $BaMg_2Al_3(Si_9Al_3O_{30})$ being present. The elemental composition (wt %) as identified by x-ray fluorescence was Al, 18.53; Si, 2.53; P, 0.16; Ca, 0.18; Ti, 0.27; Fe, 40.91; and O, 37.41. The very high concentration of iron in the deposit could cause the observed discoloration and a concomitant degradation of refractoriness and mechanical properties. The source of the iron contamination from the test configuration is unclear.

The glassy deposit on sample AD-94-2 10 mm from the exposed end contained only α-alumina as a crystalline phase. Chemical analysis of the deposit (wt %) revealed Al 33.32; Si, 10.39; Ca, 0.34; Ti, 0.62; Fe, 1.92; Na, 7.43; K, 0.43; and O, 45.54. This deposit is apparently a soda-lime silicate glass with α-alumina crystals present, as observed in Fig. 24. As both these deposits are much richer in alumina and lower in silica than the original glass batch material, it appears that the primary alumina crystals dissolve in the deposit, and alumina recrystallizes upon cooling. The concentrations of iron and titanium are noteworthy because these potentially deleterious components appear to be concentrating on the test samples.

The high-purity alumina ceramic samples, AD-998-1 and -2, as described in Tables 3 and 4 (pp. 9—10), performed significantly better than the less pure aluminas already discussed. Sample AD-998-1 was exposed at 1450°C (2650°F) for 39 d without glass with no apparent deterioration. Sample AD-998-2 was exposed with glass at the same temperature for 85 d and experienced little dimensional deterioration. Some slumping was apparent in both samples, but it was much less than that observed at the same temperature for the AD-94 material. The test temperature appeared to be excessive for these aluminas for practical applications under the stresses anticipated in recuperator structures.

The post-test microstructure of AD-998-2 is shown in Fig. 25. The microstructure is very similar to that observed for the lower purity alumina ceramic at a lower test temperature 1400°C (2550°F) without glass in the furnace (AD-94-1). The extensive penetration of the Al_2O_3 microstructure by the melt on the surface observed in AD-94-2 (with glass) is not evident in this case. The importance of the purity of alumina ceramics in determining survival in glass tank flue gas environments is apparent from these results. Although the interface is distinct with little evidence of extensive melt penetration into AD-998-2, the porosity near the interface was apparently filled. This filling may indicate the beginning of the corrosion process described earlier for AD-94-2. If subsequent tests confirm this possibility, alumina ceramics of this type may not be viable for use in glass melting applications. The distinctly different "lathlike" crystals in the deposit are much like those identified as α-alumina in sample AD-94-2.

The x-ray diffraction analysis indicated that the brown deposit located 20 mm from the exposed end of sample AD-998-2 consisted primarily of α-alumina. No other crystalline phases were identified. Chemical analysis of this deposit (wt %) revealed Na, 10.62; Mg, 0.11; Al, 22.43; Si, 17.22; K, 0.85; Ca, 0.67; Ti, 1.03; Fe, 1.82; and O, 45.25. This composition is roughly equivalent to that of the deposit on AD-94-2 except that the silica content is higher and the alumina content is lower for 998-2, indicating that this higher purity ceramic is less soluble in the melt deposit. Thus the melt dissolved less alumina from

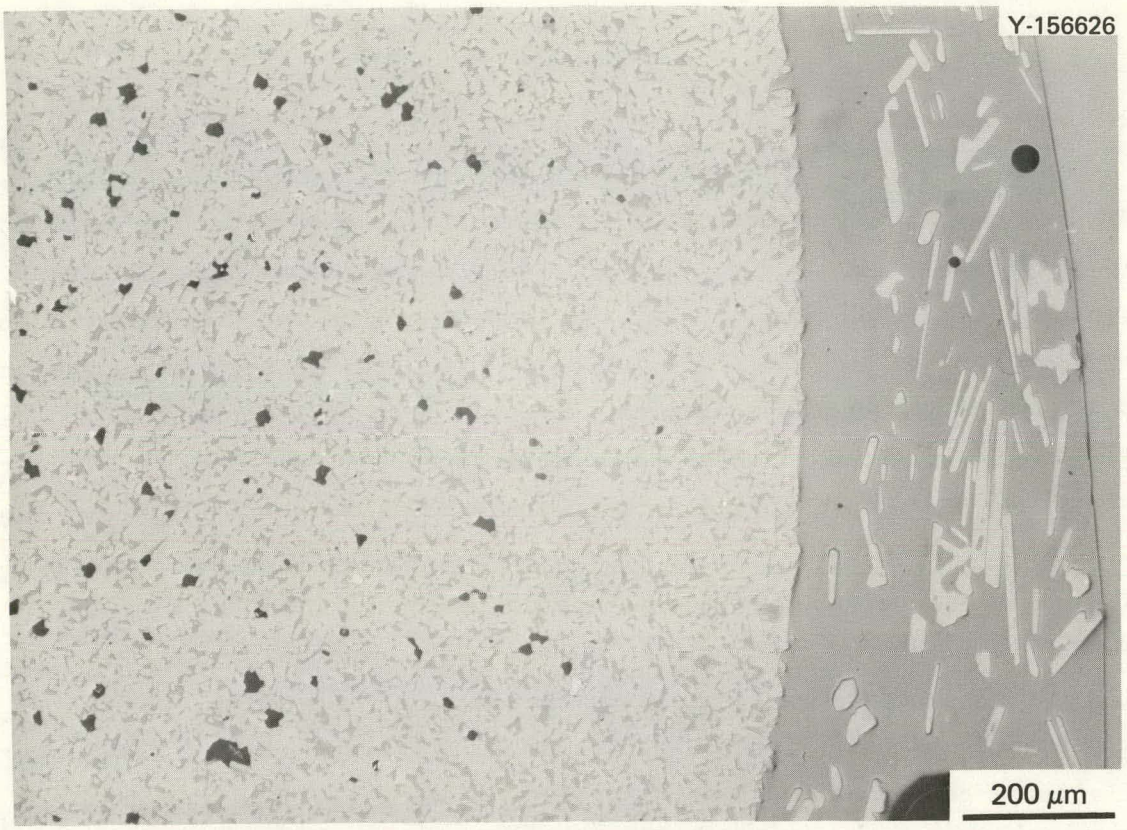

Fig. 25. Microstructure of High-Purity (99.8 wt %) Alumina (AD-998-2) Exposed at 1450°C (2650°F) for 85 d with Glass in the Furnace.

the specimen during the test. The source of magnesium is probably an adjacent sample such as cordierite, as it is unlikely that the manufacturer used magnesia as a sintering aid in AD-998.

Three samples of an alumina ceramic having the highest initial density and purity (Vistal) were tested. Their post-test appearance is shown in Figs. 26 and 27. The Vistal 1 sample, exposed at 1400°C (2550°F) for 7 d and then at 1450°C (2650°F) for 105 d without glass exhibited the best behavior of all the ceramic materials tested under these conditions. Negligible corrosion occurred, and only a loss of the surface finish was observed, in addition to a slight discoloration that was probably attributable to iron. The Vistal 2 sample was exposed at 1400°C (2550°F) for 11 d and 1450°C (2650°F) for 146 d with glass in the furnace. Some slumping was observed along with 5% reduction in diameter near the flue wall. The microstructure of the Vistal 1 sample is shown

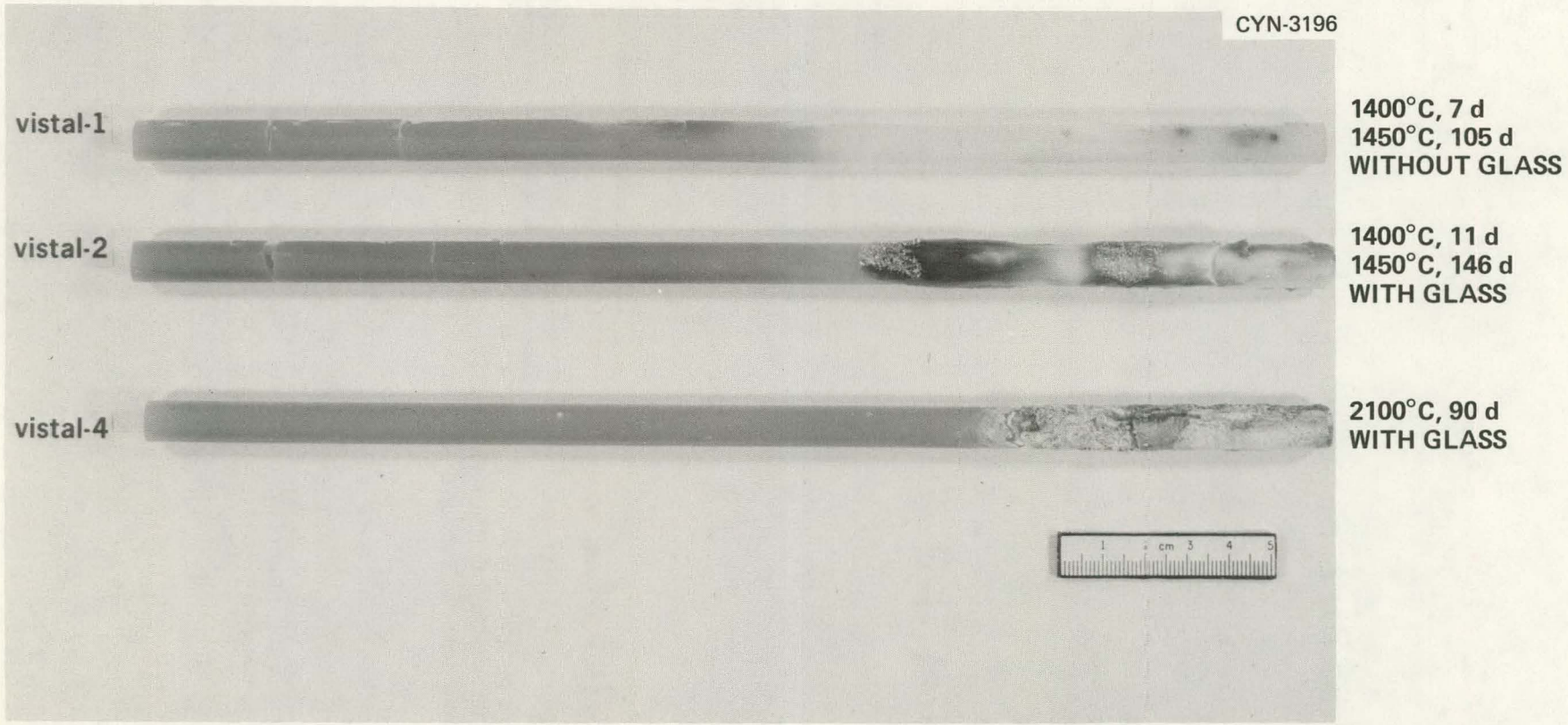

Fig. 26. High-Purity (Vistal) Alumina Exposed to Glass Furnace High-Temperature Exhaust Stream.

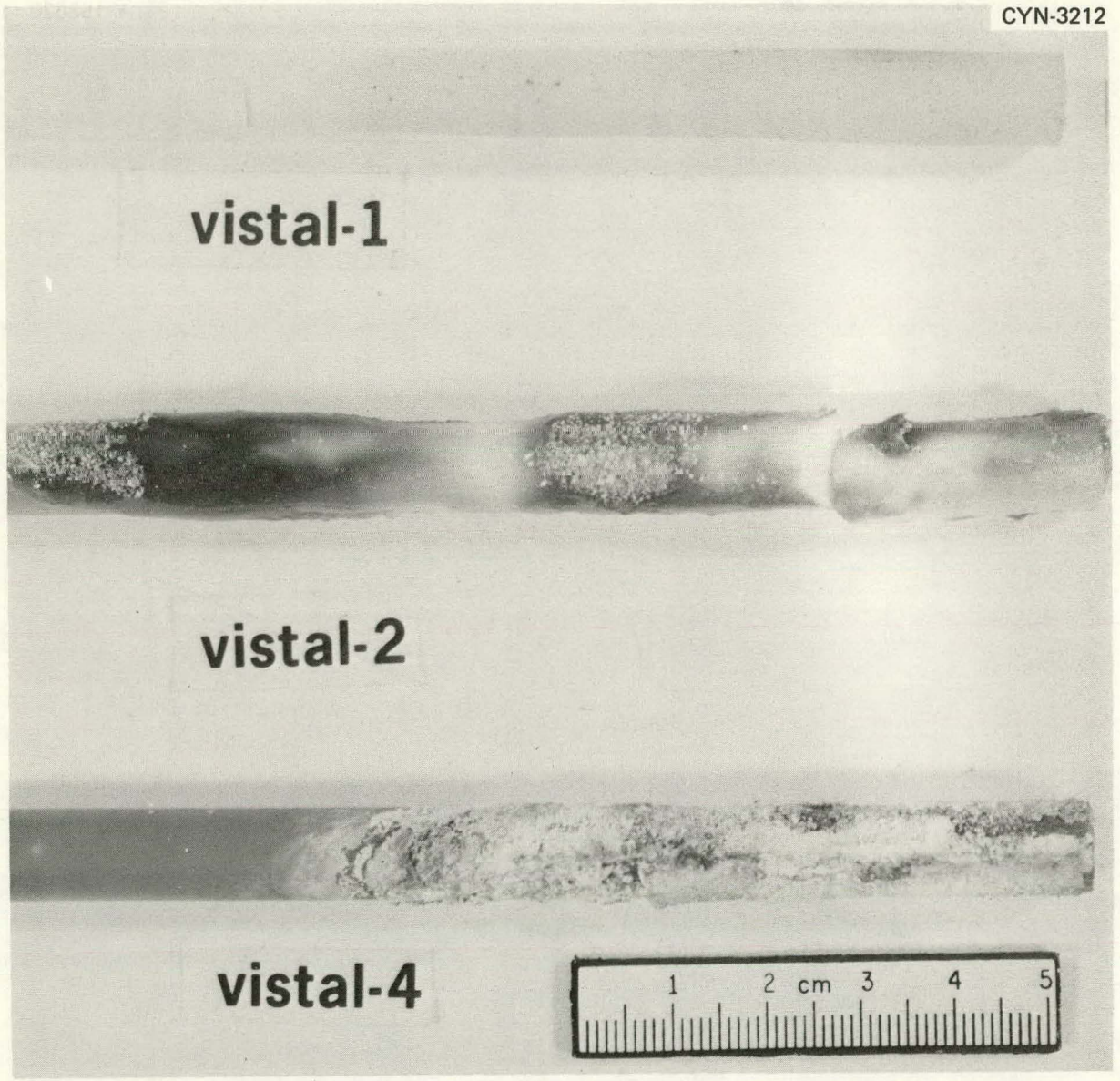

Fig. 27. Close-Up of High-Purity (Vistal) Alumina Exposed to Glass Furnace High-Temperature Exhaust Stream.

in Fig. 28. Two sections were examined: 0.1 m and 35 mm from the exposed end. Little degradation or attack is apparent in either region except for some slight penetration along the grain boundaries close to the Al_2O_3-deposit interface. The microstructure of samples Vistal 1 and 2 are compared in Fig. 29. The sharp distinct interface between the Al_2O_3 and the deposit in sample 2 is readily visible. The relatively low concentration of crystalline phase in the deposits also indicates less

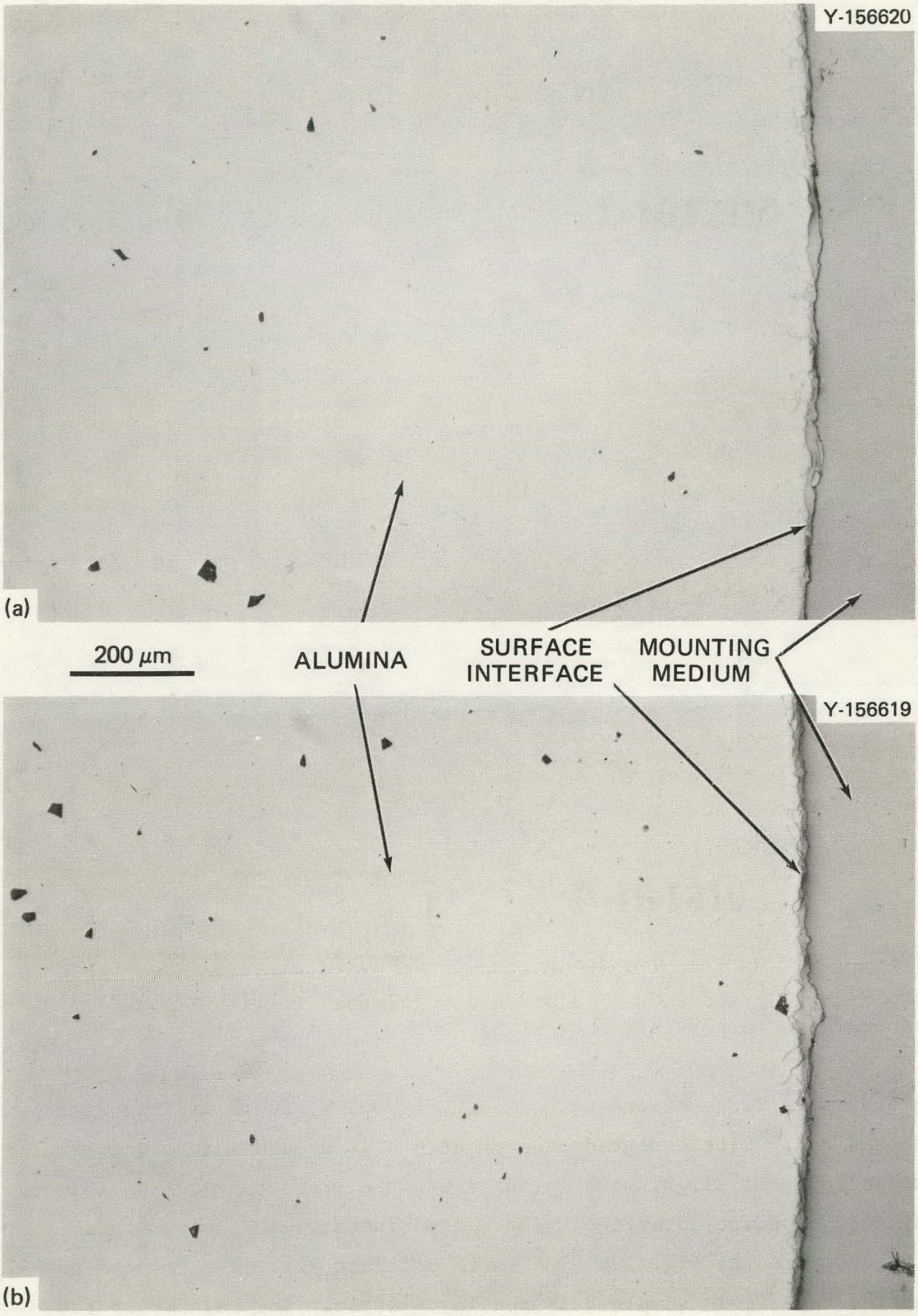

Fig. 28. Microstructure of High-Purity (Vista1) Alumina Exposed at 1400°C (2600°F) for 7 d and 1450°C (2650°F) for 105 d with No Glass in the Furnace. (a) 35 mm from exposed end. (b) 0.1 m from exposed end.

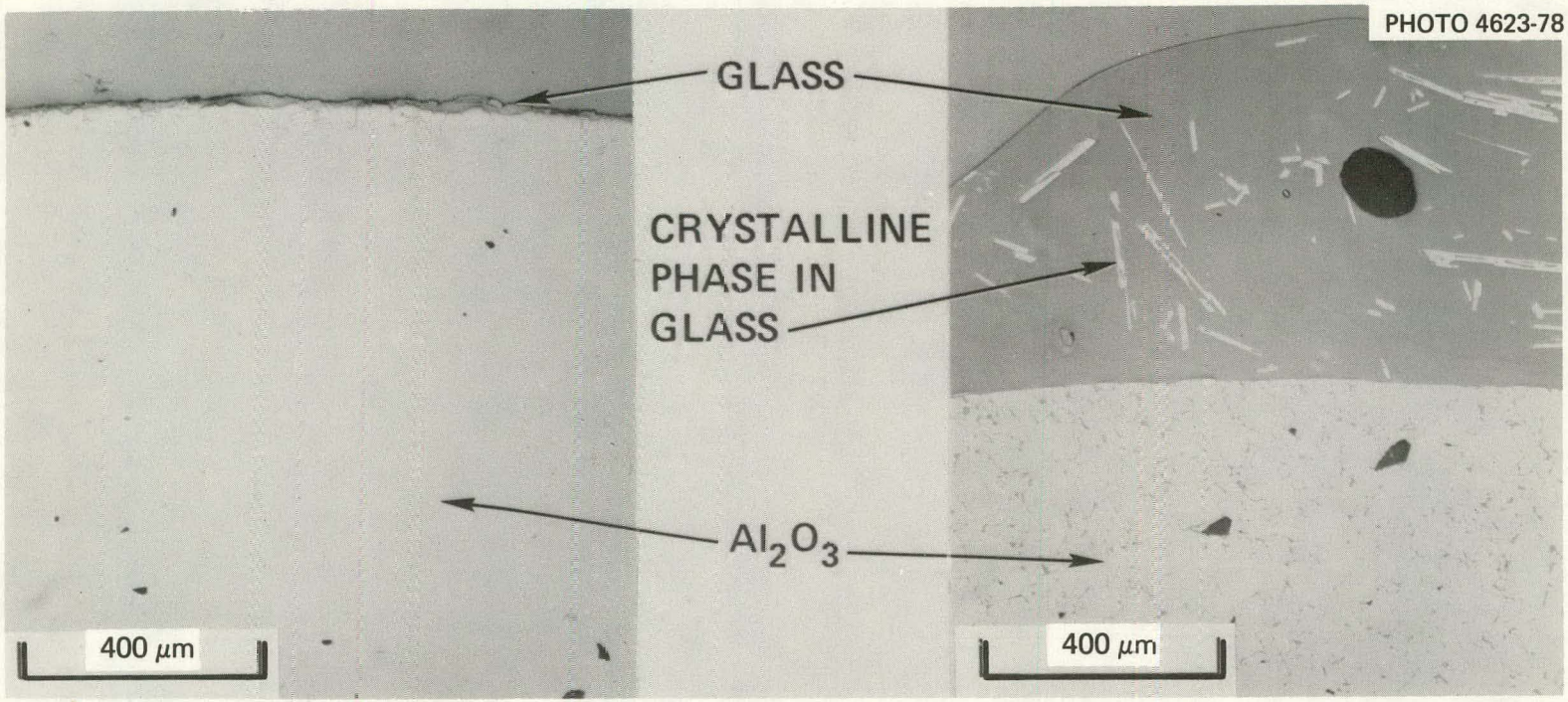

Fig. 29. Microstructure of High-Purity Vistal Aluminas Exposed to Glass Furnace High-Temperature Exhaust Stream. Left: specimen 1 exposed 7 d at 1450°C and 105 d at 1450°C without glass in the furnace. Right: specimen 2 exposed 11 d at 1400°C and 146 d at 1450°C with glass.

dissolution for this ceramic in the melt than for less pure alumina ceramics. The grains appear to be more distinct for Vistal 2, which may indicate that an amorphous phase has penetrated the ceramic and decorated the grain boundaries. Available data do not allow an unequivocable conclusion on this point.

X-ray diffraction data for Vistal alumina specimens are given in Tables A14, A15, and A16 of the Appendix. A discolored spot located 10 mm from the end of the Vistal 1 sample was essentially α-alumina, indicating that no detectable solid solution had occurred in the alumina from any contaminant elements. A brown coating located 5 mm from the end of Vistal sample 2 was more difficult to index uniquely but apparently contained $NaCa_4Al_3O_9$ and $FeO\cdot(Cr,Al)_2O_3$ or $CaO\cdot 2FeO$. The brown coating 40 mm from the end of the Vistal sample 4 contained at least two phases, including α-alumina and a sodium calcium silicate of a type such as $Na_2Ca_2(SiO_3)_3$ or $Na_4Ca(SiO_3)_3$.

Scanning electron microscopy was used to examine the microcomposition and morphology of the cross section and surface of the Vistal 2 sample and the surface in the regions of the Vistal 4 sample. Figure 30 shows the morphology of fracture sections of the interior of the Vistal 2 sample as well as the ceramic-deposit interface region. The difference in the morphology clearly shows the granular crystalline nature of the polycrystalline ceramic in contrast to the relatively featureless conchoidal fracture surface characteristic of an amorphous material. The microprobe data for the interface in Fig. 30 indicates the predominance of Si and Al plus the presence of Na, K, Ca, Ti, and Fe. The detector used was limited to elements with atomic numbers above ten. These are the elements found in similar analyses of surface deposits from the AD-94 and -998 specimens. Figure 31 of the surface of the Vistal 2 specimen 40 mm from the exposed end tested at 1400°C (2550°F) and then at 1450°C (2650°F) contained regions that appear to have been molten. These regions were surrounded by deposits that were more crystalline in appearance. Microcompositional data given in Fig. 31 are essentially identical with that seen at the specimen-deposit interface in Fig. 30.

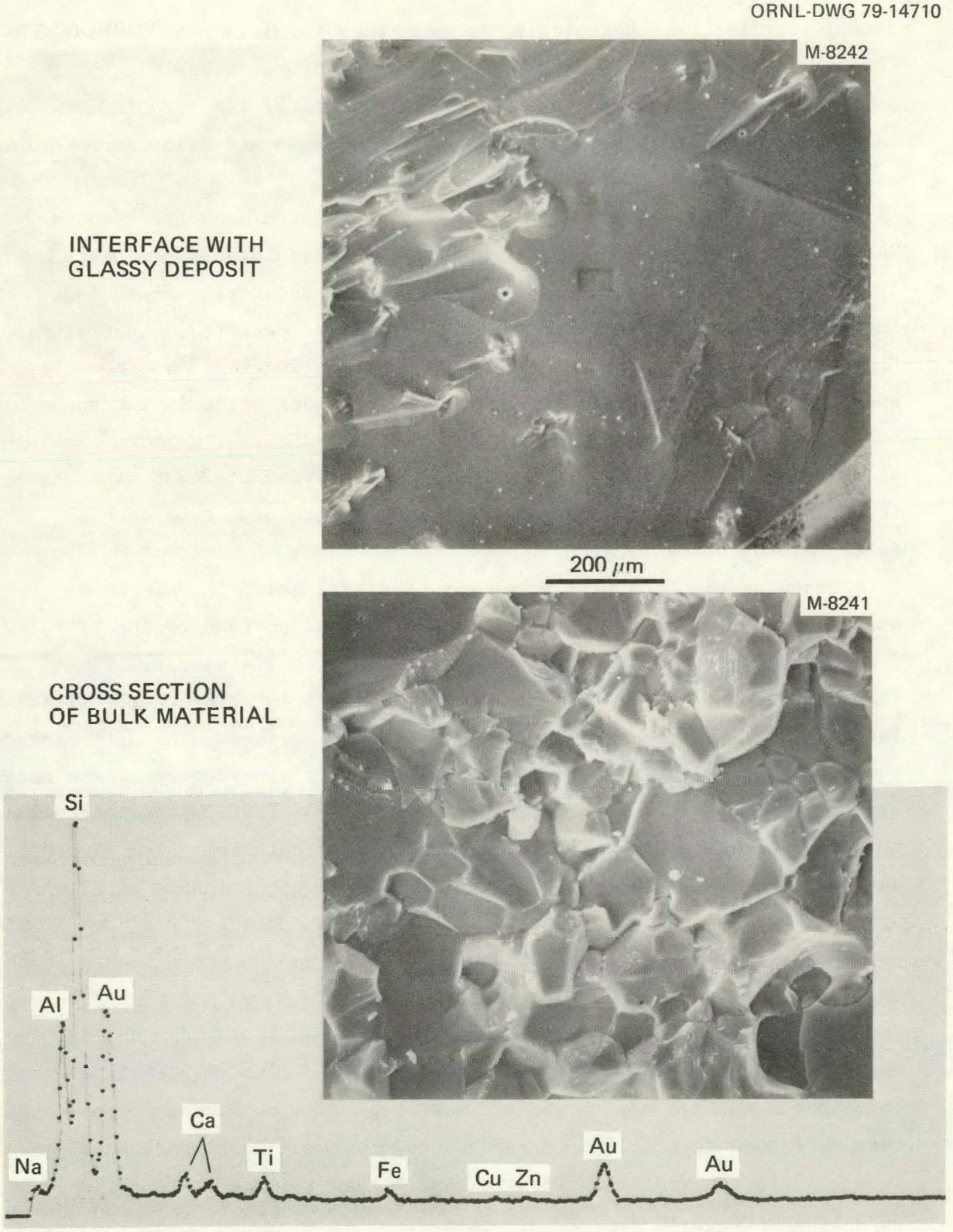

Fig. 30. Scanning Electron Micrographs and Microcompositional Analysis (EDS) of High-Purity Alumina (Vistal 2) Exposed to Glass Furnace Environment at 1450°C for 146 d and 1400°C for 11 d. Gold peaks in EDS are from conductive coating, not part of specimen.

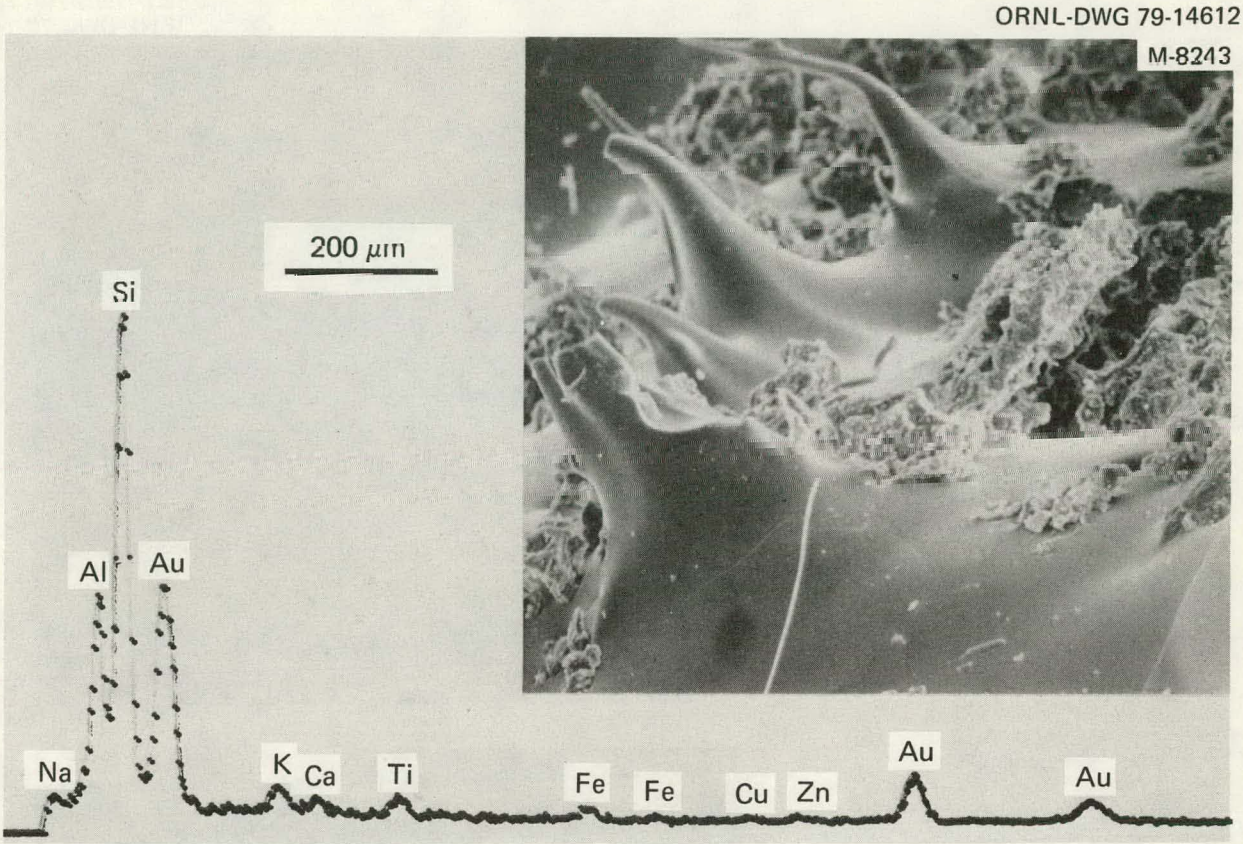

Fig. 31. Scanning Electron Micrograph and Microcompositional Analysis of Surface of High-Purity Alumina (Vistal 2) Exposed to Glass Furnace Environment at 1450°C for 146 d and 1400°C for 11 d.

Scanning electron microscopic results from the surface of the Vistal 4 specimen in Figs. 32 and 33 show two different morphologies and types of surface deposits. The more clearly developed lathlike crystals apparent in Fig. 32 contained more silicon and potassium and less sodium than the more poorly developed material shown in Fig. 33. Both these deposits from the lower temperature Vistal 4 sample contained more sodium and less aluminum than those found on the higher temperature Vistal 2 sample.

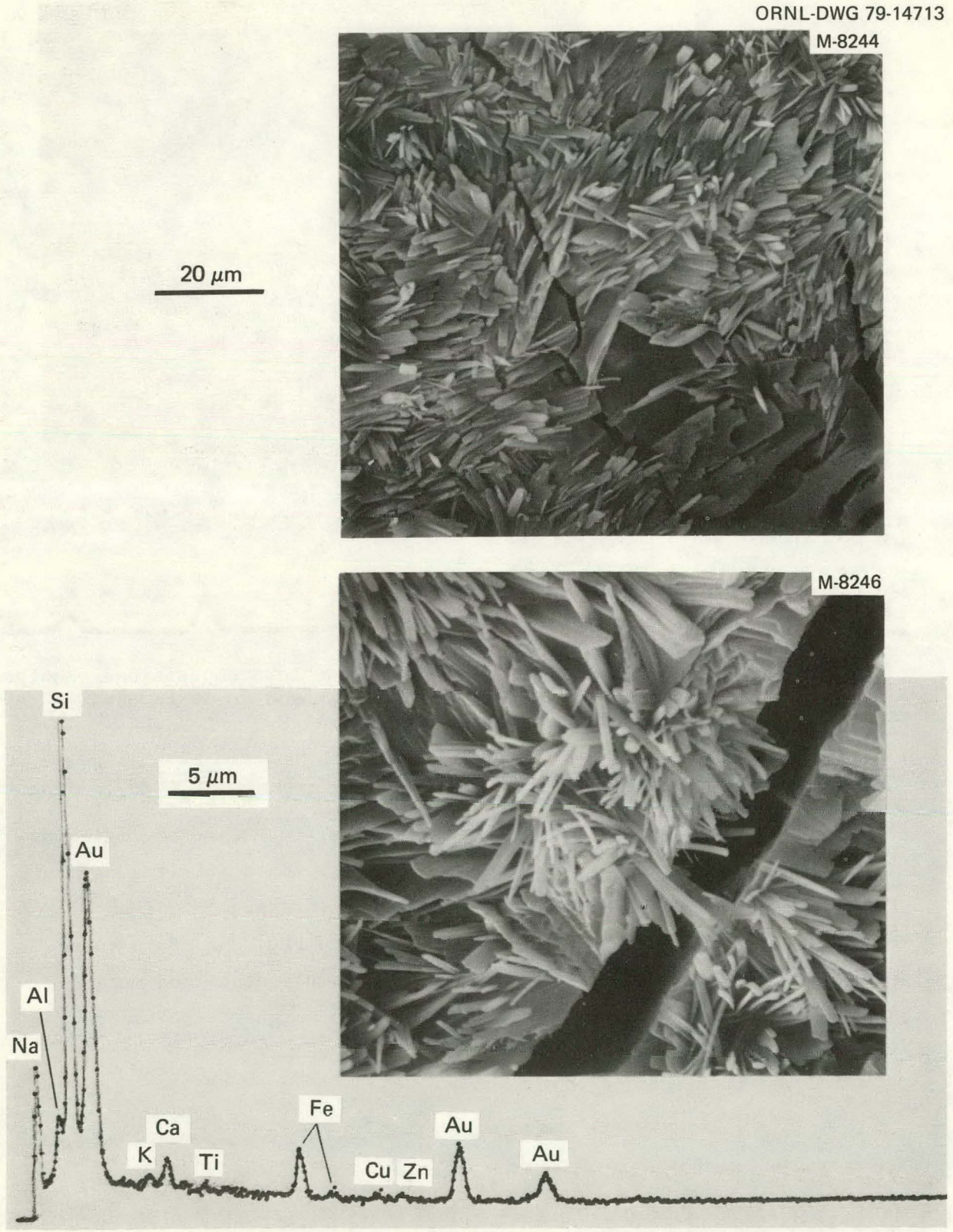

Fig. 32. Scanning Electron Micrographs and Microcompositional Analysis (EDS) of Lathlike Crystals on High-Purity Alumina (Vistal 4) Exposed to Glass Furnace Environment at 1150°C for 90 d. Gold peaks are from conductive coating, not specimen.

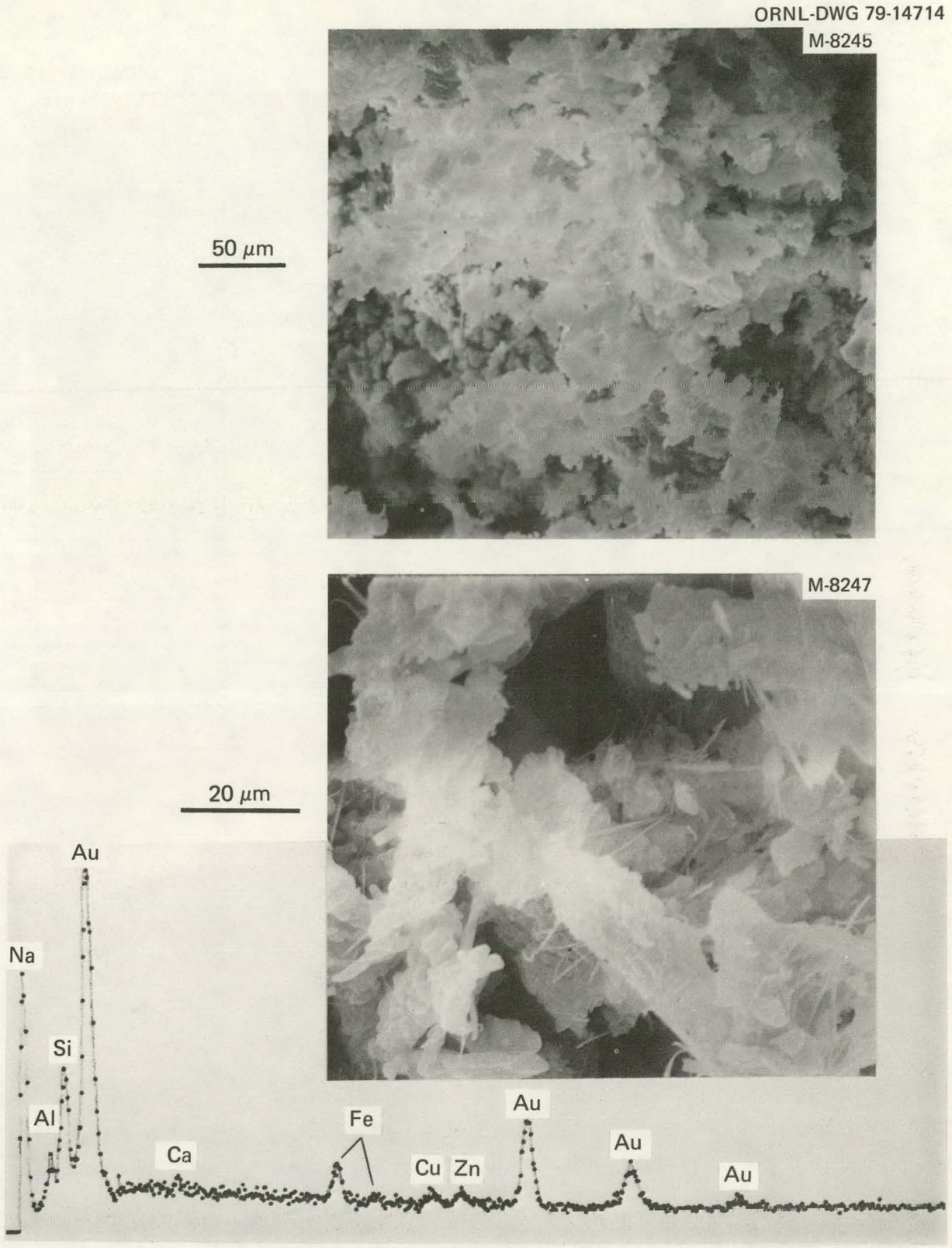

Fig. 33. Scanning Electron Microscope and Microcompositional Analysis (EDS) of Poorly Developed Surface Features on High-Purity Alumina (Vistal 4) Exposed to Glass Furnace Environment at 1150°C for 90 d. Gold lines are from conductive coating, not specimen.

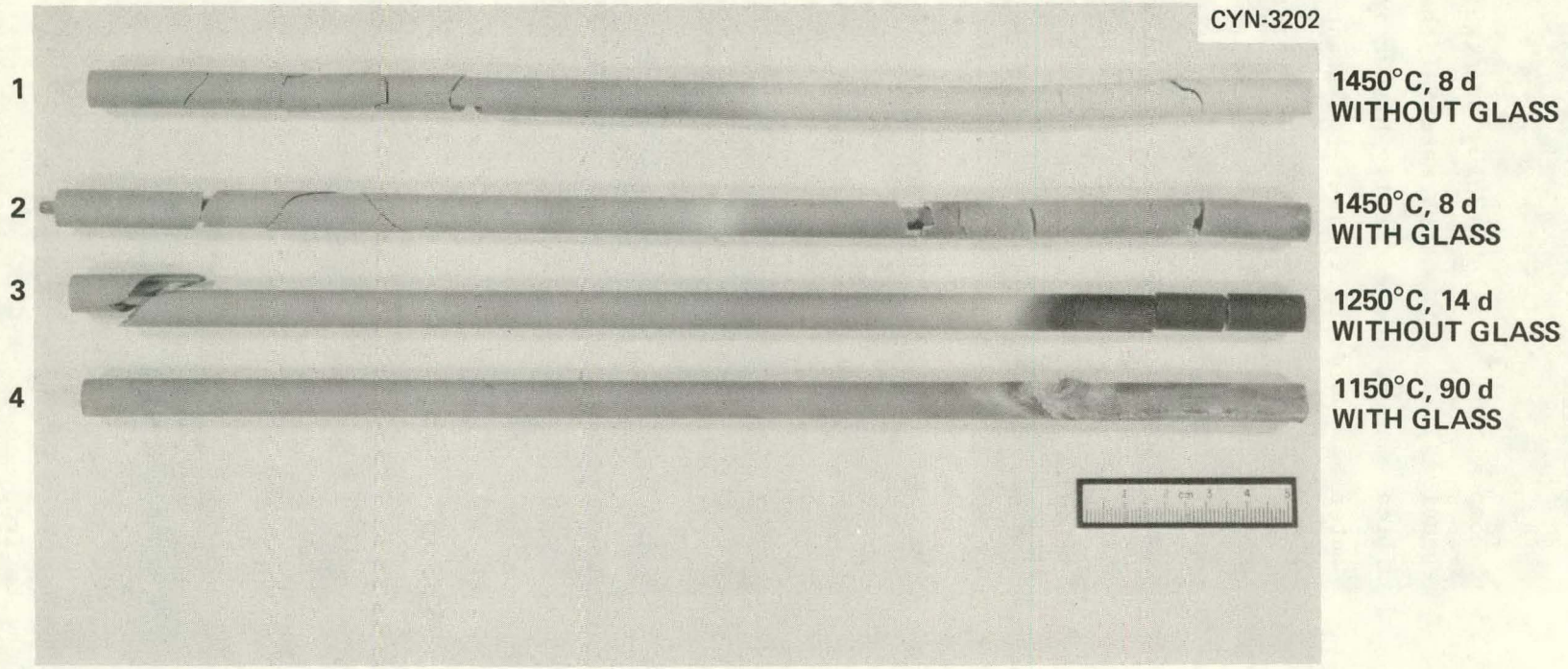

Fig. 34. Mullite Exposed to Glass Furnace High-Temperature Exhaust Stream.

Mullite

Mullite, with an ideal composition of $3Al_2O_3 \cdot 2SiO_2$ or $Al_6Si_2O_{13}$, is often employed as a less expensive, less refractory material than high-purity alumina. The high silica content and generally higher impurity concentration make mullite materials potentially less resistant to corrosion at high temperatures in a glass furnace environment.

Four mullite samples were exposed in the test matrix and are shown after testing in Figs. 34 and 35. Mullite-1 was exposed at 1450°C (2650°F) for 8 d without glass in the furnace but underwent such major deformation that it was withdrawn from the test. Mullite-2 was exposed under the same thermal conditions but with glass in the furnace. Major deformation was again observed and, in addition, crystalline growth was visible in the material. This glazing and crystal growth are particularly visible in Fig. 35.

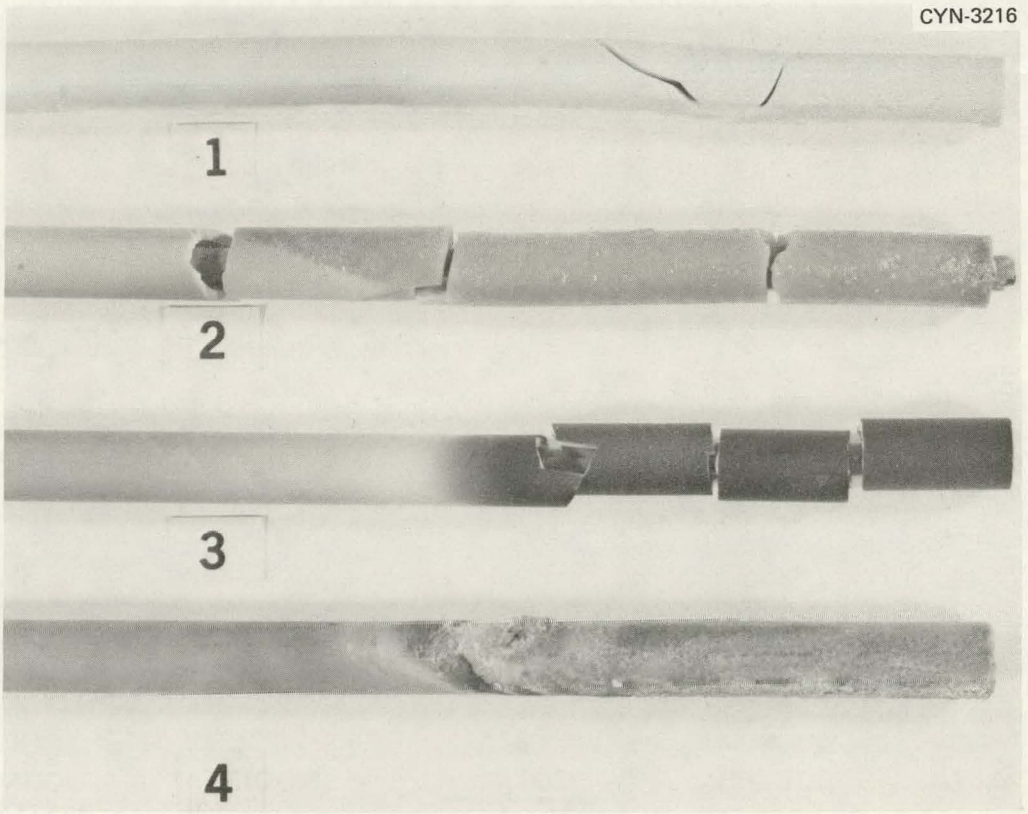

Fig. 35. Close-Up of Mullite Exposed to Glass Furnace High-Temperature Exhaust Stream.

Mullite samples 3 and 4 were exposed at significantly lower temperatures. Mullite-3 was exposed at 1250°C (2300°F) for 14 d without glass in the furnace. It exhibited extensive surface darkening and crystalline growth and was withdrawn from the test. Mullite-4 was tested for 90 d at 1050°C (2100°F) with glass and displayed discoloration and some material loss on the lower exposed side.

Ceramography of the Mullite sample 1 (Fig. 36) revealed little microstructural alteration during the relatively short high-temperature exposure. The very fine microstructure including small evenly distributed porosity is representative of ceramic bodies of this type. Only in the outer 20 μm was there an apparent increase in grain size during the test. The microstructure of the mullite sample 2 exposed to the same thermal conditions as sample 1 but with glass in the test furnace was significantly different, as is apparent in Fig. 37 of sections taken

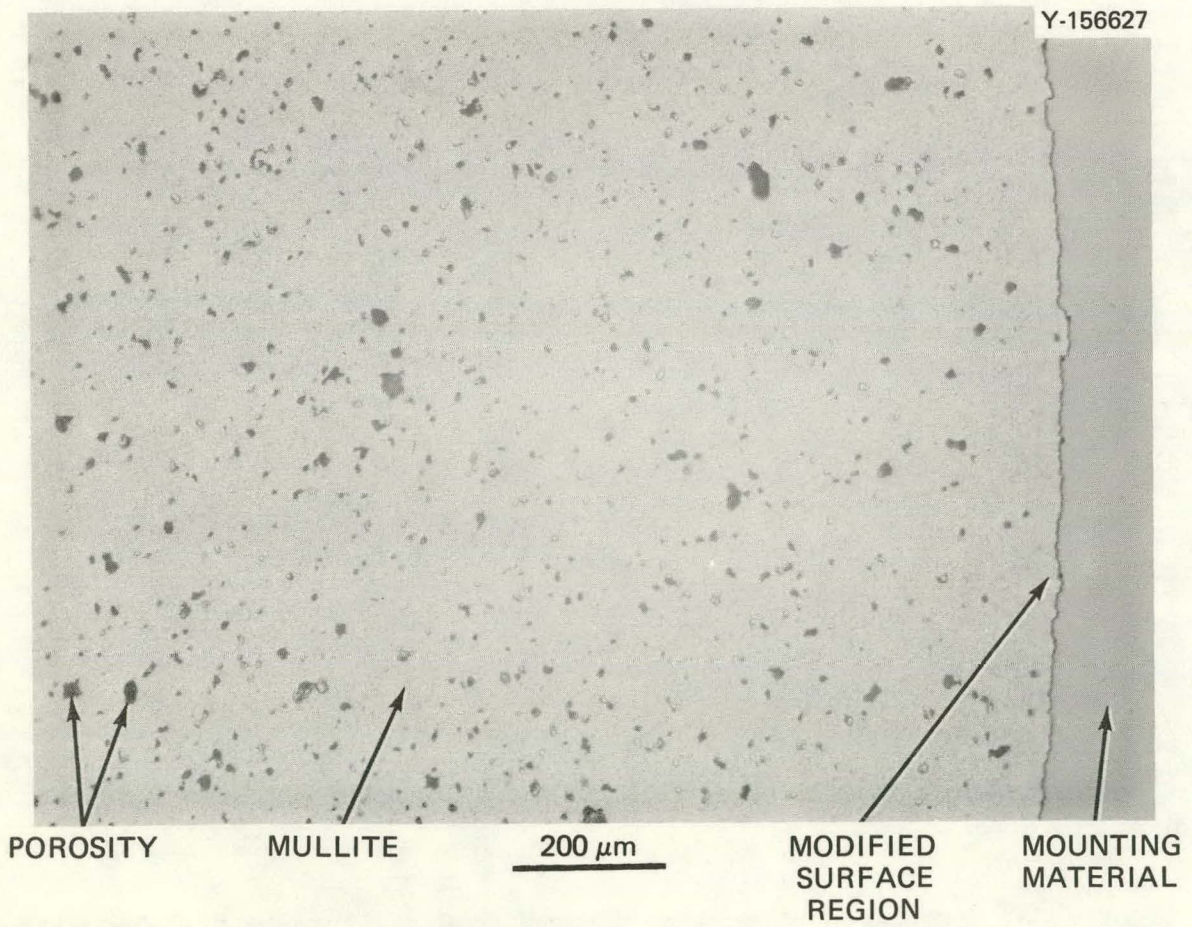

Fig. 36. Microstructure of Mullite (Sample 1) Exposed at 1450°C for 8 d with No Glass in the Furnace.

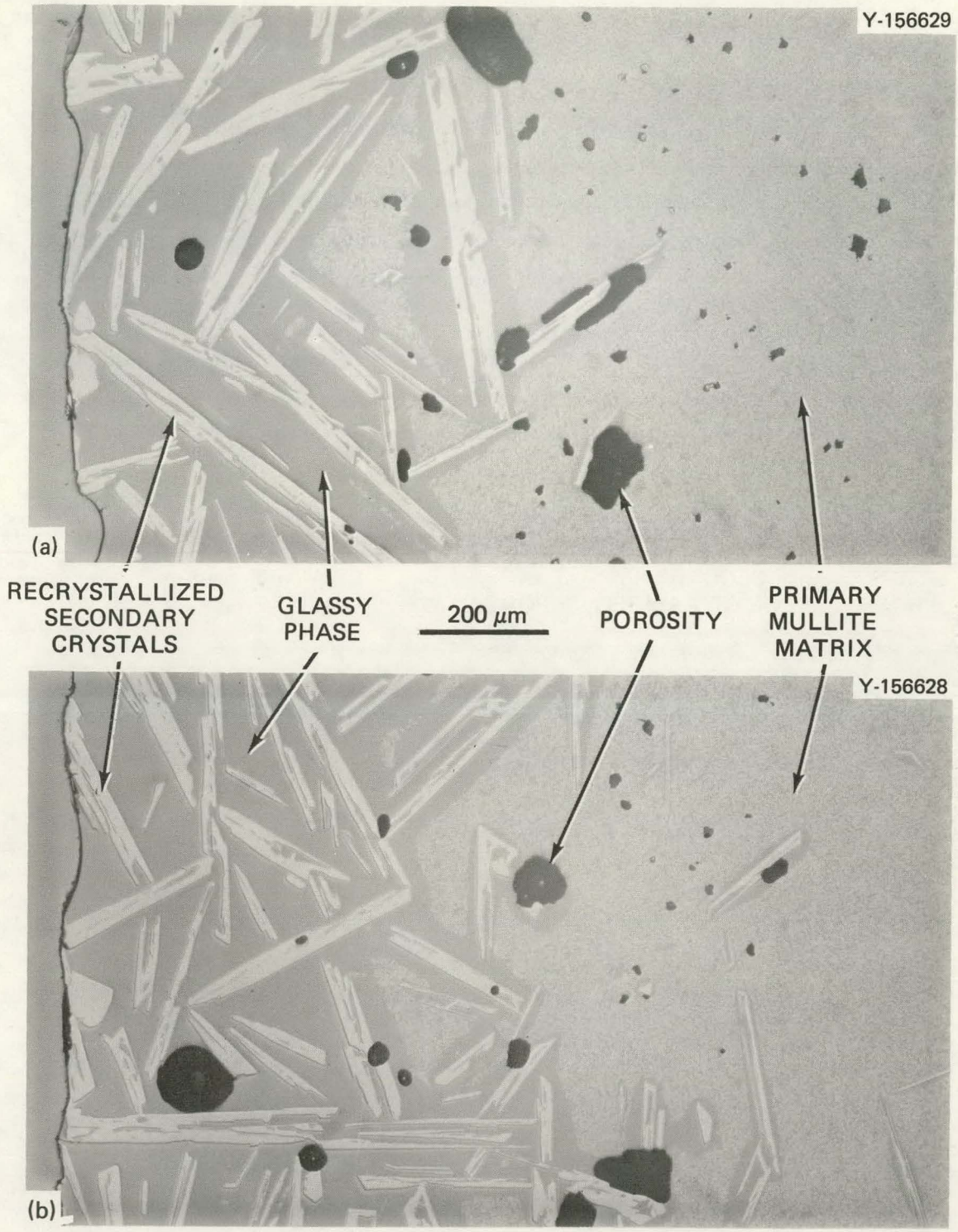

Fig. 37. Microstructure of Mullite (Sample 2) Exposed at 1450°C for 8 d with Glass in the Furnace. (a) 25 mm and (b) 50 mm from exposed end.

50 and 25 mm from the end of the exposed specimen length. The small grain size in the interior is still apparent but the outer 0.7 to 1 mm of the rod had been converted into very large lathlike crystals with aspect ratios exceeding 10 surrounded by large amounts of amorphous material. The mechanical degradation was significant, and thermal shock propreties accompanying such a conversion would, in our view, make this material of little value in glass furnace applications at these temperatures.

The microstructure of the Mullite sample 3, which was exposed at a temperature 200°C (350°F) lower than sample 1 for 14 d without glass in the furnace, shows changes similar to those in samples 1 and 2. In sample 3, the outer 200 to 300 μm had changed, as shown in Fig. 38.

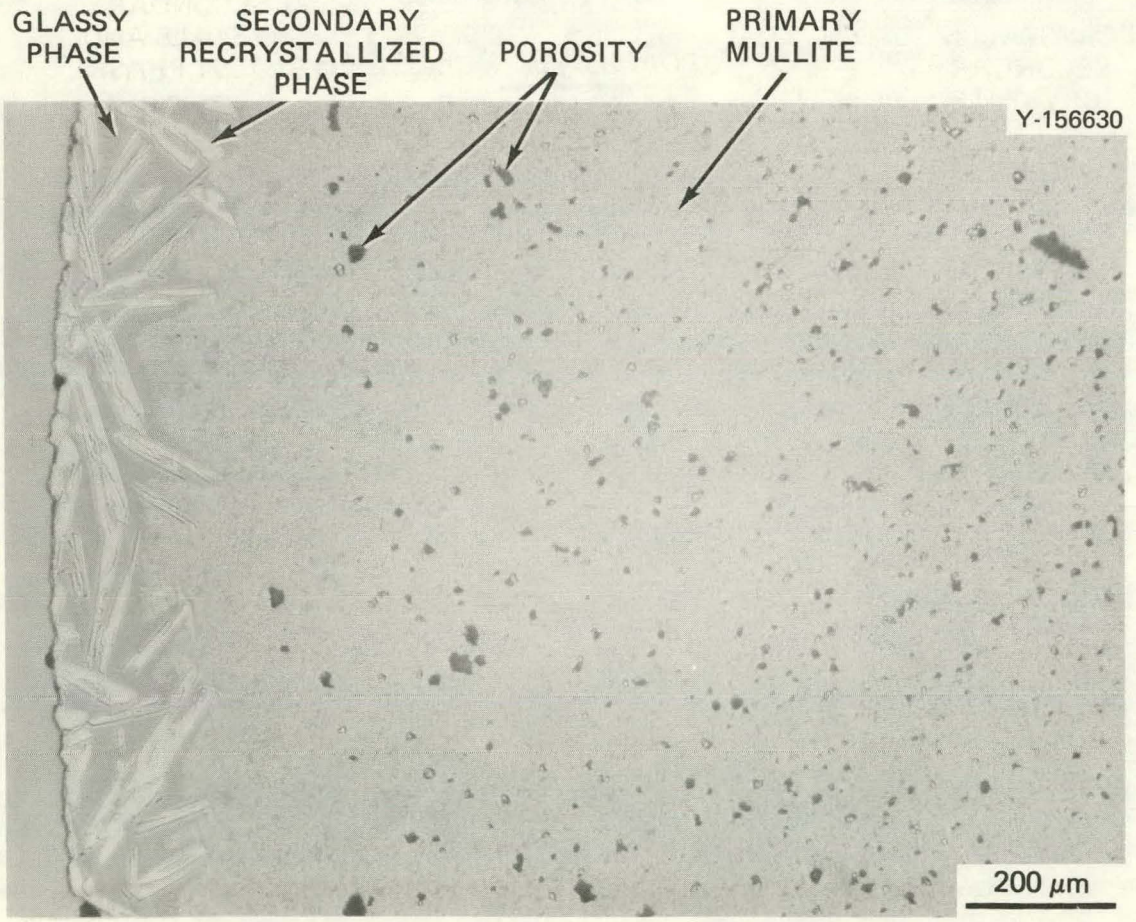

Fig. 38. Microstructure of Mullite (Sample 3) Exposed at 1250°C for 14 d with No Glass in the Furnace.

This behavior indicates that temperature alone readily changes a relatively large amount of material in this mullite ceramic, but exposure to vapors and product carryover from glass melting significantly enhances the conversion. An extensive degradation in mechanical and thermal shock properties would be anticapated for this mullite ceramic exposed to these conditions for any significant time.

Microstructural examination of mullite sample 4, which was exposed at 1150°C with glass, is shown in Fig. 39. The inside wall of the hollow tube specimen is in the initial stages of the changes noted in the previous two figures. The exterior wall shows the formation of an amorphous region about 100 μm thick in the bulk material adjacent to the interface with

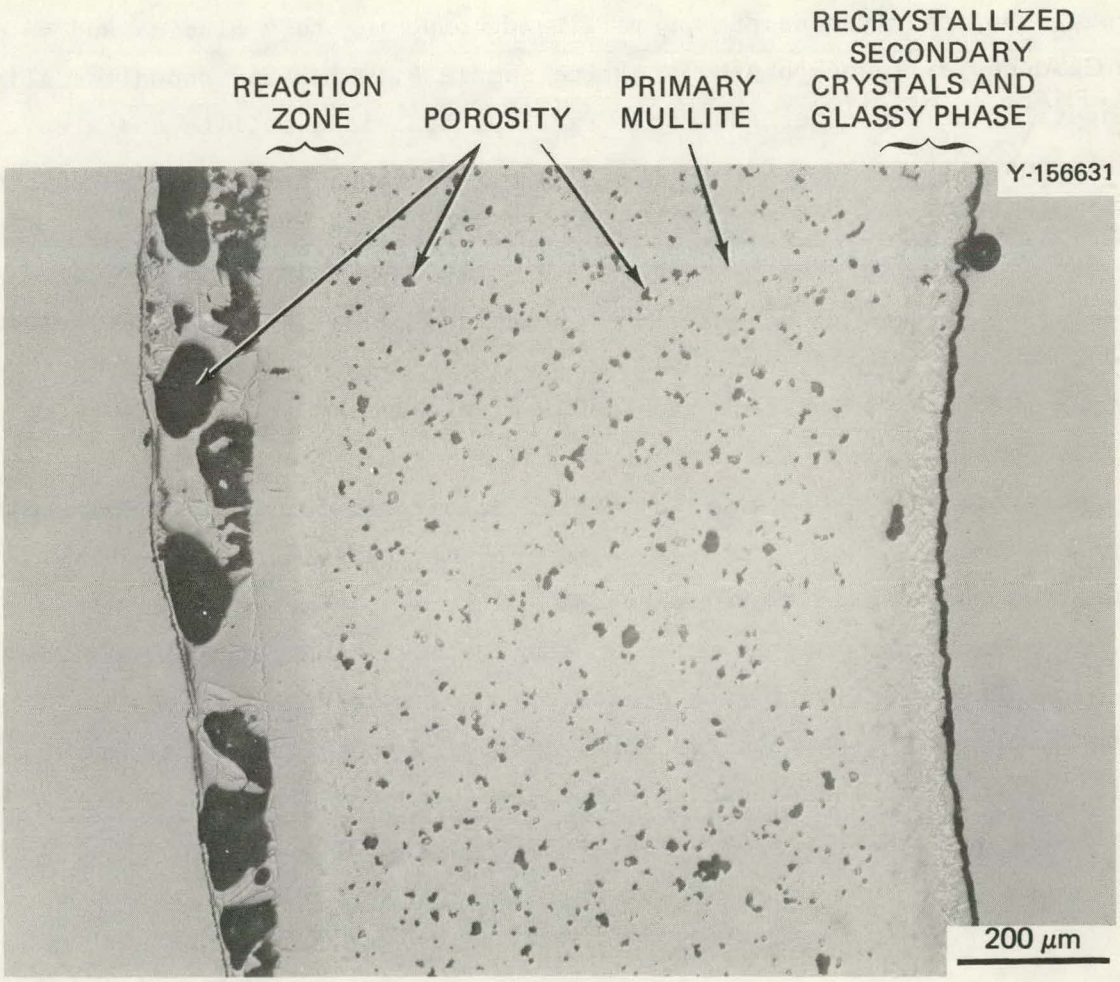

Fig. 39. Microstructure of Mullite (Sample 4) Exposed at 1150°C for 90 d with Glass in the Furnace.

the deposit. The extent of the modification of the bulk material in such a comparatively short time (90 d) makes serious consideration of mullite for use in this environment very questionable even for temperatures as low as 1150°C (2100°F).

X-ray diffraction analysis of the mullite sample 1 was done for two locations; 1A, 25 mm from the cold end, and 1B, 50 mm from the exposed end. Sample 1A, which would be expected to represent "as-received" material, contained mullite, $Al_6Si_2O_{13}$, as the only identifiable crystalline phase. Sample 1B, which had shown negligible microstructural change, also contained only mullite as a crystalline phase. Mullite sample 3, 20 mm from the exposed end in the region that had shown significant microstructural modification (Fig. 38), contained crystalline mullite and possibly α-alumina plus amorphous material. The "conversion" process apparently consists of mullite decomposing to α-alumina and an amorphorous siliceous phase. Mullite sample 4, which had shown the slight conversion at the outer surface (Fig. 39), contained mullite and also a small quantity of an unidentified phase. These x-ray observations agree well with the observed microstructures described earlier.

X-ray fluorescence measurements made to determine elemental compositional analysis indicated results given in Table 6. Samples 1A, 1B and 3 had very similar aluminum, silicon, and oxygen contents, indicating that the composition remained very close to that of the initial mullite when no glass was present in the furnace. The titanium and iron contents are very comparable to those seen earlier for the high-purity aluminas and, as such, probably represent the contamination level of these two elements in these furnaces. Mullite specimen 4 has a composition more like that expected in the cooler regions of a recuperator as a result of carryover from a glass furnace with high sodium, potassium, and phosphorous contents. However, these components are still retained in the amorphous phase, as the x-ray diffraction data indicated only mullite as a crystalline phase.

Table 6. Compositional Analysis of Mullite Samples Exposed to Glass Furnace Exhaust as Determined by X-Ray Fluorescence

Specimen	Temperature		Time (d)	With or Without Glass	Content, wt %								
	(°C)	(°F)			Al	Si	K	Ti	Fe	P	S	Na	O
1A	1450	2650	8	Without	32.56	15.96	0.24	1.15	1.49				48.6
1B	1450	2650	8	Without	33.46	15.18		1.63	1.10				48.62
3	1250	2300	14	Without	31.33	16.16	0.54	1.68	1.95				48.35
4	1150	2100	90	With	10.94	12.00	4.26		2.18	5.93	3.36	17.38	43.95

Cordierite

Cordierite is a low-thermal-expansion compound with an ideal composition of $2MgO \cdot 2Al_2O_3 \cdot 5SiO_2$ ($Mg_2Al_4Si_5O_{18}$) and is relatively inexpensive and of moderate refractoriness. The increasing interest in its use in heat exchangers, recuperators, and regenerators is largely because of its excellent thermal shock resistance and fabricability. Five samples of cordierite were evaluated in this study, as shown in Figs. 40 and 41.

Cordierite specimen 1 was exposed at 1425°C (2600°F) for 117 d without glass in the furnace. After exposure for 5 d the hot end slumped and fell to the bottom of the furnace flue, where it remained for the rest of the 117 d until it could be recovered. When recovered, the sample was badly deteriorated and curled and was not examined further. Specimen 2, exposed to the same temperature with glass, also lost its end and was not examined further. Apparently 1425°C (2600°F) is above the temperature stability range of this material.

Specimen 3 was exposed at 1250°C (2300°F) for 14 d without glass in the furnace and showed blistering, darkening, expansion, and bloating with concomitant curvature development. Its microstructure is shown in

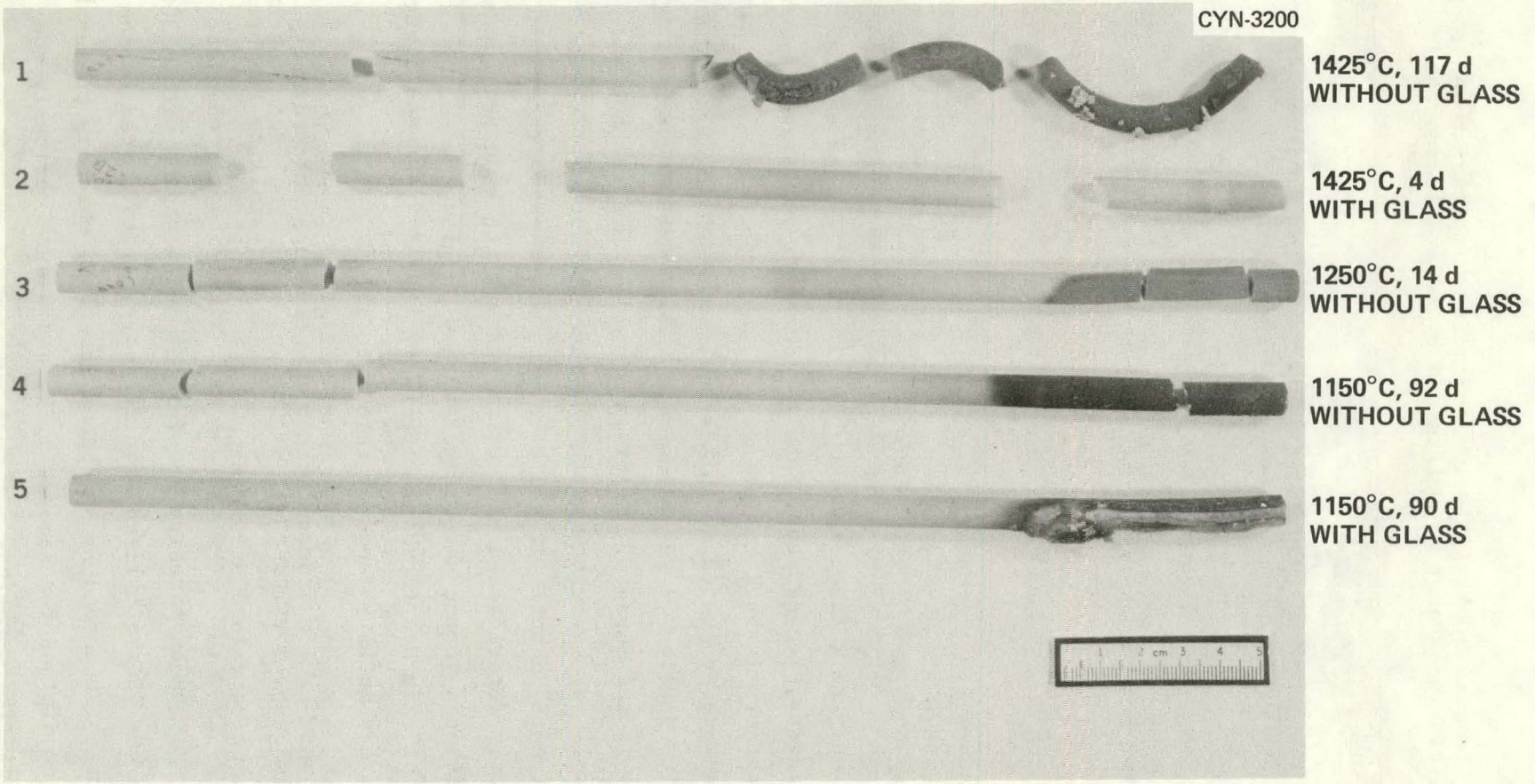

Fig. 40. Cordierite Exposed to Glass Furnace High-Temperature Exhaust Stream.

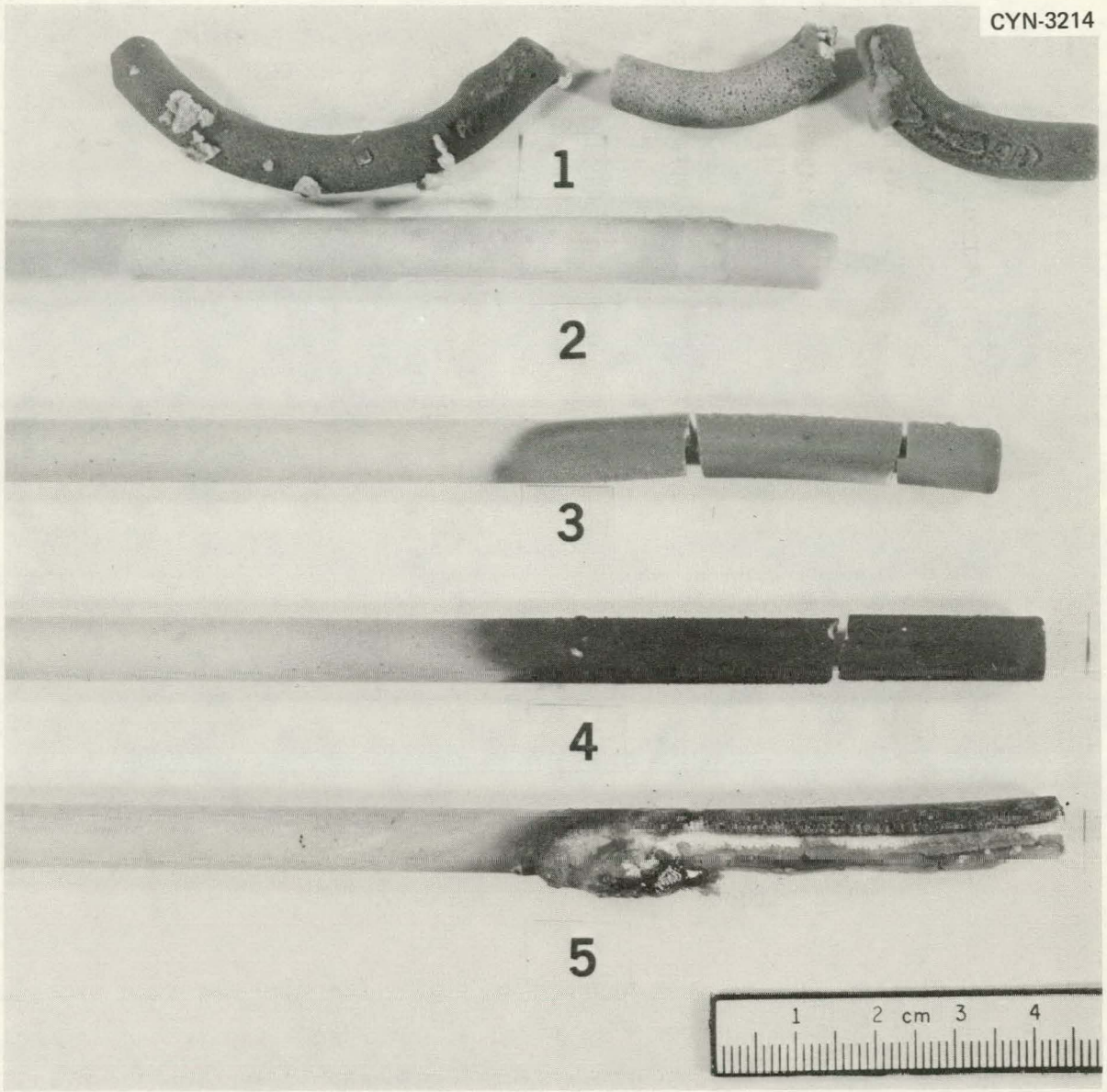

Fig. 41. Close-Up of Cordierite Exposed to Glass Furnace High-Temperature Exhaust Stream.

Fig. 42. The very fine characteristic microstructure of cordierite ceramics, consisting of almost indistinguishable crystalline features and widely dispersed fine porosity, has been significantly changed. Large, almost continuous porosity has formed, and a region within 300 μm of the surface has recrystallized significantly, as evidenced by the equiaxed crystals surrounded by amorphous material, which is presumably a glass. The conditions for samples 1, 2, and 3 were obviously too severe for cordierite ceramics.

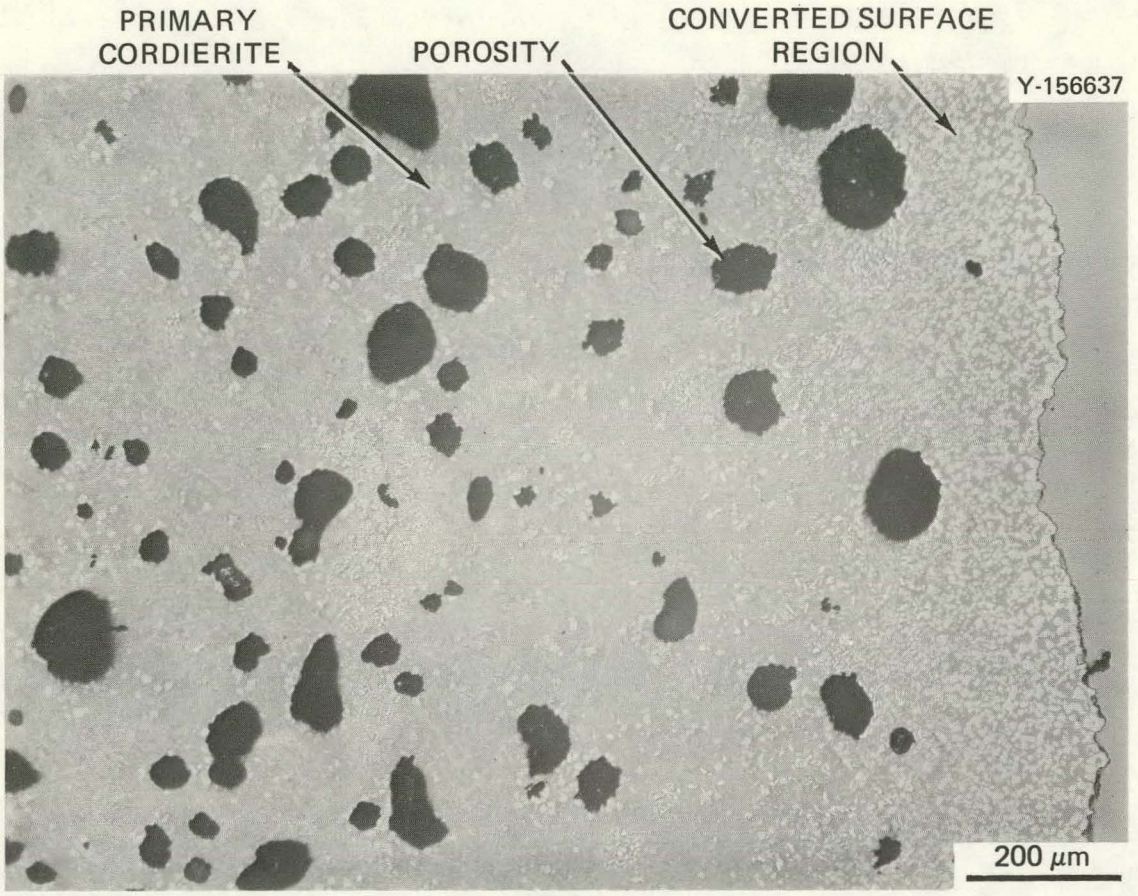

Fig. 42. Microstructure of Cordierite (Sample 3) Exposed at 1250°C (2300°F) for 14 d Without Glass in the Furnace.

Cordierite sample 4 was exposed at 1150°C (2100°F) for 92 d without glass in the furnace. After this time, slight edge rounding and significant discoloration had occurred. The ceramographic section shown in Fig. 43 demonstrated the characteristic microstructure in the interior of the specimen with coalescence of the porosity and a modified equiaxed microstructure near the surface. A lighter colored second phase at the interface between the ceramic and the coating is believed to result from metallic impurities, particularly iron, which are responsible for the observed discoloration as well as the microstructural modification.

The final specimen, cordierite 5, was also exposed at 1150°C (2100°F) for 90 d but with glass in the furnace. It was significantly deformed, with substantial deterioration on the side toward the furnace. Two metallographic sections were analyzed: (A) 50 and (B) 15 mm from the

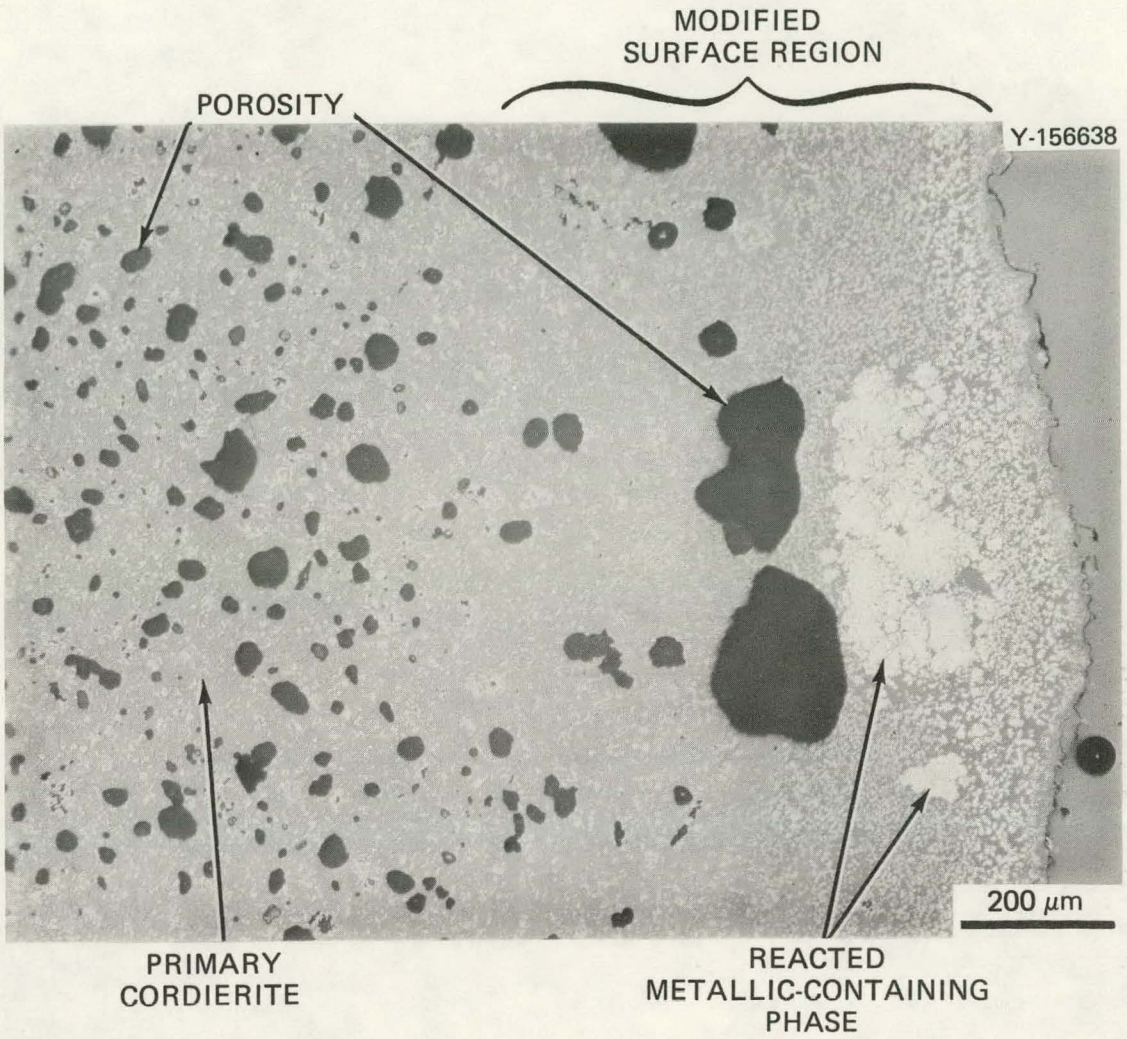

Fig. 43. Microstructure of Cordierite (Sample 4) Exposed at 1150°C (2100°F) for 92 d Without Glass in the Furnace.

exposed end. As seen in Fig. 44, the microstructures are similar, with a 0.7 to 0.9-mm-thick zone of coalesced porosity and possibly recrystallized material intermediate between the bulk material and the surface deposit. The cracks in section A of this sample may have been caused during ceramographic preparation. The depth and type of the modification in the structure of this ceramic as well as the observed behavior of the bulk material would indicate that even at 1150°C (2100°F) cordierite is not a viable structural material in this environment.

X-ray diffraction and microcompositional analyses were conducted on samples 3, 4, 5A, and 5B. Sample 3 contained mullite, indialite

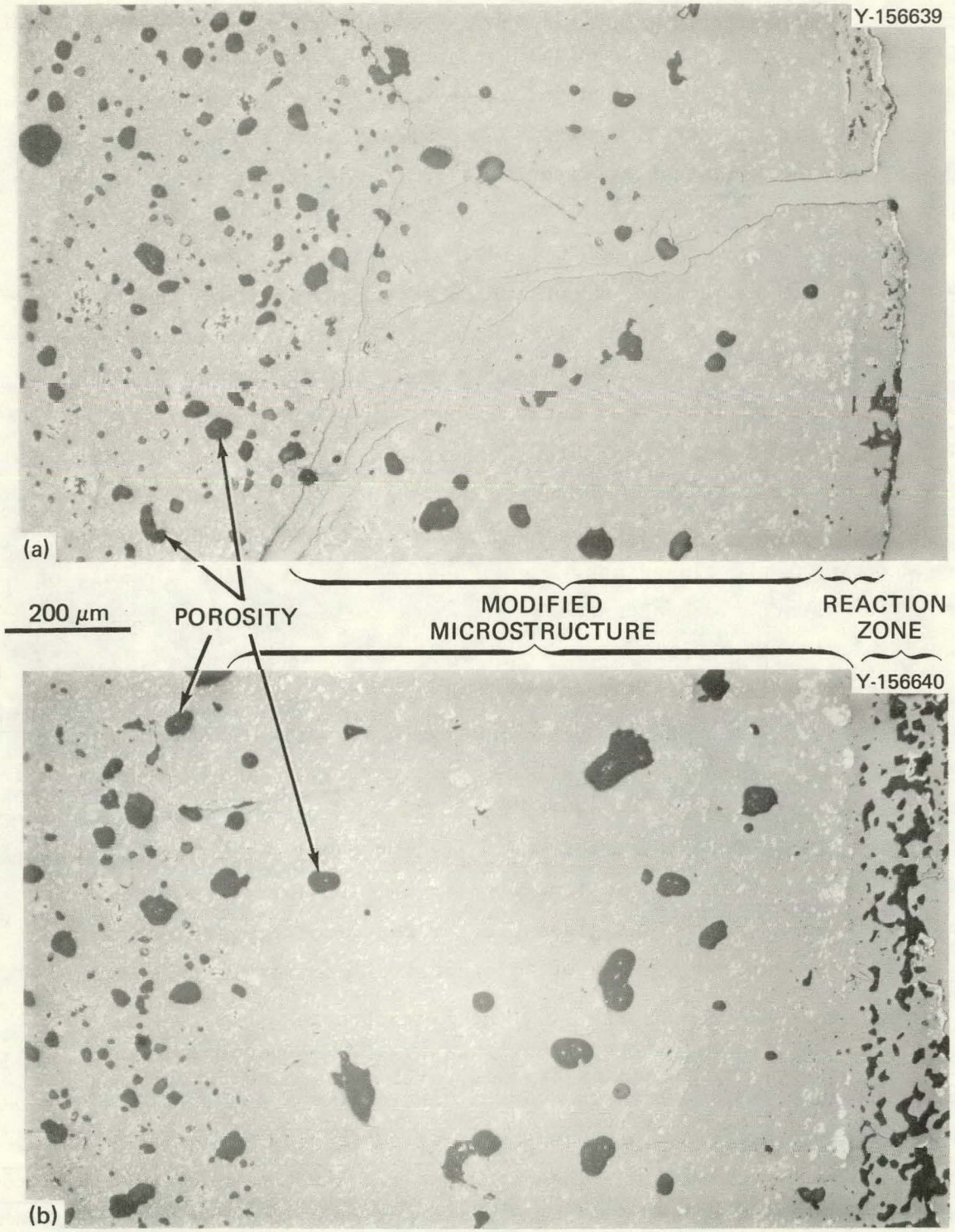

Fig. 44. Microstructure of Cordierite (Sample 5) Exposed at 1150°C (2100°F) for 90 d. (a) Section A, 50 mm from the exposed end. (b) Section B, 15 mm from the exposed end.

(a polymorphic low-temperature form of $Mg_2Al_4Si_5O_{18}$) or cordierite (a high-temperature polymorph of $Mg_2Al_4Si_5O_{18}$), $MgAl_2O_4$, and some unidentified phase(s). Sample 4 contained indialite (or cordierite) and possibly silica with some unknown phase(s) like those found for sample 3. These observations are consistent with the significant modification of the microstructure at 1250°C (2300°F) seen in Fig. 42 and the less significant changes observed at 1150°C (2100°F) in Fig. 43. The high-temperature decomposition of cordierite normally results in mullite and/or silica. The decomposition process is strongly temperature sensitive in the region included in the furnace tests. Sample 5, which contained more of the glassy surface deposit, indexed fairly well as $Na_6Al_4Si_4O_{17}$ (5A) and $Na_3KAl_4Si_4O_{16}$ (5B), with some missing lines and different intensities than those reported in the literature. These phases also agree well with those expected from glass batch carryover for a conventional glass tank. Confirmation that they are a result of batch carryover is demonstrated by the high sodium content, which is not found in the base ceramic.

Elemental compositional analysis of the cordierite samples is shown in Table 7. Higher sodium and calcium contents were present in samples exposed to glass batch carryover from the furnace. The high concentrations of these "fluxing" elements, which form low melting or amorphous aluminosilicates, probably account for the poor structural stability of cordierite in the test environment. We find it extremely unlikely that cordierite could be used in commerical glass plant recuperators regardless of the temperatures employed because of this chemical compatibility problem.

Table 7. Compositional Analysis by X-Ray Fluorescence of Cordierite Samples Exposed to Glass Furnace Exhaust

Sample	With or Without Glass	Temperature (°C)	Exposure (d)	Content, wt %								
				Na	Mg	Al	Si	K	Ca	Ti	Fe	O
3	Without	1250	14	7.08	4.03	21.16	18.4	1.00		0.20	2.03	46.11
4	Without	1150	92	5.80	3.94	19.58	18.0	1.02	0.13	0.32	5.79	45.46
5A	With	1150	90	16.52	3.88	10.65	17.5	0.39	4.67	1.35	3.13	41.91
5B	With	1150	90	14.06	2.85	19.95	15.7	0.31	1.57		1.68	43.85

Silicon Nitride

Silicon nitride (Si_3N_4) ceramics have been the subject of extensive research and development in recent years in an attempt to develop a high-temperature structural material with mechanical properties suitable for use in highly stressed heat engine components, such as turbine blades, at 1250 to 1300°C. Because of the background of information generated in recent years on this material and its promise as an advanced high-temperature structural material, it was also included in the test matrix. As its high-temperature chemical compatibility with glass tank carryover was expected to be poorer than that of silicon carbide or alumina, only four samples were evaluated. Three of these samples are shown in Figs. 45 and 46.

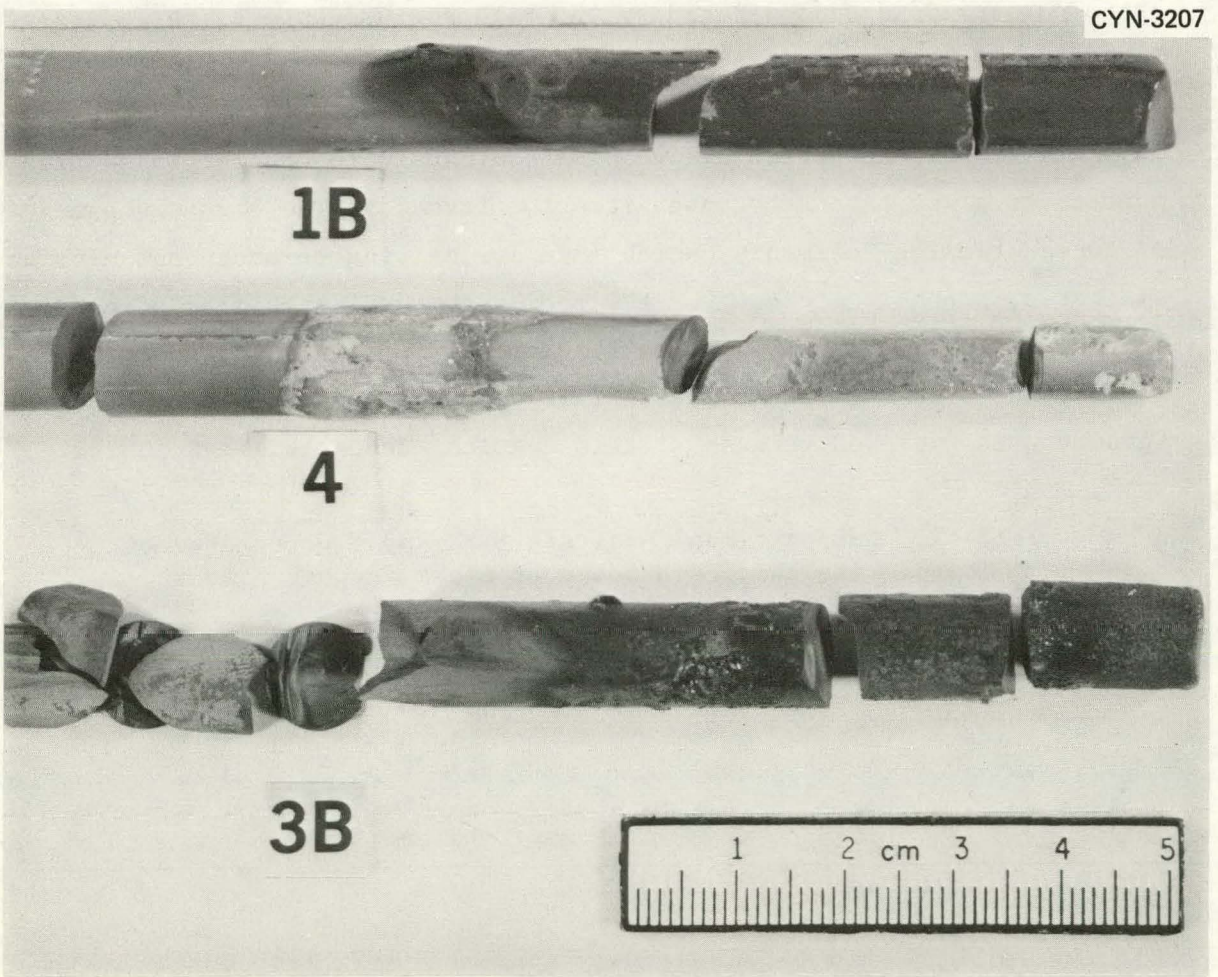

Fig. 45. Close-Up Silicon Nitride Exposed to Glass Furnace High-Temperature Exhaust Flue.

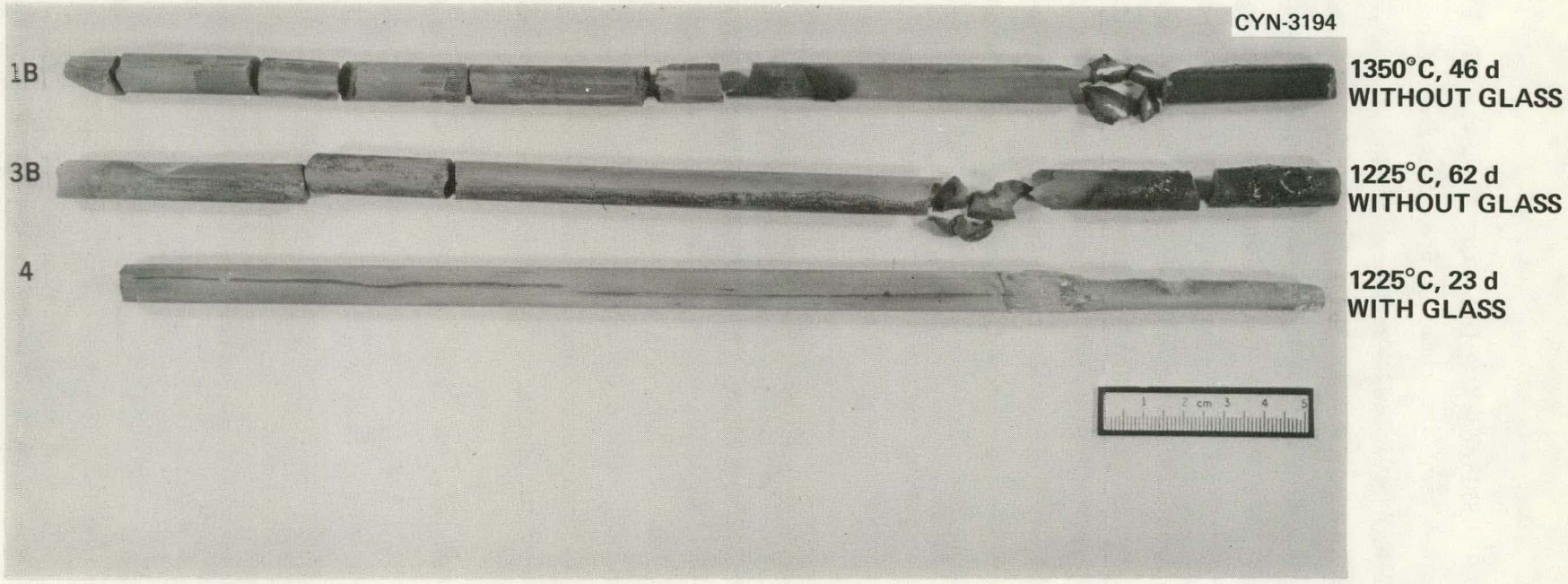

Fig. 46. Silicon Nitride Samples Tested in Glass Furnace High-Temperature Exhaust Flue.

Sample 1B was exposed at 1350°C (2450°F) for 46 d without glass in the furnace and was broken during its removal from the test flue. A slight deterioration of the sample surface was evident. Sample 2, exposed at the temperature for 70 d with glass in the furnace, showed evidence of major strength degradation, as it broke easily upon removal from the test flue despite considerable care. Some surface changes judged to be deterioration were observed as well. The poor mechanical behavior may be attributed to intrinsic defects in the as-manufactured material, but this possibility was not pursued further. The microstructure varied significantly across the specimen diameter for all silicon nitride samples. This behavior is illustrated for sample 1B in Fig. 47. A coating attributed to oxidation of the nitride consists of amorphous glass and no obvious crystalline phases. The surface of the sample at the interface between this coating and the bulk ceramic appears to be selectively etched in that major components appear to be preferentially removed during exposure.

Sample 3B, exposed at 1225°C (2250°F) for 62 d without glass in the furnace, also exhibited a glazing on the surface and broke very easily upon removal from the test flue in a manner analagous to the previous samples. Microstructural results shown in Fig. 48 are analogous to those of sample 1B in Fig. 47. The microstructure varies considerably across the post-test sample cross section, and some major components are removed selectively near the surface. Crystals were distributed in the amorphous coating on this specimen.

Sample 4 was exposed at 1225°C (2250°F) for 23 d with glass in the furnace, underwent a major decrease in diameter over its exposed length, and was withdrawn from the test. Silicon nitride loss was significantly worse than that seen for the sample exposed without glass in the furnace at 1350°C (2450°F) for longer times. This increase in mass loss at low temperatures when exposed to glass batch carryover is reminiscent of the behavior of silicon carbide noted earlier in this report. The microstructure (shown in Fig. 49) consisted of an amorphous layer on the sample surface similar to that in sample 1B. The silicon nitride had a microstructure much like that observed at the center of the two specimens discussed previously. The sample mass loss was apparently such

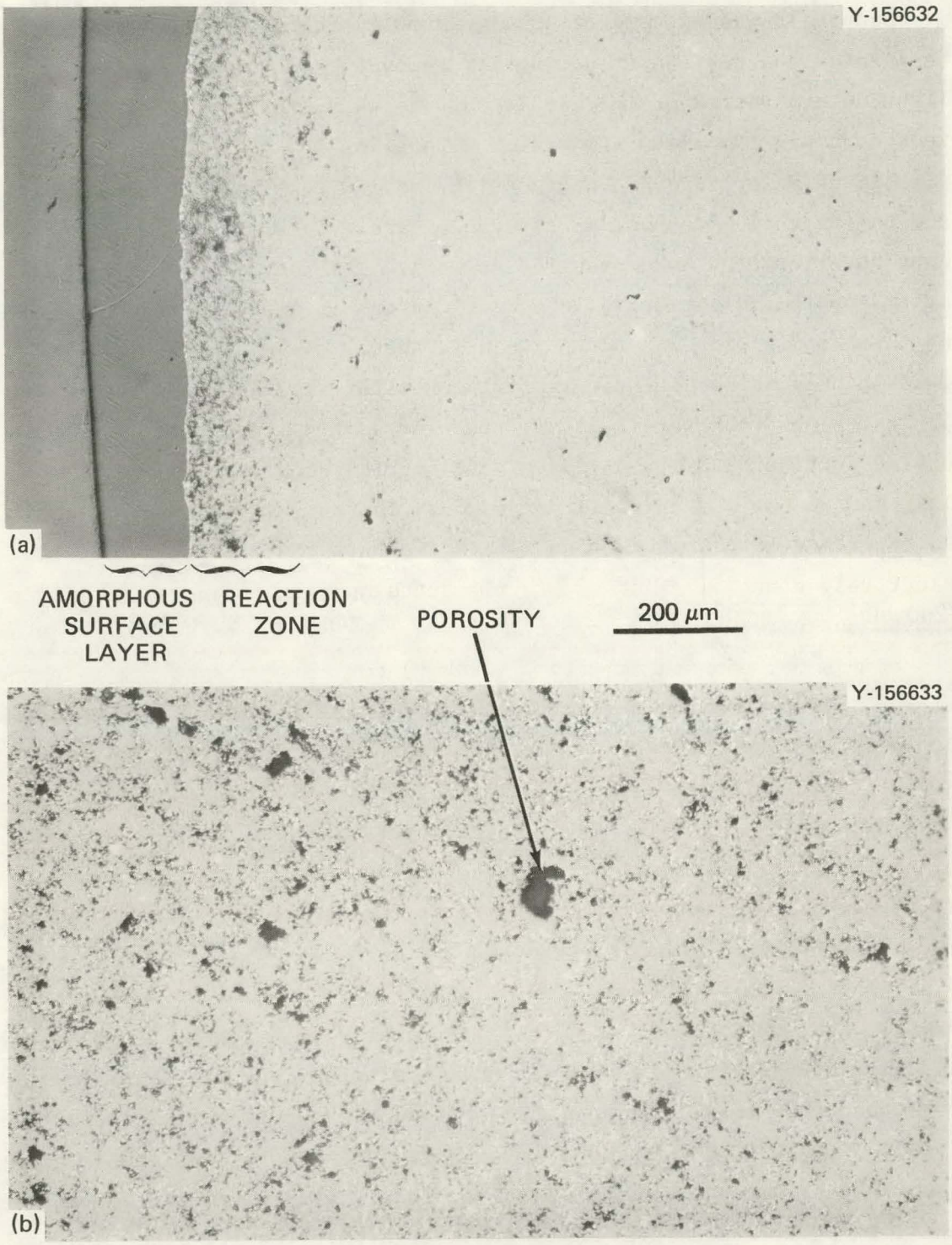

Fig. 47. Microstructural Variation in Silicon Nitride Cylindrical Test Specimen (Sample 1B) Exposed at 1350°C (2450°F) for 46 d Without Glass. (a) Outside surface of rod. (b) Center of rod.

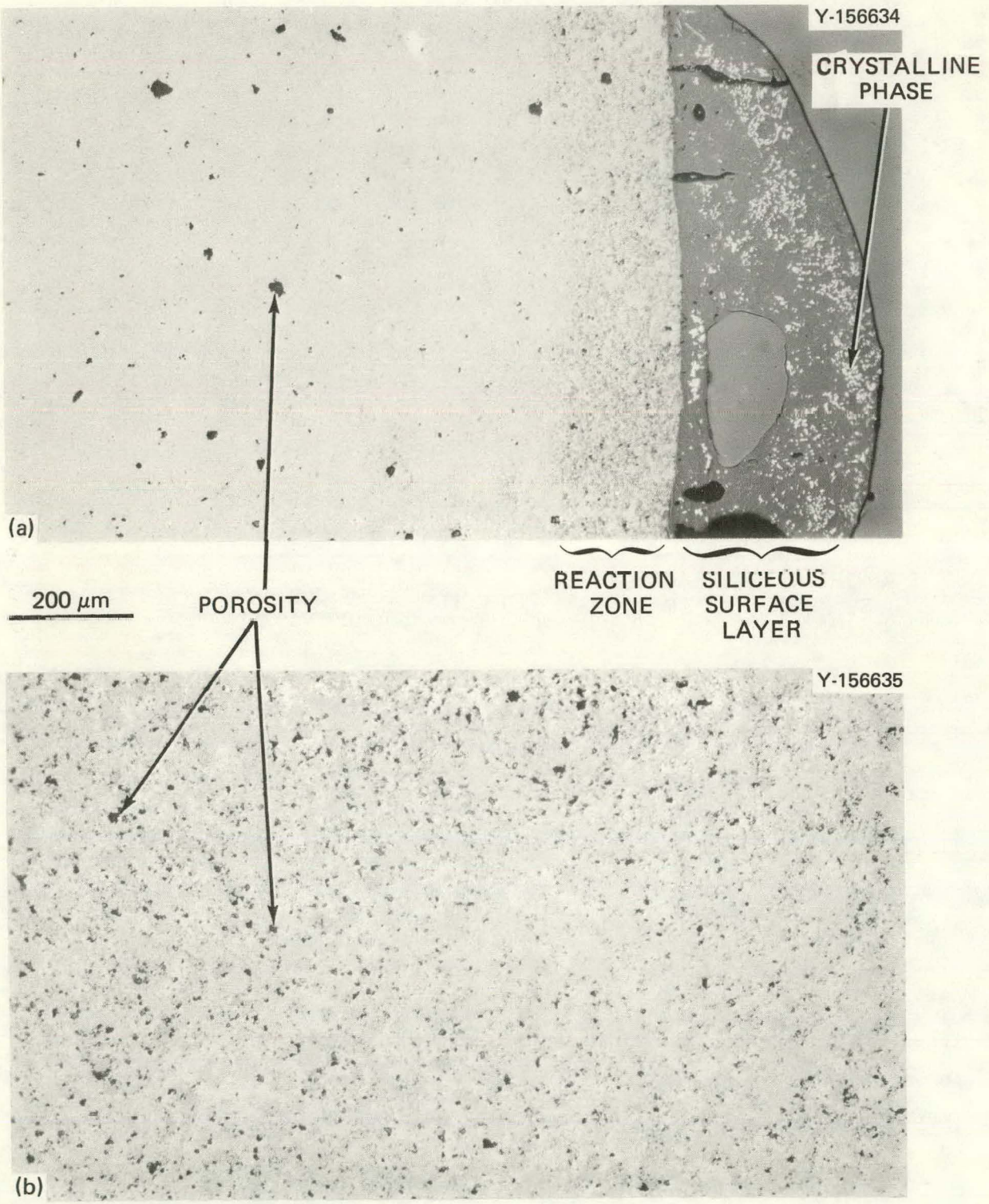

Fig. 48. Microstructural Variation in Silicon Nitride Cylindrical Test Specimen (Sample 3B) Exposed at 1225°C (2250°F) for 62 d Without Glass. (a) Outside surface of rod. (b) Center of rod.

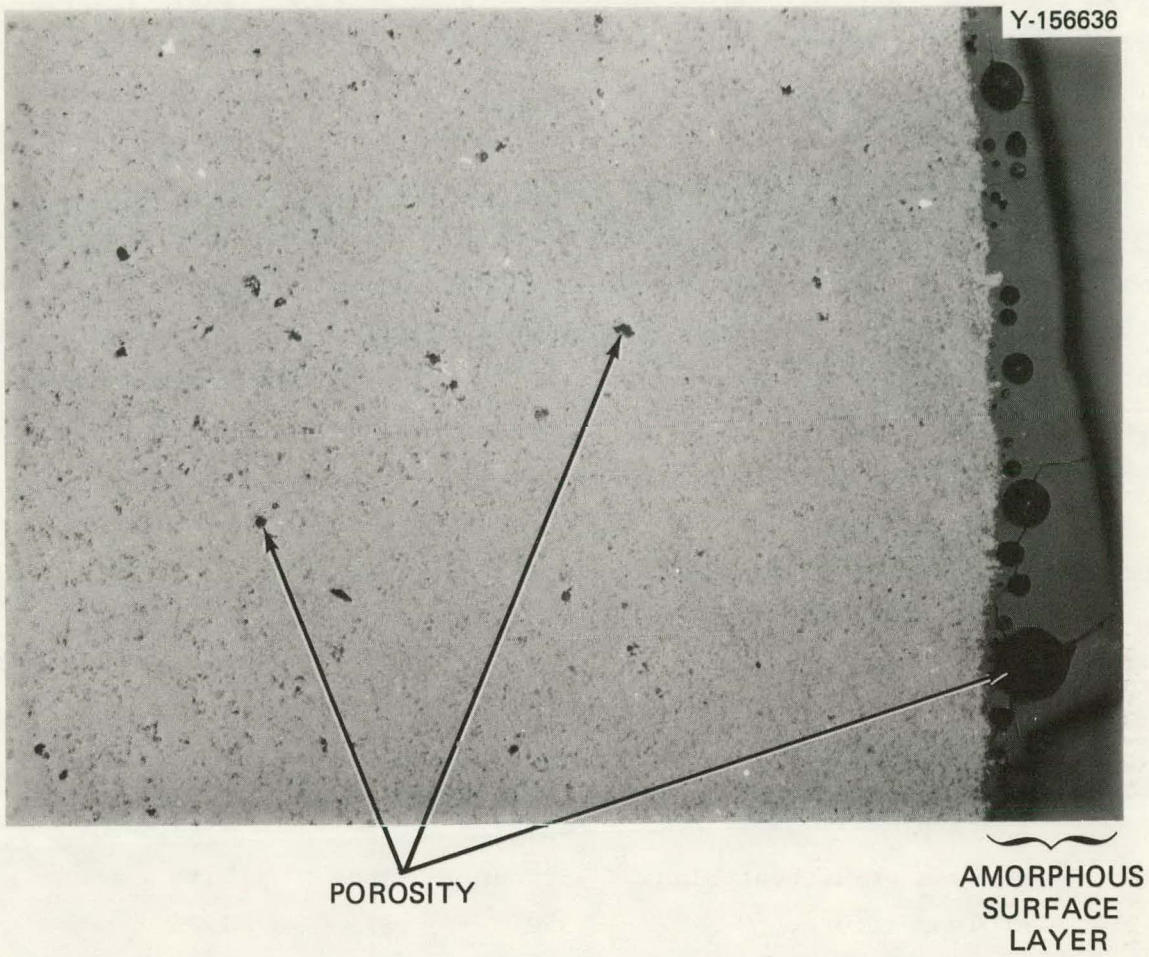

Fig. 49. Microstructure of Silicon Nitride (Sample 4) Exposed at 1225°C (2250°F) for 23 d with Glass in the Furnace.

that the surface section shown in Fig. 49 is close to the original centerline of the specimen. This observation and those on samples 1B and 3B suggest that the cross-sectional microstructural variation observed in these post-test cylindrical rod samples was not caused by the exposure environment or thermal conditions but rather was present in the as-manufactured material. Unfortunately, no archive material was available to substantiate this conclusion.

X-ray diffraction analysis results revealed that cristobalite (SiO_2) is the poorly developed crystalline phase present in the coating on sample 1B and that the coating on sample 4 was essentially amorphous with only one diffraction line attributable to cristobalite. These

results agree with the surface microstructures shown in Figs. 47 and 49, which had no well-defined crystalline phase in the surface coatings. The coating on sample 3B had optically observable crystalline phases, and the x-ray results indicated well-developed cristobalite and α-Fe_2O_3 phases plus unidentifiable peaks. These results agree with other reported oxidation studies of silicon nitride, wherein the nitride ceramic acquired an oxidation protective coating of amorphous SiO_2. The source of the iron to produce the Fe_2O_3 in the coating on sample 3B is unknown. It may have originated from the stainless steel samples tested in the same flue, from other furnace refractories, or from within the nitride ceramic itself.

Elemental analyses of the post-test coatings are given in Table 8. The high sodium content in the coating of sample 4 was anticipated because this sample was exposed to sodium from the glass melting process

Table 8. Compositional Analysis of Silicon Nitride Exposed to Glass Furnace High-Temperature Exhaust Stream

Sample	1B	3B	4
With or Without Glass	Without	Without	With
Temperature, °C	1350	1225	1225
Exposure, d	46	62	23
Content, wt %			
Si	31.14	30.49	29.08
Al	8.22	7.11	2.73
Na	9.83	1.20	20.04
Fe	0.68	7.32	2.75
K	0.78	1.23	1.08
Ca		0.96	
Ti	1.61	0.52	
Mg		1.26	
Ni		1.63	
Cr		0.73	0.21
O	47.7	47.5	44.1

via vapor transport and batch carryover. Since this sample experienced the highest corrosion and mass loss and the coating did not contain many of the other often deleterious impurities such as Ti, Mg, and Ni (see 3B) and had less than half the iron in sample 3B, we conclude that the sodium was a principal determinant of the stability of silicon nitride ceramics in this environment.

DISCUSSION OF RESULTS

Silicon Carbide

Resistance of silicon carbide ceramics to chemical attack and to reaction in oxidizing environments has been the subject of a considerable amount of investigation in recent years. The high melting point and low vapor pressure of silicon carbide give it exceptional stability at high temperatures in vacuum and inert atmospheres. It has also been found to be "stable" in oxidizing environments under certain conditions.

The stability of silicon carbide at high temperatures in oxidizing environments has been shown to be due to the formation of a dense protective silica film on the surface. The oxidation process obeys a parabolic dependence on time,[6] in which the rate can be quite low at temperatures in the range 1200 to 1500°C. The ability of the oxide film to form a contiguous protective layer is proposed in the literature to explain the oxidation resistance of silicon carbide in intermediate temperature ranges, where the oxidation rate is a minimum.[7] At temperatures above 1700°C, the weight loss of silicon carbide in oxidizing environments is reported[8] to vary linearly with time as a result of mass loss by evaporation of SiO. At 2000°C, the vapor pressure of silicon carbide, in fact, reaches about 1.3 Pa.[9]

Jorgensen et al.[10] indicated that oxidation of silicon carbide in oxygen is impeded because cristobalite forms at higher temperatures instead of vitreous silica, ostensibly because of a change in the diffusion rate of oxygen through the protective film. When atmospheric

moisture was present in the gas phase, as was the case in the current tests, the reaction rate through the vitreous silica increased by a factor of approximately 35 at 923°C. Similar data were not available for the effects of moisture on oxidation temperatures at which cristobalite formation is favored.

The correlation of these silicon carbide oxidation mechanisms with the material losses given in Table 5 (p. 37) was not straightforward. Oxidation of commercially available KT SiC in air has been reported to extend to a depth of 3 μm at 1000 to 1300°C in 100 h. In similar studies, so-called "pure" SiC oxidized slightly slower to produce an oxidation depth of 1.5 μm at 1300°C to 0.3 μm at 1000°C in 100 h in oxygen.[10-12]

The maximum observed corrosion in this study was 3 mm in 2500 h at 1225°C. If the reported experimental oxidation results on silicon carbide are linearly extended by a factor of 25 (from 100 to 2500 h), which is a pessimistic assumption because of the known parabolic oxidation dependence, the material conversion would amount to 75 μm, which is only 0.025 times the actual observed silicon carbide loss.

A more complex and destructive corrosion mechanism or combination of mechanisms in addition to oxidation is therefore required to explain the relatively high corrosion rate observed in this work at temperatures near 1200°C. Our observed silicon carbide losses were lower at the higher test temperatures. At test temperatures of about 1200°C the high corrosion rates may be a result of the formation of a vitreous film that either provides limited protective capability or actively reacts with the silicon carbide. At the higher temperatures, the formation of some other phase(s) may somehow reduce this reaction rate.

Results of the analyses of the x-ray diffraction patterns of samples exposed to glass in the furnace were discussed previously. The coating on sintered α-SiC sample 2, which was badly corroded, contained very little crystalline material, while the coating on sample 3 (1450 and 1550°C) contained a considerable quantity of crystalline phases. The KT sample 3 test at lower temperature (1225°C), which resulted in more material loss, had a coating containing poorly developed crystalline

phases, whereas the less extensively corroded KT-4 sample (1550°C) contained a considerable amount of crystalline material. The relative lack of development of crystalline phases in the coating of the samples tested at the lower temperature appears to correlate reasonably well with the greater observed corrosion.

Observed compositional differences in the sample coatings associated with different sample test locations and temperatures in the flue could also have a major influence in determining the various corrosion rates. Comparison of the microcompositional analysis of the coatings removed from the Vistal alumina ceramic exposed at high temperature (Fig. 32, p. 52, 1400 and 1450°C, sample Vistal 2) with those formed at lower test temperatures (Figs. 33 and 34, 1150°C, Vistal 4) and at higher temperatures on NC-430 SiC (sample 2 at 1450°C, in Fig. 11, p. 24) clearly indicates that the coatings formed on samples tested at lower temperatures contain much higher sodium, potassium, and iron concentrations. The well-established "fluxing" ability and solubility of these species in siliceous melts could explain the increased attack at lower temperatures. This could be particularly true if the silicate melt films formed had lower viscosities at a given temperature than the corresponding relatively pure vitreous silica film. A reduction in the viscosity of the protective film would increase the diffusion of various ionic species and hence probably increase the reaction rates.

Reported investigations of the corrosion of silicon carbide by alkali salts in various partial pressures of oxygen support this phenomenological explanation of the observed results. The normally excellent oxidation resistance of silicon carbide derived from formation of a contiguous silicon dioxide coating has been observed to change to other modes of behavior under certain conditions, including accelerated corrosion in the presence of oxides.[8,13,14] McKee and Chatterji[14] found that basic oxides can dissolve the protective SiO_2 coating on silicon carbide to form silicates with accelerated corrosion. Additionally, when the oxygen partial pressure at the SiC interface with the coating is below a certain value, active oxidation can occur, forming gaseous species at the interface. This process results in rapid corrosion, particularly

if the evolved gaseous species can react with a silicate-forming melt.[14-16] This behavior was observed for silicon carbide at temperatures as low as 900°C when alkaline salt melts were present.

The blisters and bubble formation observed on the silicon carbide samples in this study are indicative of gaseous evolution from active oxidation at low oxygen partial pressures.[14] Gaseous SiO and CO are formed at the interface betwen the SiO_2 layer and the SiC surface according to the equation

$$SiC + O_2 \rightarrow SiO(g) + CO(g) .$$

The ability of these gases to pass through the protective silica layer as they are generated depends upon the viscosity of the layer. As sodium (or other alkali) is added to the silica from condensation from the flue gas stream, the viscosity decreases dramatically. This increased fluidity permits more rapid release of the gaseous SiO and CO and more rapid diffusion of O_2 through to the interface to react with freshly exposed SiC and increase the rate of material loss and conversion. As temperature is increased and less alkali condenses on the silica layer, the film viscosity remains high and gaseous transport is impeded. If viscosity is sufficiently high, the silica acts as an effective oxidation protective barrier to limit corrosion once initial oxidation has occurred.

Recent work by other investigators would support our hypothesis that sodium contamination of the protective silica film is the critical degradation mechanism.[17] Pierson and Hanna[18] reported that the most prevelant species present in typical glass melting furnace flue gas streams is Na_2SO_4, which melts at 843°C and forms a eutectic at 800°C with 72 mol % SiO_2. The protective SiO_2 layer is thus easily attacked by Na_2SO_4 to form a relatively low-viscosity liquid, which flows readily from the silicon carbide surface and continually exposes new surface to the gas stream. Additionally, Smith[17] has reported that the protective SiO_2 film that forms on SiC at 1200°C, if contaminated with impurities such as iron and alumina, becomes too fluid at higher temperatures to

provide adequate protection for the silicon carbide. These observations are consistent with our observations that very thin vitreous films were found on those tubes with high corrosion rates whose post-test coatings had the highest sodium contents. Thicker, partially crystallized coatings were found on the less corroded samples whose coatings had lower sodium contents.

These conclusions cause considerable concern over the potential for utilization of silicon carbide ceramics in oxidizing environments containing sodium, particularly at temperatures above about 800°C. These temperature and atmosphere conditions include those common to many of the proposed applications of this material, particularly in ceramic heat exchangers. The presence of alkalies from hot topping compounds used in steel soaking pits as well as from soda-lime glass production and in various dirty fuel ashes and slags requires a critical determination of the suitability of silicon carbide ceramics in new or advanced applications.

Alumina

The higher purity alumina ceramics were more stable in the furnace tests than the less pure alumina ceramics, which contained silica as a major impurity. The Vistal ceramic was unquestionably the most stable alumina ceramic tested relative to its resistance to corrosion by species from the glass melting process. Sodium carbonate, caustic soda, and sodium peroxide can reportedly be fused in higher purity alumina vessels with little observed reaction.[19] It follows that high-purity alumina is resistant to the degradation by sodium compounds at moderately high temperatures in this environment.

The presence of even small amounts of certain impurities in alumina ceramics, particularly silica, strongly affects the high-temperature mechanical properties and the resistance to corrosion. The performance of 85% Al_2O_3 compositions was unacceptable, even at 1150°C (2250°F). Ceramics with purity levels of 94% Al_2O_3 had somewhat improved behavior, but the material is clearly not a serious structural material candidate

for use at 1400°C (2550°F) in a glass furnace environment. Alumina ceramics of 99.8% Al_2O_3 showed significant performance improvement such that use temperatures of about 1400°C (2550°F) would be marginal for long-term exposure in these environments. The >99.8%-pure Vistal material performed satisfactorily even up to 1450°C (2650°F).

The present high cost of Vistal-type aluminas and the relatively good performance of silicon carbides at very high temperatures, 1300 to 1550°C under conditions where alkalies do not concentrate in the oxidation protective coating, suggests that ceramic heat exchangers constructed of both materials may be a cost effective design approach. Use of silicon carbide at temperatures in the range 1400 to 1550°C, under low alkali deposition conditions would be effective in the hotter portion of a waste heat recovery heat exchanger. Commercial high purity aluminas are not recommended at such high temperatures because of their high creep rates. Use of alumina ceramics such as AD-998 in regions where the potential for alkali deposition is higher and service temperatures are lower (about 1350°C) may be a very feasible design approach to a recuperator for use in these environments.

Mullite and Cordierite

As described in some detail in the results section, both mullite ($3Al_2O_3 \cdot 2SiO_2$) and cordierite ($2MgO \cdot 2Al_2O_3 \cdot 5SiO_2$) were unsatisfactory for use in glass furnace environments, even at temperatures as low as 1150°C. The mullite material was the better of the two, with microstructural modification occurring at 1150°C, which would be anticipated to lead to failure in service times too short to provide economically viable heat recovery systems. Cordierite was so severely attacked, even at 1150°C when glass was present in the furnace, that it is unsuitable for use in this environment.

The standard mullite refractories that are available[20,21] are usually made by adding alumina to available clays to approximate the required bulk composition of mullite after the ceramic is fired during fabrication. These bodies are subject to considerable chemical attack

under conditions of the tests reported here, because of the nature of the bonding phase, which gives these materials their mechanical integrity. More recently introduced mullites are fabricated by adding alumina to previously synthesized "mullite," which is somewhat high in silica, with finely divided mullite as a bonding material. These mullite ceramics can be of very high purity, contain at least 70% Al_2O_3, and have been found to be superior to some more expensive clay-bonded aluminas.[19]

These materials have found extensive use in crucibles for melting corrosive materials and in slagging environments as well as in the glass industry, particularly in use for borosilicate glass manufacturing environments, where fluxing by the alkalies present in soda-lime glasses is not a problem. These materials could, therefore, possibly be used at lower temperatures in heat recovery systems for carefully selected applications not requiring the alkali resistance of pure aluminas.

Cordierite has been found in other investigations, including industrial recuperator demonstration projects, to be unsuitable for use in glass furnace applications.[22] In view of its high silica content, low refractoriness, and low-temperature eutectics with alkalies and silicates, this conclusion is not surprising.

Silicon Nitride

The performance of silicon nitride in these tests was analogous to that observed for silicon carbide. The silicon nitride samples showed dramatically increased corrosion at lower temperatures when high levels of sodium were present in the surface deposits. This situation was apparently aggravated by considerable microstructural variation across the sample cross section in the particular silicon nitride selected for the tests. Some component appeared to be selectively removed from the nitride during test exposure, although the nitride was reported to be primarily Si_3N_4.

A considerable body of literature has recently evolved out of development efforts to utilize silicon nitride as a high-temperature load-bearing structural ceramic material. The efforts have only recently been

directed towards improved understanding of the high-temperature oxidation and corrosion properties. Recent oxidation studies of Si_3N_4 have shown that on exposure to oxygen at high temperature this material forms a protective coating, which remains coherent for several hundred hours below 1350°C. Above 1350°C the coating spalls for oxidation times exceeding 20 to 30 h.[23-25] It was also found that oxidation is controlled by inward oxygen diffusion through the coating with subsequent release of $N_2(g)$ at the nitride-coating interface. This release of N_2 causes bubbles that can expand with sufficient pressure to cause film rupture. The corrosion scale formed contained large amounts of $MgSiO_3$ resulting from preferential diffusion of magnesium through the film from the substrate. Magnesium is used in fabricating some types of silicon nitride ceramics. The formation of multicomponent silicates substantially decreased the oxidation resistance of silicon nitride ceramics at temperatures at which the film exists essentially as a liquid.

These observations coincide with the observation of selective removal of a major component from the nitride in the severely attacked samples examined in this study. The deleterious effect of the alkalies on the protective silicate film occurs apparently in the same manner as that observed on silicon carbide.

Silicon nitride would therefore appear to have no advantage over silicon carbide for high-temperature heat-recovery systems with environments similar to those reported here. In fact, if the processing difficulties demonstrated by the observed microstructural variation in the test samples are considered, silicon carbide is a significantly more attractive material candidate. This is especially true considering the selective removal of the grain boundary phase from the Si_3N_4 observed during the test and the deleterious effect on the protective film.

CONCLUSIONS

1. Silicon carbide exposed to glass furnace exhaust gases showed enhanced corrosion at lower temperatures (1150°C) when alkalies were deposited on the carbide. Corrosion at higher temperatures (1540°C) without alkali deposition was significantly less.

2. Alumina corrosion in glass-furnace exhaust gas depends strongly upon the purity and density of the ceramic material. The lowest corrosion rate observed for all materials was for Vistal high-density, high-purity (>99.8% Al_2O_3) alumina. Alumina contents of less than 99.8% Al_2O_3 were unsatisfactory above 1400°C.

3. Mullite and cordierite are generally unacceptable for application in soda-lime glass melting environments for temperatures above 1100°C.

4. Reaction-bonded silicon nitride exhibits behavior inferior to silicon carbide in soda-lime glass furnace flue environments and displays a similar corrosion rate dependence with temperature and a similar sensitivity to accelerated corrosion because of alkalies in the protective film.

5. Materials that rely upon either a protective SiO_2 film (such as SiC or Si_3N_4) or an extensive silicate bonding phase (such as cordierite, mullite, and aluminas with $\leq$94% Al_2O_3) were severely corroded by the fluxing action of alkalies and iron in the test environment. These substances increase the fluidity of the siliceous film, resulting in unacceptable degradation and material loss.

ACKNOWLEDGMENTS

The authors would like to express their appreciation to W. H. Warwick for metallography and sample prepartion, T. J. Henson for SEM and EDS analyses, H. Keating for sample preparation and handling, J. W. Nave for photography, and O. B. Cavin and L. D. Hulett for x-ray diffraction and fluorescence analysis.

The cooperation of D. Power of Terra Tek, Inc., of Salt Lake City, Utah, in providing the exposed samples and their exposure histories is gratefully acknowledged. The assistance of P. Hastings of Millcreek Glass Company of Salt Lake City, Utah, in conducting the exposure testing and construction of the special day tank furnaces is similarly appreciated. The support of J. W. Osborne and J. Eustis of the Department of Energy made the work possible.

The authors also appreciate the assistance of G. C. Wei and E. L. Long, Jr., for review of the report for technical content and providing many valuable comments, Sigfred Peterson for editorial review, and Denise Campbell for report preparation.

REFERENCES

1. Energy and Environmental Analyses, Inc., *Energy Consumption in the Industrial Section — Data Sources for 1974 Consumption,* prepared for the Federal Energy Administration (January 1976).
2. J. R. Shorr et al., *Industrial Energy Study of the Glass Industry,* prepared for the Federal Energy Administration by Battelle Memorial Institute (December 1974).
3. Robert Drake, Glass Packaging Institute, private communication to Terra Tek Corp., August 1977.
4. Terra Tek, Inc., Salt Lake City, Utah, *High Temperature Range Recuperator, Phase I, 1st Quarterly Report,* TR 77-104 (Nov. 15, 1977).
5. *The Use and Conservation of Natural Gas in the Glass Industry,* Dynatech Report 1381 (January 1976).
6. R. F. Adamski, "Oxidation of Silicon Carbide in the Temperature Range 1200—1500°C," *J. Phys. Chem.* 63: 305—07 (1959).
7. J. H. Westbrook and E. R. Stover, "Carbides for High Temperature Applications," pp. 312—48 in *High Temperature Materials and Technology,* I. E. Campbell and E. M. Sherwood, eds., Wiley, New York, 1967.
8. C. Ervin, Jr., "Oxidation Behavior of Silicon Carbide," *J. Am. Ceram. Soc.* 41: 347—52 (1958).
9. O. Ruff, "The Formation and Dissociation of Silicon Carbide," *Trans. Electrochem. Soc.* 68: 87—109 (1935).
10. P. J. Jorgensen, M. E. Wadsworth, and I. B. Cutler, "Oxidation of Silicon Carbide," *J. Am. Ceram. Soc.* 42: 613—16 (1959).
11. K. M. Taylor, "Improved Silicon Carbide for High Temperature Points," *Mater. Methods* 44: 92—95 (October 1956).
12. "'KT' Silicon Carbide," Advanced Materials Technology 3, No. 1, 6—7 (1960), the Carborundum Company.
13. R. H. Arendt and M. J. Curran, "Corrosion of Dense Silicon Carbide in Basic Molten Salt Solutions" (abstract), *J. Electrochem. Soc.* 122: 96C (1975).

14. D. W. McKee and D. Chatterji, "Corrosion of Silicon Carbide in Gases and Alkali Melts," *J. Am. Ceram. Soc.* 59(9): 441–44 (1976).

15. E. A. Gulbransen and S. A. Jansson, "High Temperature Oxidation, Reduction and Volatilization Reactions of Silicon and Silicon Carbide," *Oxid. Met.* 6: 181–201 (1972).

16. J. E. Antell and J. B. Wallurton, "Oxidation of Silicon and Silicon Carbide in Gaseous Atmospheres at 1000–3000°C," in *Reactions Between Gases and Solids* (Proc. Conf. Advisory Group for Aerospace R and D, Paris), AGARD-CP-52, AD-702657 (February 1970).

17. J. M. Smith, "Selection of Materials," pp. 131–51 in *High Temperature Materials and Technology,* I. E. Campbell and E. M. Sherwood, eds., Wiley, New York, 1967; see p. 144.

18. W. R. Pierson and W. T. Hanna, Battelle Columbus Laboratory, private communication, Jan. 9, 1979.

19. S. W. Bradstreet, "Oxide Ceramics," pp. 235–303 in *High Temperature Materials and Technology,* Wiley, New York, 1967.

20. G. R. Remmey, "Upper Useful Limits of Commercial Superrefractories," *Am. Ceram. Soc. Bull.* 27(12): 477–85 (1948).

21. C. B. Remmey, "New Alumina-Silica Refractories," *Chem. Eng. Progr.* 44(12): 943–46 (1948).

22. K. Kohnken, GTE-Sylvania, Torwanda, Pennsylvania, personal communication, November 1978.

23. W. C. Tripp and H. C. Graham, "Oxidation of Si_3N_4 in the Range 1300 to 1500°C," *J. Am. Ceram. Soc.* 59(9–10): 399–403 (1976).

24. A. J. Kiehl et al., "Oxidation Behavior of Hot-Pressed Si_3N_4," *J. Am. Ceram. Soc.* 58(1–2): 17–20 (1975).

25. R. Kossowsky and S. C. Singhad, pp. 275–87 in *Grain Boundaries in Engineering Materials,* J. L. Walter, J. H. Westbrook, and D. A. Woodford, eds., Claitor's, Baton Rouge, La., 1975.

THIS PAGE

WAS INTENTIONALLY

LEFT BLANK

APPENDIX

THIS PAGE

WAS INTENTIONALLY

LEFT BLANK

Table A1. X-Ray Diffraction Analysis of Milky Surface Coating on Silicon Carbide NC-430-1 Exposed at 1450°C for 104 d

Observed		JCPDS 11-695 α-Cristobalite	
d, pm	I/I_0	d, pm	I/I_0
402.57	100	405	100
336.68	2	353	4
312.79	10	314	12
283.90	11	284.1	14
268.16	1		
248.34	19	248.5	20
219.62	4		
211.74	5	211.8	6
202.10	5		
201.76	5	201.9	4
194.00	4		
193.02	6	192.9	6
187.72	5	187.0	8
187.22	6		
170.04	3		
169.69	4		
169.37	4		
169.23	4	169.0	4
161.27	6	161.2	6
161.04	6		
153.61	4	153.3	4
152.08	3		
149.68	4	149.4	6
143.40	5	143.1	44
136.99	3		
136.75	3	136.5	4

Table A2. X-Ray Diffraction Analysis of Brown Scale 10 mm from End on Silicon Carbide KT-1B Exposed at 1350°C for 116 d

Observed		JCPDS 22-1319 α-SiC-21R		JCPDS 22-1273 α-SiC-6H	
d, pm	I/I_0	d, pm	I/I_0	d,pm	I/I_0
512.59	5				
486.98	5				
408.63	94				
318.21	13				
312.63	12				
262.34	19	263	70	262.1	40
257.03	4				
251.17	100	253	100	251.1	100
235.56	15	235	10		
220.29	4				
217.61	16	217	10		
214.25	3				
205.61	7				
204.66	7				
203.83	7				
202.64	9				
201.91	7	201	30		
201.01	7				
199.79	5				
191.78	8				
163.30	8	162	10		
163.01	8				
154.24	39				
153.99	79	154	80	153.7	35
145.04	5				
142.13	7	144	30		
131.47	24	131.1	70	131.1	40
129.03	4	129.3	10	128.6	15
125.85	4	125.9	30	125.6	7
124.59	8	125.9	30		
109.02	4	108.9	20		
108.74	4			108.7	15
100.01	7			100.4	15
99.80	5	099.9	50		
98.95	5	098.6	20		
97.55	6			097.3	15
97.27	4	097.3	40		

Table A3. X-Ray Diffraction Analysis of White Foam Scale 25 mm from Exposed End of Silicon Carbide NC-430-2 Exposed at 1450°C for 104 d With Glass

Observed		JCPDS 4-0379 SiO_2 α-Cristobalite	
d, pm	I/I_0	d, pm	I/I_0
504.16	4		
457.68	4		
424.51	7		
400.96	100	404	100
311.57	22	313.8	12
309.91	22		
282.86	19	284.5	14
247.48	39	248.9	18
217.72	3		
207.27	3	212.1	4
196.50	90	193.2	4
191.51	7	187.4	4
168.78	4	169.2	3
163.36	5	164.2	1
160.92	6	161.2	5
153.72	3	153.5	2
153.27	3		
152.86	3		
149.29	3	149.5	3
143.42	3	143.2	2
143.01	3	142.3	1
124.49	4	123.5	<1

Table A4. X-Ray Diffraction Analysis of Bluish-White Deposits 15 mm from Exposed End of Silicon Carbide KT-4 Exposed at 1540°C for 69 d With Glass

Observed		JCPDS 4-0379 SiO_2 α-Cristobalite		JCPDS 18-1170 Tridymite	
d, pm	I/I_0	d, pm	I/I_0	d, pm	I/I_0
815.95	7				
507.55	5				
432.81	60			433	90
429.63	84			411	100
427.62	100				
404.94	78	404	100		
401.96	60			387	20
379.74	57			382	50
323.51	8			325.0	4
312.08	10	313.8	12	312.6	<1
295.76	18			297.5	30
282.97	13	284.5	14		
276.92	7			277.6	8
261.76	5				
249.02	23	248.9	18	249	10
248.31	25			250	20
247.37	20	246.8	6		
230.36	11	234.2	<1	231	20
229.65	11			229.4	2
211.42	6	212.1	4	211.7	4
208.95	8				
208.52	10			208.6	8
208.25	8				
193.02	7	193.2	4		
192.55	8				
187.08	6	187.4	4	187.4	2
186.98	6				
172.94	5	173.6	1		
169.21	9	169.2	3	169.5	12
168.84	9				
163.07	7	164.2	1	163.5	8
160.92	8	161.2	5	160.0	10
154.23	5			154.6	2
153.88	10	153.5	2		
152.97	0			153.4	10
149.24	5	149.5	3		
143.97	6	143.2	2		
142.99	5	142.3	1		
140.27	3				
140.12	5	140.1	1		
139.94	6				
136.25	5	136.8	1		
135.09	5	135.3	1		
133.65	3	133.6	1		
130.71	4	130.1	2		
124.59	4	123.5	<1		
122.95	4				
115.49	4	115.56	<1		
109.69	4	109.89	3		

Table A5. X-Ray Diffraction Analysis of Grayish Surface Material 30 mm from Exposed End of Silicon Carbide KT-3 Exposed at 1225°C for 69 d With Glass

Observed		JCPDS 4-0379 SiO_2 α-Cristobalite		JCPDS 18-1170 SiO_2, Tridymite		JCPDS 1-1064 $Na_4Ca(SiO_3)_3$	
d, pm	I/I_0	d, pm	I/I_0	d, pm	I/I_0	d, pm	I/I_0
877.95	24						
762.68	18						
705.23	12						
428.10	58			433	90		
406.38	95	404	100	411	100	410	20
401.74	100						
392.23	24						
379.81	40			382	50	379	20
332.41	40					328	5
312.08	76	313.8	12	298	30		
248.47	56	248.9	18	250	20	268	100
227.46	24	234.2	<1	231	20		
202.30	22	202.4	3				
201.44	24						
191.66	42	193.2	4			189	60
179.45	20					180	10
165.29	22						
163.73	36	164.2	1				
163.26	37					162	20
161.03	19	161.2	5				
154.35	20	153.5	2			154	50
151.72	20						
145.89	18						
143.82	20					144	20
143.17	18	143.2	2				
139.90	08					139	10
137.19	25						
137.02	25	136.8	1				
135.02	25	135.3	1			134	40
124.55	32	123.5	<1			122	10
124.24	24						
110.82	34	111.12	1			114	10
110.53	22					111	10

Table A6. X-Ray Diffraction Analysis of Silicon Carbide KT-2 Exposed at 1350°C (47 d) and 1425°C (48 d) With Glass

Observed 40 mm from end		JCPDS 11-695 SiO_2 α-Cristobalite		JCPDS 22-1319 SiC-21		JCPDS 1-1064 $Na_4Ca(SiO_3)_3$		Whitish Deposit 30 mm from End	
d, pm	I/I_0	d, pm	I/I_0	d,pm	I/I_0	d, pm	I/I_0	d, pm	I/I_0
632.6	9							534.9	28
403.7	25					410	20	404.0	95
401.2	38	405	100			379	20		
399.6	43							403.1	100
367.0	9							407.7	44
350.4	5								
344.0	10								
328.8	24	314	12			328	5	337.6	64
296.4	4								
279.5	7	284.1	14						
264.8	6								
		263	70	268	100	268.5	36		
258.4	6								
252.0	12							253.6	32
251.1	19	248.5	20	253	100			253.8	32
245.7	10	246.5	6	247	20				
217.7	10					210	10	220.3	40
209.0	6	211.8	6					211.9	28
205.2	6	201.9	4	201	30				
199.5	8	192.9	6					202.3	26
168.9	10	169.0	4	166	10				
159.0	5	160.0	4	162	10			159.8	16
154.1	37					154	50	152.4	32
153.6	17	153.3	4	154	80				
152.4	9			151	20				
146.1	7			144	30	144	20	144.0	22
144.9	5	143.1	44						
141.3	5	142.3	1	141	20	139	10		
134.9	7	134.5	1	133.7	10	134	40	134.6	20
132.2	6	133.3	4	131.1	70			133.6	20
126.9	4	128.1	4	125.9	30			127.7	18
120.2	4	120.6	4						
119.7	100					122	10		
119.4	41	118.8	2			119	30		
114.6	3	115.6	4			114	10	109.96	16
101.2	4					101	20		
96.8	36			97.3	40			97.66	13
93.5	20			96.2	10				

Table A7. X-Ray Diffraction Analysis of Yellowish Foamed Deposit 30 to 40 mm from the End of Silicon Carbide NC-400-1 Exposed at 1400°C for 116 d Without Glass

Observed		JCPDS 11-695 SiO_2 α-Cristobalite		JCPDS 4-0379 SiO_2, α-Cristobalite	
d, pm	I/I_0	d, pm	I/I_0	d, pm	I/I_0
532.24	4				
402.16	100	405	100	404	100
337.92	5				
335.41	5	353	4		
312.63	6	314	12	313.8	12
283.83	9	284.1	14	284.5	14
268.31	3				
265.94	3				
251.84	4				
248.83	16	248.5	20	248.9	18
219.28	4				
211.15	5	212.8	6	212.1	4
202.69	4	201.9	4	202.4	3
193.25	4	192.9	6	193.2	4
187.65	4				
187.36	5	187.0	8	187.4	4
170.02	4				
169.10	4	169.0	4	169.2	3
162.42	5	163.4	2	164.2	1
161.86	5				
161.23	7	161.2	6	161.2	5
152.07	3	153.3	4	153.5	2
143.61	4				
143.28	4	143.1	44	143.2	2
110.33	2			111.12	1
110.09	2			109.98	3

Table A8. X-Ray Diffraction Analysis of Foamed Deposit 5 mm from the End of Silicon Carbide NC-400-1 Exposed at 1400°C for 116 d with Glass

Observed		JCPDS 11-695 SiO_2 α-Cristobalite	
d, pm	I/I_0	d, pm	I/I_0
494.8	2		
405.7	100	405	100
312.4	8	314	12
284.0	9	284.1	14
248.5	24	248.5	20
212.0	5	211.8	6
204.0	5	201.9	4
192.5	5	192.9	6
187.1	5	187.0	8
169.2	3	169.0	4
162.7	8	163.4	2
161.8	8	161.2	6
153.4	4	153.3	4
149.5	3	149.4	6
144.5	6	143.1	44
136.5	4	136.5	4
129.9	3	129.9	4
128.2	3	128.1	4
123.1	2	123.3	2
120.6	2	120.6	4
113.4	10		
109.7	2		
107.9	2		

Table A9. X-Ray Diffraction Analysis of Surface Coating on Sintered Alpha Silicon Carbide Sample Exposed at 1450°C for 36 d and 1425°C for 44 d Without Glass

Observed		JCPDS 4-0379 SiO_2 α-Cristobalite	
d, pm	I/I_0	d, pm	I/I_0
402.5	100	404	100
339.16	8		
335.85	8	314	12
283.90	13	284.5	14
267.85	7		
267.09	7		
247.76	22	248.5	18
219.16	3		
210.59	8	212.1	4
210.34	8		
201.66	5	202.4	3
192.66	9	193.2	4
187.51	8	187.4	4
186.65	8		
169.14	6	169.2	3
168.72	6		
160.90	6	161.2	5
153.43	3	153.5	2
151.92	3		
151.71	3		
149.52	5	149.5	3
143.68	4	143.2	2
142.88	6	142.3	1
142.11	3	140.1	1
139.94	3	140.1	1
136.92	4	136.8	1
136.54	3		
136.15	3		
128.09	4	128.2	2
118.47	4	118.4	2
117.68	3	117.62	1
110.0	4	111.12	1
110.00	4	109.89	3

Table A10. X-Ray Diffraction Analysis of Surface Coating on Sintered Alpha Silicon Carbide Sample 2 Exposed at 1450°C for 4 d and 1550°C for 17 d With Glass

Observed		JCPDS 11-695 SiO_2 α-Cristobalite		JCPDS 4-0379 SiO_2, α-Cristobalite	
d, pm	I/I_0	d, pm	I/I_0	d, pm	I/I_0
398.17	100	405	100	404	100
310.11	9	314	12	314	12
281.43	16	284.1	14	284.5	14
246.44	12	240.5	20	248.9	18
245.32	8	246.5	6	246.8	6
244.81	8				
210.50	3	211.8	6	212.1	4
200.93	4	200.9	4	202.4	3
192.87	6	192.9	6	193.2	4
192.08	18	192.9	6	193.2	4
186.23	8	187.0	8	187.4	4
172.35	2	173.0	2	173.6	1
168.31	3	169.0	4	169.2	3
160.51	5	161.2	6	160.4	2
152.75	4	153.3	4	153.5	2
149.08	4	149.4	6	149.5	3
142.71	4	143.1	44	143.2	2
139.45	4	139.8	4	140.1	1
136.19	5	136.5	4	136.8	1
133.08	4	133.3	4	133.6	1
129.57	3	129.9	4	130.1	2
127.83	3	128.1	4	128.2	2
109.50	5	118	2	109.89	3

Table All. X-Ray Diffraction Analysis of Chemically Vapor Deposited Silicon Carbide Sample 1 Exposed at 1540°C for 116 d Without Glass

Observed		JCPDS 13-651 Fe-Si-C		JCPDS 4-0379 SiO_2, α-Cristobalite	
d, pm	I/I_0	d, pm	I/I_0	d, pm	I/I_0
729.9	100	724	100		
540.7	3				
530.1	5				
470.8	8	448	20		
405.9	8	441	20	404	100
371.3	2				
341.1	2				
332.3	18	360	100	313.8	12
280.5	3	308	50	284.5	14
266.5	3				
251.0	3			248.9	18
236.2	4	240	50		
227.6	4				
200.0	2	203	50	202.4	3
188.1	4			187.4	4
177.1	2			175.6	1
174.9	2			173.6	1
171.5	2			169.2	3
162.5	3			161.2	5
148.7	2			149.5	3
144.3	1			143.2	2
141.8	1			142.3	1
131.6	1			133.6	1
128.7	1			128.2	2
117.5	1			117.6	1
115.2	1			115.5	<1

Table A12. X-Ray Diffraction Analysis of Chemically Vapor Deposited Silicon Carbide Sample 2 Exposed at 1550°C for 70 d With Glass

Observed		JCPDS 11-695 SiO_2 α-Cristobalite	
d, pm	I/I_0	d, pm	I/I_0
516.0	3		
454.0	3		
447.3	3		
401.4	100	405	100
337.7	6	353	4
334.7	8		
324.8	6	314	12
310.7	6	314	12
302.5	4		
282.7	12	284.1	14
277.9	4		
267.1	3		
248.9	7	248.5	20
247.6	13	248.5	20
246.3	23	246.5	6
217.0	6	211.8	6
208.8	6	201.9	4
199.0	7	192.9	6
190.0	6		
185.2	6	187.0	8
184.5	6		
166.9	5	169.0	4
166.3	6	163.4	2
158.9	9	160.0	4
158.5	9	161.2	6
151.2	5	153.3	4
149.5	5	149.4	6
146.9	5		
140.8	6	141.9	4
134.6	5	134.6	<2
134.2	6	133.3	4
132.1	4		
130.8	4	129.9	4
128.7	5		
127.5	4	128.1	4
125.7	4		
123.9	3		
121.9	3	121.8	4

Table A13. X-Ray Diffraction Pattern of Chemically Vapor Deposited Silicon Carbide Sample 3 Exposed at 1225°C for 92 d Without Glass

Observed		JCPDS 11-695 SiO_2 α-Cristobalite		JCPDS 3-826 $Ca_3Al_2Si_3O_{12}$	
d, pm	I/I_0	d, pm	I/I_0	d, pm	I/I_0
753.3	6				
622.1	9				
427.6	10				
404.5	100	405	100		
361.0	8	353	4		
339.3	8				
330.9	8				
309.8	12	314	12		
293.3	42			296	80
291.5	27				
283.3	17	284.1	14		
265.9	21			265	100
248.7	100	248.5	20		
242.5	8			244	60
218.6	8				
215.7	10			216	60
207.3	19	211.8	6		
202.3	11				
190.9	7	192.9	6	192	70
186.3	7	187.0	8		
182.7	10				
168.4	14	169.0	4		
165.3	5			165	80
161.9	10	161.2	6		
160.3	19	160.0	4		
159.8	18			158	90
152.7	13	153.3	4		
147.2	22	149.4	6		
144.6	12	143.1	44		
142.2	7	141.9	4		
139.1	10	139.8	4		
130.6	10	129.9	4		
127.3	6	128.1	4		
125.6	5	124.2	<2		
118.5	8	118.3	2		

Table A14. X-Ray Diffraction Analysis of High-Purity Vistal Alumina Sample 1 Exposed at 1400°C for 7 d and 1450°C for 105 d Without Glass

Observed		JCPDS 11-695 SiO_2 α-Cristobalite	
d, pm	I/I_0	d, pm	I/I_0
346.67	30	348	80
254.42	71	255	90
237.11	61	238	40
216.10	1	216.5	<1
208.14	94	209	100
173.98	35	174	50
159.94	100	160	80
151.36	6	151.4	6
140.43	34	140.4	30
140.23	54	140	30
137.28	61	137	50
133.56	2	133.7	2
127.53	2	127.6	4
123.93	8	123.9	16
123.43	13	123.43	8
119.30	1		
118.94	3	118.98	8
116.03	1	116.00	<1
114.74	4	114.70	6
112.43	8	112.55	6
109.96	6	109.88	8
108.26	9	108.31	4
107.99	6		
107.80	9	107.81	8
104.29	25	104.26	14
101.75	11	101.75	2
99.82	13	99.76	12
98.29	1	98.19	4

Table A15. X-Ray Diffraction Analysis of Brown Coating 5 mm from the End of High-Purity Vistal Alumina Sample 2 Exposed at 1400°C for 11 d and 1450°C for 146 d With Glass

Observed		JCPDS Standards					
		$NaCa_4Al_3O_9$		$FeO \cdot (Cr,Al)_2O_3$		$CaO \cdot 2FeO$	
d, pm	I/I_0	d, pm	I/I_0	d, pm	I/I_0	d, pm	I/I_0
322.84	24			295	60		
322.39	24						
243.25	12						
242.64	12						
241.09	45	267	100	252	100	259	40
226.83	10						
225.80	28	219	80	207	70	224	100
225.24	14						
199.56	39	191	80				
167.96	27						
155.05	100	155	100	160	90	159	80
136.80	48	134	60	146	90	135	50
133.94	26			110	60		
121.25	7	121	60				
120.96	6						
120.53	9						
116.63	5						
112.58	6					112	20
106.06	3					103	30
102.69	7	102	60			100	50
98.42	11			85	60	92	50

Table A16. X-Ray Diffraction Analysis of Brown Coating 40 mm from the End of High-Purity Vistal Alumina Sample 4 Exposed at 1150°C for 90 d With Glass

Observed		JCPDS Standards							
		α-Al_2O_3		$Na_2ZnSiO_4 \cdot H_2O$		$Na_2Ca_2(SiO_3)_3$		$Na_4Ca(SiO_3)_3$	
d, pm	I/I_0	d, pm	I/I_0	d,pm	I/I_0	d, pm	I/I_0	d, pm	I/I_0
435.29	10					443	10		
418.21	63							410	20
371.62	27					378	30	379	20
351.38	10	347.9	75						
334.63	21								
330.22	52					337	50	328	5
301.29	8								
290.34	14			293	50				
279.34	5			272	30				
265.58	100					265	100	268	100
261.44	77			262	50				
256.70	66			256	100				
254.61	13	255.2	90						
252.48	7					252	5		
245.52	5								
234.42	10					236	10	237	10
227.09	25					225	5		
223.29	5								
214.13	11					215	5	218	10
208.27	11	208.5	100						
186.61	92					187	60	189	60
181.93	13								
180.22	10					180	10		
179.74	10			175	10				
177.62	5							180	10
173.52	5	174.0	45			174	10	172	5
164.76	6					164	10		
161.82	7	160.1	80					162	20
154.54	22					155	20	154	50
151.99	19					152	30		
148.61	14								
148.49	14								
146.91	5								
139.58	6	137.4	50			139	80	134	40
133.24	5					133	20		
133.00	4								
131.07	4					130	20		
118.82	5					133	20	122	10
117.63	5					118	10	119	30
117.33	4					113	20		
101.27	4					101	10		
99.16	4					099	20		
98.99	4								

ORNL/TM-6970

INTERNAL DISTRIBUTION

1–2. Central Research Library
3. Document Reference Section
4–5. Laboratory Records Department
6. Laboratory Records, ORNL R.C.
7. ORNL Patent Section
8. R. A. Bradley
9. G. W. Brassell
10. R. S. Carlsmith
11. R. S. Crouse
12. R. G. Donnelly
13. J. I. Federer
14. W. Fulkerson
15. T. G. Godfrey
16. R. J. Gray
17–19. M. R. Hill
20. W. J. Lackey
21. R. R. Judkins
22. L. E. McNeese
23. A. E. Pasto
24. H. E. Reesor
25. A. C. Schaffhauser
26. J. E. Selle
27. G. M. Slaughter
28. R. R. Suchomel
29–43. V. J. Tennery
44. S. M. Tiegs
45. T. N. Tiegs
46. G. C. Wei
47. R. W. Ballufi (Consultant)
48. A. L. Bement, Jr. (Consultant)
49. W. R. Hibbard, Jr. (Consultant)
50. E. H. Kottcamp, Jr. (Consultant)
51. M. J. Mayfield, Jr. (Consultant)
52. J. T. Stringer (Consultant)

EXTERNAL DISTRIBUTION

53–56. AIRESEARCH MANUFACTURING COMPANY OF CALIFORNIA, 2525 W. 190th St., Torrance, CA 90509

M. Coombs
D. Kotchick
K. Styhr
D. Schwab

57. ALCOA RESEARCH LABORATORIES, ALUMINUM COMPANY OF AMERICA, Alcoa Center, PA 15069

R. G. LaBar

58. ALPHA GLASS INC., 301 East El Segundo Blvd., El Segundo, CA 90245

T. Williams

59. ARGONNE NATIONAL LABORATORY, Materials Science Division, 9700 South Cass Ave., Argonne, IL 60439

D. S. Kupperman

60–61. ARMCO STEEL CORPORATION, Research Center South, Middletown, OH 45043

B. H. Baker
R. L. Shultz

62. ANCHOR HOCKING COMPANY, Lancaster, OH 43135

R. S. Harris

63–65. BABCOCK AND WILCOX REFRACTORIES COMPANY, P.O. Box 923, Augusta, GA 30903

A. V. Illyn
R. C. Oxford
S. Young

66. BABCOCK AND WILCOX COMPANY, P.O. Box 1260, Lynchburg, VA 24505

E. M. Anderson

67–69. BATTELLE COLUMBUS LABORATORIES, 505 King Ave., Columbus, OH 43401

W. H. Duckworth
C. W. Kistler, Jr.
J. R. Schorr

70–71. BETHLEHEM STEEL CORPORATION, Homer Research Laboratory, Bethlehem, PA 18017

R. H. Herron
W. J. Smothers

72. BICKLEY FURNACES, INC., 550 State Road, Philadelphia, PA 19114

J. R. McGaughey

73. BROCKWAY GLASS COMPANY, Central Laboratory, Brockway, PA 15824

J. Langensiepen

74–76. CARBORUNDUM COMPANY, Niagara Falls, NY 14302

J. A. Bonar, Refractories Division, P.O. Box 337
L. H. Sweet, Manager Technical Department, P.O. Box 808
G. W. Weber, High Performance Silicon Carbide, P.O. Box 832

77. C-E MINERALS COMPANY, 901 E. 8th Ave., King of Prussia, PA 19406

R. E. Nelson

78. CHATTANOOGA GLASS COMPANY, 400 W. 45th Street, Chattanooga, TN 37410

R. Neeley

79. COORS PORCELAIN COMPANY, 600 9th Street, Golden, CO 80401

T. H. Nielson

80. CORHART REFRACTORIES COMPANY, 1600 W. Lee Street, Louisville, KY 40210

    P. Papa

81. CORNING GLASS WORKS, Box 432, Corning, NY 14830

    J. Wosinsky

82. DIVERSIFIED INSULATION, INC., P.O. Box 188, Hamel, MI 55340

    R. W. Anderson

83. EG&G IDAHO, INC., P.O. Box 1625, Idaho Falls, ID 83401

    A. R. Richardson

84. ELECTRIC POWER RESEARCH INSTITUTE, 3412 Hillview Ave., P.O. Box 10412, Palo Alto, CA 94303

    W. T. Bakker

85. EMHART CORPORATION, Hartford Refractories, P.O. Box 2809, Hartford, CT06101

    G. R. Rowland

86. FERRO CORPORATION, Temtek-Allied Division, One Erieview Plaza, Cleveland, OH 44114

    W. Mead

87. FLUIDYNE ENGINEERING COMPANY, 5900 Memorial Highway, Minneapolis, MN 55422

    R. R. Smyth

88–89. FORD MOTOR COMPANY, 25500 West Outer Drive, Lincoln Park, MI 48146

    J. E. Bailey, Raw Materials Specialist
    V. L. Spade, Glass Division

90–91. GENERAL ATOMIC COMPANY, P.O. Box 81608, San Diego, CA 92138

    J. E. Sheehan
    R. W. Schleicher

92. GENERAL ELECTRIC COMPANY, P.O. Box 8555, Philadelphia, PA 19101

    L. R. McCreight, Manager, Materials Research and Development

93. GLASROCK PRODUCTS, INC., 2210 Marietta Blvd., NW, Atlanta, GA 30318

    R. P. Ross

94. A. P. GREEN REFRACTORIES COMPANY, Green Blvd., Mexico, MO 65265

J. A. Crookston

95–96. GTE SYLVANIA INCORPORATED, Chemical and Metallurgical Division, Towanda, PA 18848

K. H. Kohnken
J. J. Cleveland

97. HAGUE INTERNATIONAL, 3 Adams Street, South Portland, ME 04106

I. W. Bjerklie

98. HARBISON-WALKER REFRACTORIES, Division of Dresser Industries, Inc., 2 Gateway Center, Pittsburgh, PA 15222

R. L. Yeckley, Industrial Market

99. ICI AMERICAS, INC., Specialty Chemicals Division, Wilmington, DE 19849

R. A. Fenimore

100. INLAND STEEL RESEARCH, 3001 East Columbus Drive, East Chicago, IN 46312

R. Ramey

101. INSTITUTE OF GAS TECHNOLOGY, 3424 S. State St., IIT Center, Chicago, IL 60616

C. J. Marnell

102. INTERPACE CORPORATION, Corporate Headquarters, Box 1111, Parsippany, NJ 07054

L. E. Ferreira

103. IOWA STATE UNIVERSITY, Materials Science and Engineering Department, Ames, IA 50010

T. D. McGee

104. JOHNS-MANVILLE CORPORATION, Box 5108, Denver, CO 80217

C. M. Pelanne

105. JONES AND LAUGHLIN STEEL CORPORATION, 3A, Gateway Center, Pittsburgh, PA 15230

D. Olenchut

106–107. KAISER ALUMINUM AND CHEMICAL CORPORATION, Box 870, Pleasanton, CA 94566

R. E. Ferris
M. L. Van Dreser

108. MASSACHUSETTS INSTITUTE OF TECHNOLOGY, Department of Materials Science and Engineering, Cambridge, MA 02139

H. K. Bowen

109. MONSANTO COMPANY, 800 N. Lindbergh Blvd., St. Louis, MO 63166

W. S. Netter

110. NL INDUSTRIES, 8361 Broadwell Road, P.O. Box 44040, Cincinnati, OH 45244

E. A. Thomas

111. NORTH AMERICAN MANUFACTURING COMPANY, 4455 E. 71st Street, Cleveland, OH 44105

R. W. Marshell

112. NORTH AMERICAN REFRACTORIES COMPANY, 1012 National City E. 6th Bldg., Cleveland, OH 44114

R. F. Whitford

113. NORTH AMERICAN REFRACTORIES COMPANY RESEARCH CENTER, Curwensville, PA 16833

R. A. Landy, Director of Research

114–115. NORTON COMPANY, One New Bond Street, Worcester, MA 01606

N. Ault
L. J. Trostel, Jr.

116–117. OWENS-ILLINOIS, INC., P.O. Box 1035, Toledo, OH 43666

L. Baumer
R. H. Redwine, Kimble Division

118. PULLMAN-SWINDELL, 441 Smithfield Street, Pittsburg, PA 15222

R. J. Moffat

119. THE REFRACTORIES INSTITUTE, 1102 One Oliver Plaza, Pittsburgh, PA 15222

B. S. Tucker

120. ROCKETDYNE DIVISION, ROCKWELL INTERNATIONAL, 6633 Canoga Ave., Canoga Park, CA 91304

H. W. Carpenter

121–122. SOLAR DIVISION OF INTERNATIONAL HARVESTER, 2200 Pacific Hwy., San Diego, CA 92112

A. G. Metcalfe
M. E. Ward

123. SOLAR ENERGY RESEARCH INSTITUTE, 1536 Cole Boulevard, Golden Colorado 80401

B. L. Butler

124–125. TERRATEK, University Research Park, 420 Wakara Way, Salt Lake City, UT 84108

R. Harrison
D. Power

126. THERMAL TRANSFER, 1100 Rico Road, Monroeville, PA 15146

G. L. Hanson

127. TRANE THERMAL COMPANY, Brook Road, Conshohocken, PA 19428

H. Orr

128–129. UNITED STATES STEEL CORPORATION, Research Center, 125 Jamison Lane, Monroeville, PA 15146

C. K. Russell
W. Vance

130. UNIVERSITY OF ILLINOIS, Ceramics Dept., Urbana, IL 61801

J. A. Nelson

131. VIRIGINIA POLYTECHNIC INSTITUTE AND STATE UNIVERSITY, Department of Materials Engineering, Blacksburg, VA 24061

J. J. Brown

132. WARREN ASSOCIATES, 22230 Bassett Street, Canoga Park, CA 91303

J. W. Warren

133. WESTINGHOUSE ELECTRIC CORPORATION, Research Center, Beulah Road, Pittsburgh, PA 15235

R. Crekrila

134. ZIRCOA PRODUCTS, 31501 Solon Road, Solon, OH 44139

H. L. Johns

135. DOE, FOSSIL ENERGY DIVISION, Fuel Utilization, E 178-GTN, Washington, 20545

M. Perlsweig

136. DOE, IDAHO OPERATIONS OFFICE, Idaho Falls, ID 83401

W. H. Thielbahr

137—140. DOE, INDUSTRIAL PROGRAMS, Office of Assistant Secretary, Conservation and Solar Energy, Forrestal Bldg., 1000 Independence Ave., Room 2H085, Washington, DC 20585

J. N. Eustis
D. G. Harvey
J. W. Osborne
Ralph Sheneman

141. DOE, MATERIALS PLANNING AND DEVELOPMENT SECTION, Planning and Systems Engineering Division, MS C156-GTN, Washington, DC 20545

S. J. Dapkanas

142. DOE, OAK RIDGE OPERATIONS OFFICE, P.O. Box E, Oak Ridge, TN 37830

Assistant Manager, Energy Research and Development

143—169. DOE, TECHNICAL INFORMATION CENTER, P.O. Box 62, Oak Ridge, TN 37830

☆ U. S. GOVERNMENT PRINTING OFFICE: 1979-640-245-297